2016

METHODOLOGY FOR ANALYZING EPOXY-CNT PHONONIC CRYSTALS FOR WAVE ATTENUATION AND GUIDING

Madhu Kolati
Michigan Technological University, mkkolati@mtu.edu

METHODOLOGY FOR ANALYZING EPOXY-CNT PHONONIC CRYSTALS FOR WAVE ATTENUATION AND GUIDING

By
Madhu Kolati

A DISSERTATION
Submitted in partial fulfillment of the requirements for the degree of
DOCTOR OF PHILOSOPHY
In Mechanical Engineering-Engineering Mechanics

MICHIGAN TECHNOLOGICAL UNIVERSITY
2016

This dissertation has been approved in partial fulfillment of the requirements for the Degree of DOCTOR OF PHILOSOPHY in Mechanical Engineering-Engineering Mechanics.

Department of Mechanical Engineering-Engineering Mechanics

Dissertation Co-Advisor: *Dr. Craig Friedrich*

Dissertation Co-Advisor: *Dr. Gregory Odegard*

Committee Member: *Dr. John Jaszczak*

Committee Member: *Dr. Reza Yassar*

Department Chair: *Dr. William W. Predebon*

To my family

TABLE OF CONTENTS

TABLE OF FIGURES

LIST OF TABLES

ACKNOWLEDGMENTS

I am extremely thankful to Dr. Friedrich Craig and Dr. Gregory Odegard for granting me the opportunity to perform research in this new and exciting field of phononic crystals. This was a tremendous learning opportunity to me as a researcher. Professor Craig's expertise in variety of engineering disciplines and Professor Odegard's knowledge in the field of solid mechanics have been the strengths for this research. I'm grateful for their guidance and support. I would also like to thank Professor John Jaszczak for accepting to serve on my advisory committee. I'm thankful to Professor Reza Shahbazian-Yassar for serving on my advisory committee.

ABSTRACT

Phononic crystals (PhnCs) control, direct and manipulate sound waves to achieve wave guiding and attenuation. This dissertation presents methodology for analyzing nanotube materials based phononic crystals to achieve control over sound, vibration and stress mitigation. Much of the analytical work presented is in identifying frequency band gaps in which sound or vibration cannot propagate through these PhnCs. Wave attenuation and mitigation analysis is demonstrated using finite element simulation. Engineering principles from current research areas of solid mechanics, solid-state physics, elasto-dynamics, mechanical vibrations and acoustics are employed for the methodology. A considerable effort is put to show that these PhnCs can indeed be designed and manufactured to build applications for frequency filtering, vibration isolation, wave guiding and stress mitigation.

1 INTRODUCTION

1.1 INTRODUCTION

Phononic crystals (PhnCs) are periodic materials which take advantage of periodicity to control the propagation of elastic or acoustic waves. These materials are not readily available in nature and therefore have to be tailored to achieve control over mechanical waves. In the past decade, researchers from diverse fields have shown interest in this field of study and have been successful in developing it. Today, the field of "Acoustic Metamaterials and Phononic Crystals"[1] stands as an independent field of study offering potential applications for wave confinement and guiding. Novel effects like negative refraction, acoustic cloaking, imaging and lensing are also being enabled by their use[2].

PhnCs available today assume a scatterer of less than $1/3^{rd}$ of the strength of a carbon nanotube [3] and since carbon nanotube materials are readily available today and have shown to exhibit very high strength [4], A phononic crystal based on the high stiffness of carbon nanotubes and low stiffness of epoxy is analyzed for wave confinement and guiding characteristics. These PhnCs are analyzed for sound, vibration, stress guiding and attenuation. The basic concepts related to acoustic metamaterials are introduced and then methods for calculating dispersion relations are presented. Potential applications for these PhnCs are illustrated in this Chapter.

1.2 BASIC CONCEPTS

The concept of meta-materials was first derived by the Russian scientist Victor Veselago[5] when dealing with electromagnetic wave propagation. He formulated his hypothesis for electromagnetic wave propagation for a medium which would behave as if the permittivity and permeability were negative. By applying Maxwell's equations to such hypothesis, he predicted that the incoming wave would deviate from following the conventional path as shown in Figure 1.1.

Maxwell's equation for electromagnetic wave propagation in a medium is given by,

$$\nabla^2 \mathbf{E} = \epsilon\mu \frac{\partial^2 \mathbf{E}}{\partial t^2}$$ (Wave equation)

$$\mathbf{E} = \mathbf{E_0} e^{(\mathbf{k}.\mathbf{r} - \boldsymbol{\omega} \mathbf{t})}$$ (Solution for the wave equation)

Where **E** is the electric field, ∈ and μ are the permittivity and permeability of the medium, ω is angular frequency, υ is the wave speed and $\boldsymbol{k}$ is the wave vector.

$$\boldsymbol{k} = \frac{\omega}{v}$$

The refractive index **n** for a medium is given by $\mathbf{n} = \pm\sqrt{\in \boldsymbol{\mu}}$

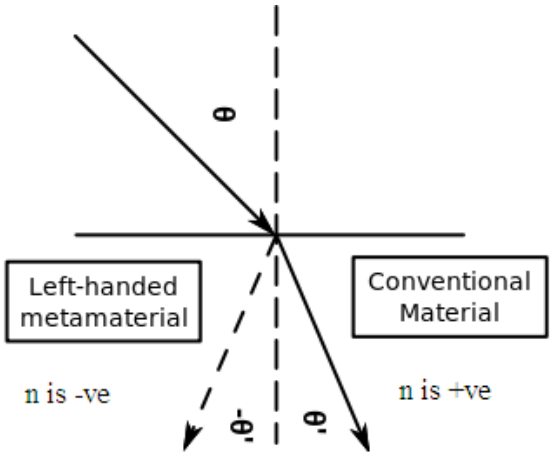

Figure 1.1. Conventional material vs metamaterial

This hypothesis was not realized practically until Pendry [6] proposed the designs of artificial structured materials. The term negative index, does not imply that materials really possess negative properties, but rather only achieve the effect of wave bending due to periodic variation of material properties. This theory has also been realized in Phononic crystals [7] for acoustic applications which create a similar effect of negative bulk modulus and density by completely reflecting incoming sound waves. This wave deviation from

the conventional path is achieved by Bragg's mechanism or local resonances and not by negative properties.

1.3 PHONONIC CRYSTALS

Phononic crystals are a branch of acoustic meta-materials [8] which make use of wave scattering and interference phenomena to create frequency band gaps within which waves cannot propagate. This effect is achieved by periodically arranging materials with varying elastic and density properties in the PhnC. This periodic variation causes the speed of sound to vary in the PhnC and in turn reflect or scatter the incoming wave. Reflection also occurs when the wave-length of the incoming wave is an integer multiple of the PhnCs periodic length.

1.4 1D PHONONIC CRYSTAL

Phononic crystals [9] can be broadly categorized according to the direction of periodicity. They could be either periodic in one direction as shown in Fig 1.2 or multiple directions as shown Fig 1.3 & Fig 1.4. PhnCs that are periodic only in one direction exhibit a frequency band gap only in a single direction. The waves travelling in the direction of the periodicity of the PhnC will be completely attenuated while the waves travelling perpendicular to the PhnC will not undergo any enhanced attenuation. This can be explained due to the fact that the traveling waves encounter impedance mismatch only in one direction. The waves traveling in the 1D PhnC have either transverse or longitudinal polarization and this makes the wave equation much easier to solve and model. Although single periodicity imposes a limitation, these PhnCs are much easier to design and manufacture compared to 2D and 3D periodic PhnCs. 1D PhnCs have also been proposed for seismic attenuation in buildings[10] and also to confine vibrations in cellular phones.

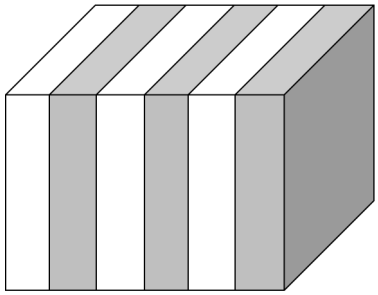

Figure 1.2. Phononic crystal periodic in one direction

1.5 2D PHONONIC CRYSTAL

PhnCs that are periodic in two directions as shown in Fig 1.3 exhibit a frequency band gap for waves traveling parallel, perpendicular and also at an inclined angle in the plane of PhnC. The waves travelling in-plane will be highly attenuated while the waves travelling out of plane of the PhnC will not undergo any enhanced attenuation. This can be explained due to the fact that the traveling waves encounter impedance mismatch only in the plane of the PhnC. Unlike 1D PhnC, the waves where the transverse and longitudinal waves are uncoupled, 2D PhnCs have coupled longitudinal and traverse waves and this makes the wave equation complicated to solve and model. Numerical methods such as Plane Wave Expansion, Finite Difference and Finite Element Methods are needed to solve for the dispersion relation. 2D PhnCs provide much better band gap capabilities compared to 1D PhnC by offering complete attenuation of coupled shear and transverse modes. 2D PhnCs can give rise to frequency filters for wave confinement and guiding by simply removing one or many inclusions from the matrix[11]. Although, out of plane properties impose a limitation, these PhnCs are much easier to design and manufacture compared to 3D periodic PhnCs. They can be very useful for isolating vibrations in Coriolis gyroscopes, micro resonators and oscillators[12].

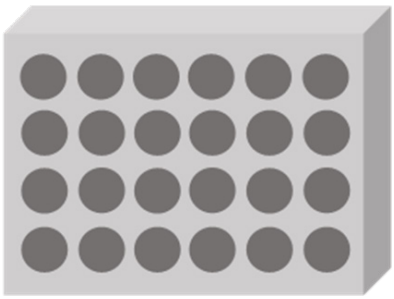

Figure 1.3. Phononic crystal periodic in two directions

1.6 3D PHONONIC CRYSTAL

PhnCs that are periodic in three directions as shown in Figure 1.4 exhibit a complete frequency band gap for waves traveling in any direction and polarization. 3D PhnCs have generated interest among researchers because of the complete band gap for complete sound and vibration isolation[13]. This unique property of a complete band gap cannot be achieved in 1D and 2D PhnCs since they possess only partial band gaps. Waves with any polarization and incidence angle will be completely attenuated by the 3D PhnC since the traveling waves encounter impedance mismatch in all directions. Unlike 1D PhnC, where the transverse and longitudinal waves are uncoupled, 3D PhnCs have coupled longitudinal and traverse waves and this makes the wave equation complicated to solve and model. Numerical methods must be relied upon for dispersion calculations. 3D PhnCs provide much better band gap capabilities compared to 1D PhnC by offering complete attenuation of coupled shear and transverse modes. 3D PhnCs can give rise to complete sound isolation and vibration isolating applications which can be useful in high-precision mechanical systems[14]. In 3D Phononic crystals, introducing deviation from periodicity in one of the directions can give rise to Anderson localization. This can be achieved by introducing planar defects in subsequent layers or by progressively changing the properties of subsequent layers or changing the size of geometry and position of embedded scatterer in subsequent layers. In all these cases, periodicity still remains in the other two directions. This introduction of impurity planes gives rise to propagation modes within the frequency band gap of the pure crystal.

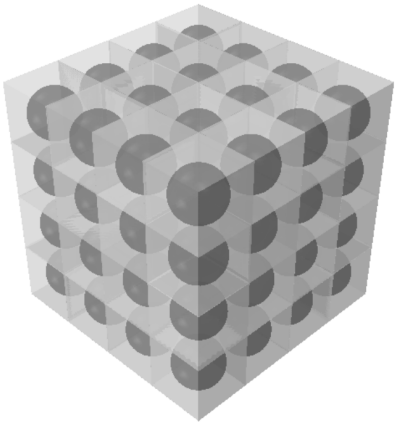

Figure 1.4 Phononic crystal periodic in three directions

1.7 PHOTONIC CRYSTALS

Many of the fundamental concepts for phononic crystals were derived from photonic crystals and semiconductors. Photonic crystals exhibit similar frequency band gap effect against electromagnetic waves due to varying permittivity and permeability of the system. They have interesting properties of light confinement and localization leading to applications such as optical waveguides, selective filters and lenses[15]. Phononic crystals are considered as mechanical analogues of photonic crystals. Semiconductors exhibit a similar band gap effect against electron flow leading to electronic and conduction properties. The table 1.1 shows the similarities between photonic and phononic crystal.

Table 1.1 Band structure related properties of Photonic and Phononic crystals [3]

Property	Photonic crystal	Phononic crystal
Materials	Made of dielectric materials	Made of elastic materials
Parameters	Electromagnetic permeability and permittivity	Mass density and speed of sound
Waves	Electromagnetic	Mechanical (Sound or vibrational)
Polarization	Transverse	Longitudinal, Transverse and Coupled shear and compressional

1.8 METHODS

Band gap calculations are computationally intensive. First the inhomogeneous material constitutive equations of the system are derived in terms of Eigen value models. The frequency dependency of the system is identified by solving the obtained dispersion relation for the wave vectors in the Brillouin zone. The Floquet Bloch theorem is used for periodic boundary conditions.

1.8.1 Plane wave expansion method for band gap calculations

Methods such as plane wave, finite difference and finite elements are used to calculate the band gaps. Although these methods have some advantages over each other, the plane wave expansion method [16] calculates the band structure assuming the displacement field and periodic variation of the sound speed in terms of Fourier components. This method is widely popular in the photonics community for calculating dispersion in photonic crystals. While this method has been widely used for band structure calculations, its main disadvantage occurs when there is a huge mismatch in the mechanical properties within the PhnC i.e. elasticity, density and sound speed, since capturing this mismatch would require a large number of Fourier components. Since Epoxy-CNT PhnCs do fall into this area because of the huge mismatch in mechanical properties, the plane wave expansion method was avoided for band gap calculations for these PhnCs. Kushwaha [16] calculated the band structure using the plane wave method for a composite made of Ni alloy cylinders in an Al alloy matrix with a 35% volume fraction.

The density and displacement field, expressed using Fourier series in a plane wave expansion method are,

$$\rho(r) = \sum_{\boldsymbol{G}} \rho(\boldsymbol{G})\, e^{\boldsymbol{iG.r}}$$

$$u(r,t) = e^{i(\boldsymbol{K.r}-\omega t)} \sum_{\boldsymbol{G}} \boldsymbol{u_K}(\boldsymbol{G})\, e^{\boldsymbol{iG.r}}$$

Where $\boldsymbol{G}$ is the reciprocal lattice vector and $\boldsymbol{K}$ the Bloch wave vector.

$\rho(r)$ and $u(r,t)$ are the density and displacement.

1.8.2 Finite difference method for band gap calculations

The Finite difference method being computationally intensive takes into account the finiteness of the model and is mostly used to calculate the transmission coefficient of the PhnC. It does so by discretizing space and time derivatives of the constitutive equation with forward, backward and central difference schemes. It can calculate the displacement field effectively inside the PhnC and can be used for direct comparison with experimental data. Additional boundary conditions are specified on the external edges to mimic the real model. Although this method is better when used for 1D and 2D PhnCs, it becomes computationally intensive for 3D PhnCs. The equations below are shown as an example.

Constitutive equations for inhomogeneous two dimensional PhnC:

$$\rho\frac{\partial^2 u}{\partial t^2} = \frac{\partial \sigma_{xx}}{\partial x} + \frac{\partial \sigma_{xy}}{\partial y}$$

$$\rho\frac{\partial^2 v}{\partial t^2} = \frac{\partial \sigma_{xy}}{\partial x} + \frac{\partial \sigma_{yy}}{\partial y}$$

$$\sigma_{xx} = (\lambda + 2\mu)\frac{\partial u}{\partial x} + \lambda\frac{\partial v}{\partial y}$$

$$\sigma_{yy} = (\lambda + 2\mu)\frac{\partial v}{\partial y} + \lambda\frac{\partial u}{\partial x}$$

$$\sigma_{xx} = \mu\left(\frac{\partial u}{\partial y} + \frac{\partial v}{\partial x}\right)$$

The space derivatives are discretized using the central difference approximation

$$\frac{\partial u}{\partial x} = \left[u\left(i+\frac{1}{2},j,k\right) - u\left(i-\frac{1}{2},j,k\right)\right]/\Delta x$$

$$\frac{\partial v}{\partial y} = \left[u\left(i,j+\frac{1}{2},k\right) - u\left(i,j-\frac{1}{2},k\right)\right]/\Delta y$$

Where i and j are grid points and Δx, Δy dimensions.

1.8.3 Finite element method for band gap calculations

The finite element method uses piecewise solutions to approximate the entire behavior of the domain. For static calculations these piecewise solutions are assembled into global matrices in terms of stiffness and displacement. For dynamic calculations these piecewise solutions are assembled in terms of global stiffness, damping and mass matrices and are solved to meet the imposed boundary conditions. For static analysis the force or displacement is assumed to be a linear function and for modal analysis they are assumed to be either a sine, cosine or a periodic function that satisfies observed phenomena and the governing differential equation. Most finite element solvers like ABAQUS and MSC NASTRAN assume either a sine or cosine function and calculate the mode shapes present in the PhnC. While this is useful, in turns out to be a disadvantage for dispersion calculations. For dispersion calculations, the displacement or force must be assumed to be a periodic function in terms of the wave vector and angular frequency. The standard FEM solvers assume displacement function in terms of angular frequency and do not include the wave vector. Because of this limitation the parametric FEM solver COMSOL was chosen for dispersion calculations. ABAQUS is used for frequency response and wave propagation analysis. The equations below show this use.

$u(\boldsymbol{x}, t) = \sin(\omega t)\ or\ \cos(\omega t)$ - Displacement function assumed by ABAQUS & MSC Nastran. $u(x, t) = \sin(\boldsymbol{k}.\boldsymbol{x} - \omega t)\ or\ \cos(\boldsymbol{k}.\boldsymbol{x} - \omega t)$ - Displacement function assumed by COMSOL.

Where **k** is the wave vector and ω the angular frequency

$$[M]\left[\ddot{U}\right] + [K][U] = 0$$

$$|[K] - \omega^2[M]| = 0$$

The above modal equations are solved by COMSOL to predict all the possible mode shapes present in the PhnC in terms of frequency or wave vector.

2 LITERATURE REVIEW

Research in the field of acoustic metamaterials has been very promising and novel concepts like acoustic cloaking [17, 18] and negative refraction [19, 20] are being enabled by their use. Steven Cummer from Duke University has proposed a 3D acoustic cloaking device made of plastic sheets with holes. This cloak alters the trajectory of the interacting sound waves making it appear as if it has reflected off a flat surface[21-23]. This possibility of altering sound waves to create novel effects has attracted many researchers to field of Acoustic metamaterials and Phononic crystals[8, 24].

Acoustic metamaterials and Phononic crystals achieve control over sound waves based on local resonances and Bragg's reflection. Novel effects such as frequency filtering, demultiplexing, collimation, guiding and imaging with accompanying experiments has been published in this field[25]. Today, the field of Acoustic metamaterials and Phononic crystals stands as an independent field with wide publications. The field of Electromagnetic metamaterials [26] have paved the way for acoustic metamaterials, since the control of waves is common to both the fields. Optical metamaterials affect the propagation of electromagnetic waves by either, altering or reflecting the incident waves. Photonic crystals are one similar field where most of the concepts and methods for calculating band gaps in Phononic crystals are relied upon. Photonic crystals are similar to phononic crystals in that material properties remain a periodic function. This periodic change in material properties causes scattering of electromagnetic and acoustic waves[15, 27-29]. Periodic change in permeability and permittivity of the materials is fundamental for affecting electromagnetic wave propagation in Photonic crystals. Periodic change in density and elastic modulus is fundamental for affecting mechanical waves in Phononic crystals. Both fields rely on Bragg's mechanism for destructive interference of the waves to cause attenuation.

Periodic structures are known in the field of acoustics for sound transmission loss [30] capabilities. However, structures that can possess transmission loss for a wave entering in all directions are rare and this is where the field of Phononics has gained its reputation and

has become a field of study of its own. The famous experiment conducted in the field of Phononics was measuring the transmission loss of the sculpture designed by Eusebio Sempere.[7] This sculpture is made of periodic array of hollow steel cylinders and attenuates sound strongly at a certain range of frequencies. Phononic crystals have a range of applications in the area of wave guiding, sound focusing, thermal management, and vibration mitigation.

Zhengyou Liu et al. [31] fabricated a sonic crystal based on the concept of Local resonance. This crystal exhibits gaps or dips in transmission properties which show large attenuation of the input sound pulse. This 2cm slab was made of lead balls coated with rubber and embedded in hard matrix of epoxy. Large attenuation of the input sound pulse was observed at 380 and 1350 Hz. This experiment has sparked interest in the search for locally resonant structures which can be two orders of magnitude smaller than the wavelength they affect.

Theoretical methods for calculations of frequency band gaps are crucial to phononic crystals. Kushwaha et al. [16] presented a theory for band structure calculations in periodic elastic composites. The material properties such as mass density, longitudinal speed of sound and transverse speed of sound are position dependent. The method was based on the plane wave expansion method which is widely used in the photonics area [32, 33]. Material properties such as mass density and speed of sound are expressed in terms of Fourier series and Bloch wave vector. Bloch Floquet boundary conditions are used to solve for the Eigen frequencies and wave vectors. Frequency band gaps were calculated for transvers modes of nickel alloy cylinder embedded in aluminum alloy matrix and vice versa. The cylinders are assumed to form a square lattice. Frequency band gaps were found to exist in these composites within which vibration and sound is prohibited. A parametric study of the dependence of the band gap on the filling fraction was also investigated as part of this method.

Po-Feng Hsieh et al. [34] calculated frequency band gaps for three dimensionally periodic phononic crystals using a Finite difference time domain method. In this research, band structures for a phononic crystal made of steel spheres embedded in

epoxy matrix were calculated. A very narrow band gap was found to exist in these phononic crystals.

Xiang et al [10] proposed Phononic crystals made of concrete and rubber as periodic foundations for resisting earthquake vibrations. In that paper, they experimentally validated their results through shake table tests. The results showed that the vibration was highly attenuated at the predicted longitudinal and transverse band gaps. The steel building structure that was mounted on the periodic foundation was less responsive in case of earth quake events. The steel structure showed a greater response without the concrete-rubber periodic foundation.

Gorishnyy et al [35] proposed Phononic crystals for thermal management. Since heat is related to electrons and phonons, controlling phonons at such a small scale would result in thermal management. This would mean making Phononic crystals for very small wavelengths i.e. in GHz- THz frequencies range. Using interference lithography, researcher's manufactured a 6-micron thick epoxy layer film on glass substrate with air holes. The lattice periodicity for the structure is approximately 1.36 microns. They predicted band gaps in the 1 GHz range and concluded that these gaps affect the thermal conductivity and heat capacity.

Otsuka et al[36] have shown Phononic crystals for wave guiding at 1GHz frequency range. They manufactured a surface Phononic crystal made of crystalline silicon with microscopic air holes with 5.6-micron diameter. The designed wave guides match the experimental and theoretical band gap data.

Phononic crystals have potential applications in sound, vibration and thermal areas. These crystals can be designed for sonic, ultrasonic and hypersonic frequencies. Crystals designed to operate at sonic frequencies could lead to potential applications in architectural acoustics and seismic isolation. Crystals designed to operate at ultrasonic frequencies could lead to potential applications in imaging and non-destructive testing. Crystals designed to operate at hypersonic frequencies could lead to potential applications in acousto-optics and thermal management[37].

3 ONE-DIMENSIONAL EPOXY-CNT PHONONIC CRYSTALS

3.1 INTRODUCTION

One dimensional Phononic crystals are periodic in one direction. These PhnCs can either block or guide incoming waves in one direction. These PhnCs have potential application in vibration, sound, and stress mitigation applications based on the frequency range and dimensions [38, 39]. The frequency range blocked by these PhnCs depend on the dispersion characteristics[40].

In this chapter, the basic theory governing phononic crystals is presented. Basic concepts related to mass-spring lattice vibrations are presented in order to introduce the concepts governing phononic crystals. Concepts including Brillouin zone, frequency band gaps, reciprocal lattice vectors and dispersion relation are explained. Basic equations governing mass spring vibrations are solved assuming a plane wave solution. Dispersion relation and frequency band gaps is explained via MATLAB generated plots.

Subsequently, the dispersion relation for the actual PhnC is derived using elasticity theory [10]. Bloch-Floquet [41, 42]periodic boundary conditions and interfacial stress-strain conditions are used to arrive at the Eigen value relation. The band gap diagrams for transverse and longitudinal wave types are calculated. To correlate the band gap data, frequency response and stress attenuation figures are developed using the finite element method. Based on the correlated results, a conclusion is arrived at the transmission properties of the Epoxy-CNT PhnC.

3.2 SINGLE MASS LATTICE VBRATIONS

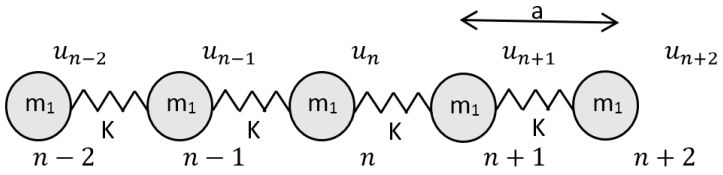

Figure 3.1 Single mass lattice

Consider a single mass lattice as shown in Fig 3.1

Where

u_n = displacement of mass from equilibrium position

m_1 = mass

K = spring stiffness

n = position

a = lattice distance or distance between mass centers

Considering only opposing forces due to neighboring masses,

$$m_1 \frac{d^2 u_n}{dt^2} = K(u_{n+1} - u_n) + K(u_{n-1} - u_n) = K(u_{n+1} + u_{n-1} - 2u_n) \quad \text{3.1 eq}$$

A harmonic solution can be assumed for displacement of the masses,

$$u_n(t) = A_1 e^{i(\boldsymbol{k}na - \omega t)} \quad \text{3.2 eq}$$

$$u_{n+1}(t) = A_1 e^{i(\boldsymbol{k}(n+1)a - \omega t)} \quad \text{3.3 eq}$$

$$u_{n+2}(t) = A_1 e^{i(\boldsymbol{k}(n+2)a - \omega t)} \quad \text{3.4 eq}$$

Where $\boldsymbol{k} = \frac{2\pi}{\lambda}$ is the one dimensional wave vector with wavelength λ and A_1 is the amplitude of oscillation. Substituting the above solutions into the equation of motion gives,

$$i^2 m_1(\omega^2) e^{i(\boldsymbol{k}na-\omega t)} = K(e^{i(\boldsymbol{k}(n+1)a-\omega t)} + e^{i(\boldsymbol{k}(n-1)a-\omega t)} - 2e^{i(\boldsymbol{k}na-\omega t)}) \quad \text{3.5 eq}$$

$$-m_1(\omega^2) e^{i\boldsymbol{k}na} = K(e^{i\boldsymbol{k}(n+1)a} + e^{i\boldsymbol{k}(n-1)a} - 2e^{i\boldsymbol{k}na}) \quad \text{3.6 eq}$$

$$m_1(\omega^2) = K(-e^{i\boldsymbol{k}a} - e^{-i\boldsymbol{k}a} + 2) \quad \text{3.7 eq}$$

$$m_1(\omega^2) = K(-(\cos(\boldsymbol{k}a) + i\sin(\boldsymbol{k}a)) - (\cos(-\boldsymbol{k}a) + i\sin(-\boldsymbol{k}a)) + 2) \quad \text{3.8 eq}$$

$$m_1(\omega^2) = K(-2\cos(\boldsymbol{k}a) + 2) \quad \text{3.9 eq}$$

$$m_1(\omega^2) = 2K(1 - \cos(\boldsymbol{k}a)) \quad \text{3.10 eq}$$

$$m_1(\omega^2) = 4K\sin^2\frac{\boldsymbol{k}a}{2} \quad \text{3.11 eq}$$

This gives the relation between frequency and wave vector, i.e. the Dispersion Relation

$$\omega = \sqrt{\frac{4K}{m_1}}\left|\sin\frac{\boldsymbol{k}a}{2}\right| \quad \text{3.12 eq}$$

Assuming for example the following values: a = 0.01 m; K = 0.001 N/m; m1 = 0.1 kg;

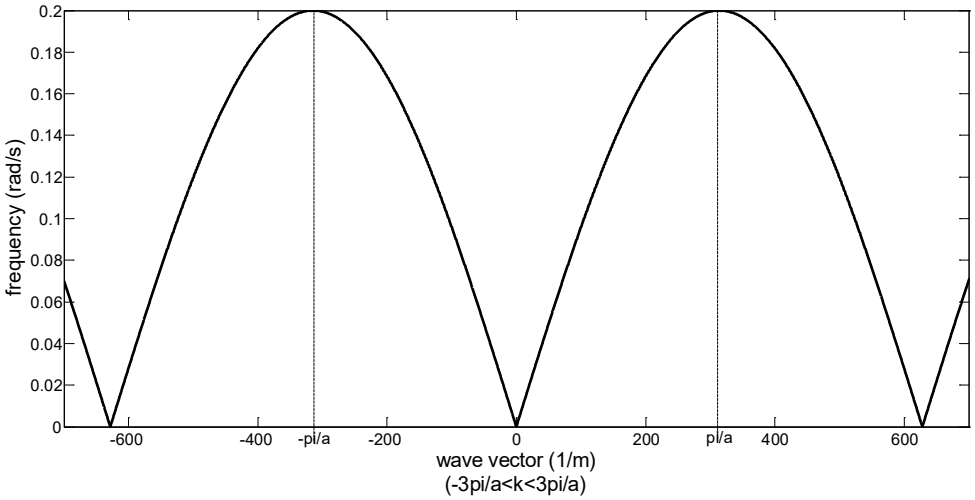

Figure 3.2 Frequency vs wave vector figure for the single-mass lattice

Figure 3.2 shows that the frequency varies periodically with the wave vector. All the information necessary for the frequency and wave vector lies in the intervals of –pi/a to pi/a and no new information is produced beyond these limits. This interval is called the

Brillouin zone and the limits –pi/a to pi/a are termed the reciprocal lattice vectors. Brillouin zone and reciprocal lattice vectors are used to calculate the frequency band gaps present in semiconductors, photonic crystals and phononic crystals[43].

3.3 DOUBLE MASS LATTICE VIBRATIONS

Consider a double mass-spring model shown in Figure 3.3

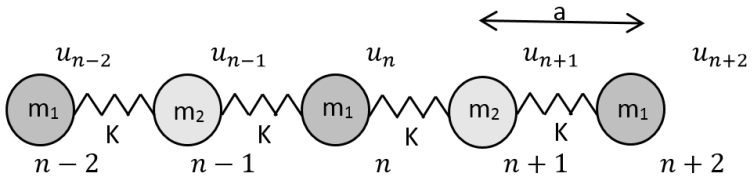

Figure 3.3 Double-mass lattice

Considering only opposing forces due to neighboring masses, gives

$$m_1 \frac{d^2 u_n}{dt^2} = K(u_{n+1} - u_n) + K(u_{n-1} - u_n) = K(u_{n+1} + u_{n-1} - 2u_n) \quad \text{3.13 eq}$$

$$m_2 \frac{d^2 u_{n+1}}{dt^2} = K(u_{n+2} - u_{n+1}) + K(u_n - u_{n+1}) = K(u_{n+2} + u_n - 2u_{n+1}) \quad \text{3.14 eq}$$

A harmonic solution in the form of a traveling wave is assumed for displacements

$$u_n(t) = A_1 e^{i(\boldsymbol{k}na - \omega t)} \quad \text{3.15 eq}$$

$$u_{n-1}(t) = A_2 e^{i(\boldsymbol{k}(n-1)a - \omega t)} \quad \text{3.16 eq}$$

$$u_{n+1}(t) = A_2 e^{i(\boldsymbol{k}(n+1)a - \omega t)} \quad \text{3.17 eq}$$

$$u_{n+2}(t) = A_1 e^{i(\boldsymbol{k}(n+2)a - \omega t)} \quad \text{3.18 eq}$$

Substituting these solutions in the equation of motion gives

$$i^2 m_1(\omega^2) A_1 e^{i(\boldsymbol{k}na - \omega t)} = K(A_2 e^{i(\boldsymbol{k}(n+1)a - \omega t)} + A_2 e^{i(\boldsymbol{k}(n-1)a - \omega t)} - 2A_1 e^{i(\boldsymbol{k}na - \omega t)}) \quad \text{3.19 eq}$$

$$i^2 m_1(\omega^2) A_2 e^{i(\boldsymbol{k}(n+1)a-\omega t)} \quad \text{3.20 eq}$$

$$= K(A_1 e^{i(\boldsymbol{k}(n+2)a-\omega t)} + A_1 e^{i(\boldsymbol{k}na-\omega t)} - 2A_2 e^{i(\boldsymbol{k}(n+1)a-\omega t)})$$

$$(2K - m_1\omega^2)A_1 - (2K\cos(\boldsymbol{k}a))\,A_2 = 0 \quad \text{3.21 eq}$$

$$-(2K\cos(\boldsymbol{k}a))\,A_1 + (2K - m_2\omega^2)A_2 = 0 \quad \text{3.22 eq}$$

The determinant of the matrix formed by 3.21 and 3.22 must be zero for a solution,

$$(2K - m_1\omega^2)(2K - m_2\omega^2) - 4K^2 cos^2 \boldsymbol{k}a = 0 \quad \text{3.23 eq}$$

This results in a quadratic equation,

$$m_1 m_2(\omega^2)^2 - 2K(m_1 + m_2)\omega^2 + 4K^2(1 - cos^2 \boldsymbol{k}a) = 0 \quad \text{3.24 eq}$$

$$\omega^2 = K\left[\frac{1}{m_1} + \frac{1}{m_2}\right] \pm K\sqrt{\left[\frac{1}{m_1} + \frac{1}{m_2}\right]^2 - \frac{4\sin^2 \boldsymbol{k}a}{m_1 m_2}} \quad \text{3.25 eq}$$

There are two solutions depending on the sign.

Acoustic or Low frequencies

$$\omega^2 = K\left[\frac{1}{m_1} + \frac{1}{m_2}\right] - K\sqrt{\left[\frac{1}{m_1} + \frac{1}{m_2}\right]^2 - \frac{4\sin^2 \boldsymbol{k}a}{m_1 m_2}} \quad \text{3.26 eq}$$

Optical or High frequencies

$$\omega^2 = K\left[\frac{1}{m_1} + \frac{1}{m_2}\right] + K\sqrt{\left[\frac{1}{m_1} + \frac{1}{m_2}\right]^2 - \frac{4\sin^2 \boldsymbol{k}a}{m_1 m_2}} \quad \text{3.27 eq}$$

Assuming for example the following values for illustration: a = 0.01m (10mm), K=0.001 N/m (1N/mm), m1 = 0.1 kg and m2=0.2 kg

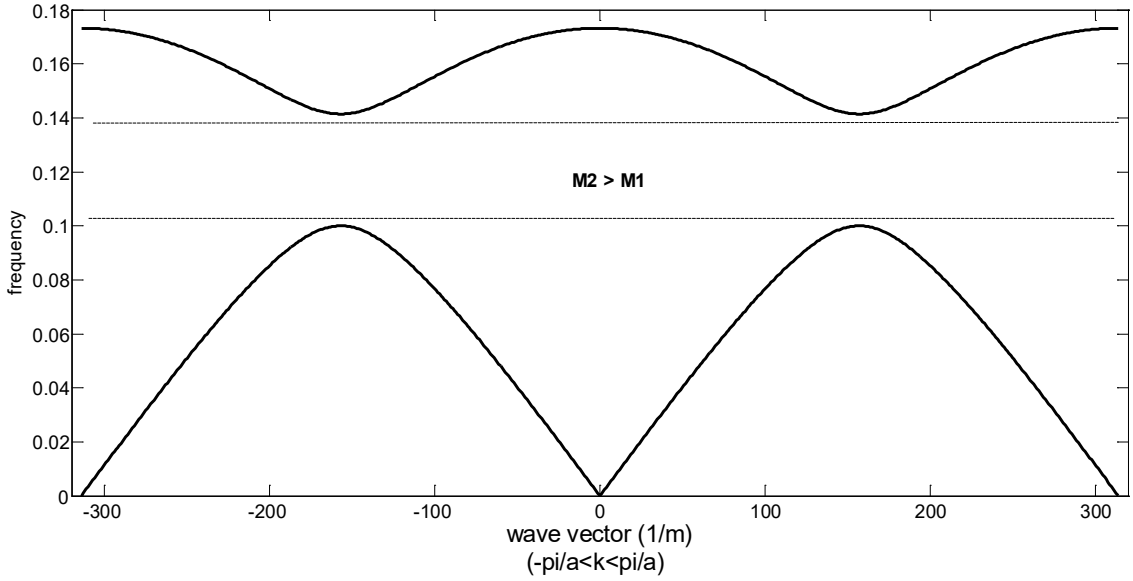

Figure 3.4 Frequency vs wave vector figure for double-mass lattice

As shown in Figure 3.4, a frequency band gap arises for the double mass model due to the difference in the two masses. The width of this gap also depends on the difference between the two masses. This analogy is used in phononic crystals where the contrast in densities and elastic properties of materials is critical.

Normalized Amplitudes:

Calculating the amplitude and phases of the two masses vibrating at a certain frequency gives,

$$(2K - m_1\omega^2)A_1 - (2K\cos(\boldsymbol{k}a))\,A_2 = 0 \qquad \text{3.28 eq}$$

$$\frac{A_1}{A_2} = \frac{(2K\cos(\boldsymbol{k}a))}{(2K - m_1\omega^2)} \qquad \text{3.29 eq}$$

$$-(2K\cos(\boldsymbol{k}a))\,A_1 + (2K - m_2\omega^2)A_2 = 0 \qquad \text{3.30 eq}$$

$$\frac{A_1}{A_2} = \frac{(2K - m_2\omega^2)}{(2K\cos(\boldsymbol{k}a))} \qquad \text{3.31 eq}$$

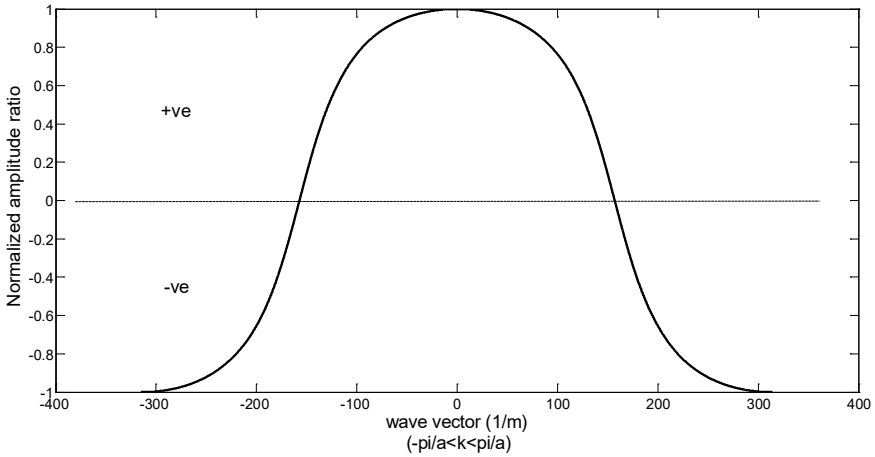

Figure 3.5 Amplitude ratio of the two masses for low frequencies

As seen from Figure 3.5, the amplitude ratio for the two masses are positive and negative from 0 to pi/a, a positive ratio would mean the two masses move in phase with respect to each other and a negative ratio would mean the two masses move out of phase w.r.t each other. The wave could either be a right or left traveling wave. Understanding of mode shapes is critical to predict the behavior of phononic crystals under external excitation. This figure gives an insight into modes present in a periodic material.

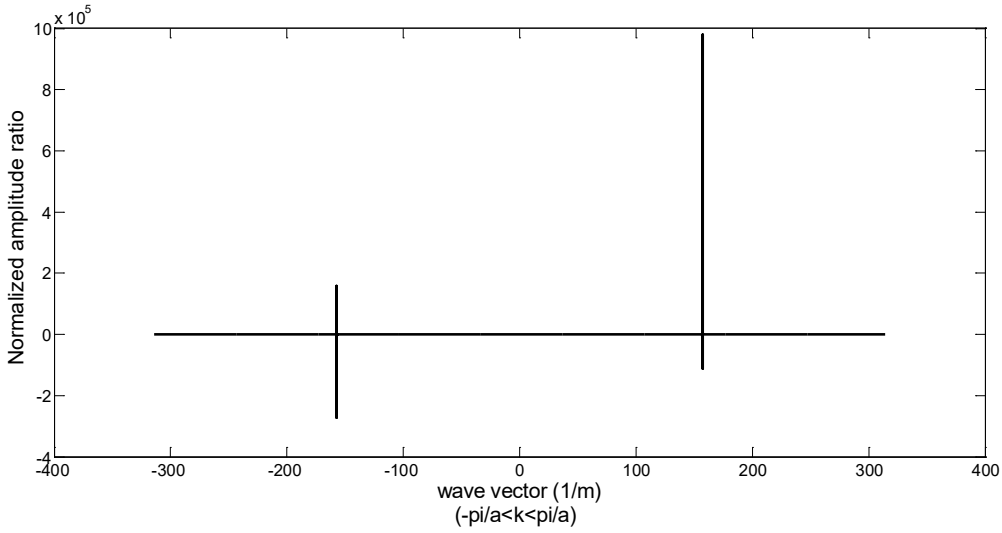

Figure 3.6 Amplitude ratio for the two masses for high frequencies

As seen from Figure 3.6, the amplitude ratio for the two masses are zero from 0 to +/- pi/a, meaning the two masses move out of phase with respect to each other representing a

standing wave. The equations used in Section 3.2 and 3.3 are clearly presented in the text book “Solid State physics by Charles Kittel[43]”.

3.4 WAVE PROPAGATION IN 1D MEDIUM

In this section the dispersion relation[10] for the 1D layered periodic PhnC is derived using the theory of elasticity. First the 1D wave propagation equations for longitudinal and transverse wave types are derived and a displacement solution accounting for backward and forward moving waves is assumed. This assumption accounts for wave transmission and reflection occurring in the PhnC. The displacement and stress boundary conditions at the interface are applied along with the Floquet periodic boundary conditions for the unit cell. The dispersion relation for the periodic PhnC is derived by substituting the displacement solution in the interfacial and periodic boundary conditions. Later, the band gap for an actual Epoxy-CNT PhnC is calculated by the derived dispersion relation. The equations used in Section 3.4 are clearly presented in the text book “Introduction to elastic wave propagation by A. Bedford[44]”.

Consider the following unit cell with layers A and B as shown in Figure 3.7.

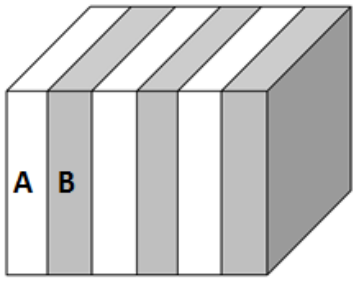

Figure 3.7 1D Phononic crystal

$$h1 = thickness\ of\ layer\ A$$

$$h2 = thicknesss\ of layer\ B$$

For longitudinal waves propagating in A, $\frac{\partial^2 u_a}{\partial t^2} = {C_{la}}^2 \frac{\partial^2 u_a}{\partial x^2}$ where $C_{la} = \left(\frac{\lambda_a + 2\mu_a}{\rho a}\right)^{\frac{1}{2}}$

For longitudinal waves propagating in B, $\frac{\partial^2 u_b}{\partial t^2} = {C_{lb}}^2 \frac{\partial^2 u_b}{\partial x^2}$ where $C_{lb} = \left(\frac{\lambda_b + 2\mu_b}{\rho b}\right)^{\frac{1}{2}}$

For transverse waves propagating in A, $\frac{\partial^2 u_a}{\partial t^2} = {C_{ta}}^2 \frac{\partial^2 u_a}{\partial x^2}$ where $C_{ta} = \left(\frac{1}{\mu_a}\right)^{\frac{1}{2}}$

For transverse waves propagating in B, $\frac{\partial^2 u_b}{\partial t^2} = {C_{tb}}^2 \frac{\partial^2 u_b}{\partial x^2}$ where $C_{tb} = \left(\frac{1}{\mu_b}\right)^{\frac{1}{2}}$

Where a general solution is given by,

$$u_a(x,t) = A_a e^{i(\boldsymbol{k_a} x - \omega t)} + B_a e^{i(-\boldsymbol{k_a} x - \omega t)} \quad \text{3.32 eq}$$

$$u_b(x,t) = A_b e^{i(\boldsymbol{k_b} x - \omega t)} + B_b e^{i(-\boldsymbol{k_b} x - \omega t)} \quad \text{3.33 eq}$$

The displacement at the interface is equal for the two adjoining layers,

$$u_a(h1,t) = u_b(0,t) \quad \text{3.34 eq}$$

Substituting gives,

$$A_a e^{i(\boldsymbol{k_a} h1 - \omega t)} + B_a e^{i(-\boldsymbol{k_a} h1 - \omega t)} = A_b e^{i(\boldsymbol{k_b} 0 - \omega t)} + B_b e^{i(-\boldsymbol{k_b} 0 - \omega t)}$$

$$A_a e^{i(\boldsymbol{k_a} h1 - \omega t)} + B_a e^{i(-\boldsymbol{k_a} h1 - \omega t)} = A_b e^{i(-\omega t)} + B_b e^{i(-\omega t)}$$

$$A_a e^{i(\boldsymbol{k_a} h1)} + B_a e^{i(-\boldsymbol{k_a} h1)} = A_b + B_b$$

$$A_a e^{i(\boldsymbol{k_a} h1)} + B_a e^{i(-\boldsymbol{k_a} h1)} - A_b - B_b = 0$$

The stress at the interface is equal for the two layers,

$$\sigma_{12_a}(h1,t) = \sigma_{12_b}(0,t) \quad \text{3.35 eq}$$

The normal stress is given by,

$$\sigma_{11_a} = \left(\frac{1}{\lambda_a + 2\mu_a}\right) \frac{\partial u_a}{\partial x}$$

$$\sigma_{11_b} = \left(\frac{1}{\lambda_b + 2\mu_b}\right)\frac{\partial u_b}{\partial x}$$

The shear stress is given by,

$$\sigma_{12_a} = \mu_a \frac{\partial u_a}{\partial x}$$

$$\sigma_{12_b} = \mu_b \frac{\partial u_b}{\partial x}$$

$$\sigma_{12_a}(h1, t) = \sigma_{12_b}(0, t)$$

$$\mu_a\left(A_a i\boldsymbol{k_a} e^{i(\boldsymbol{k_a}h1-\omega t)} + B_a i\boldsymbol{k_a} e^{i(-\boldsymbol{k_a}h1-\omega t)}\right) = \mu_b\left(A_b i\boldsymbol{k_b} e^{i(\boldsymbol{k_b}0-\omega t)} + B_b i\boldsymbol{k_b} e^{i(-\boldsymbol{k_b}0-\omega t)}\right)$$

$$\mu_a\left(A_a i\boldsymbol{k_a} e^{i(\boldsymbol{k_a}h1-\omega t)} + B_a i\boldsymbol{k_a} e^{i(-\boldsymbol{k_a}h1-\omega t)}\right) = \mu_b\left(A_b i\boldsymbol{k_b} e^{i(-\omega t)} + B_b i\boldsymbol{k_b} e^{i(-\omega t)}\right)$$

$$\mu_a\left(A_a i\boldsymbol{k_a} e^{i(\boldsymbol{k_a}h1)} + B_a i\boldsymbol{k_a} e^{i(-\boldsymbol{k_a}h1)}\right) = \mu_b(A_b i\boldsymbol{k_b} + B_b i\boldsymbol{k_b})$$

$$\mu_a A_a\boldsymbol{k_a} e^{i(\boldsymbol{k_a}h1)} + \mu_a B_a\boldsymbol{k_a} e^{i(-\boldsymbol{k_a}h1)} - \mu_b A_b\boldsymbol{k_b} - B_b\boldsymbol{k_b} = 0$$

From Bloch-Flouqet Theorem,

$$u_a(x, t) = A_a e^{i(\boldsymbol{k_a}\boldsymbol{x}-\omega t)} + B_a e^{i(-\boldsymbol{k_a}\boldsymbol{x}-\omega t)}$$

$$u_a(x, t) = \left(A_a e^{i(\boldsymbol{k_a}\boldsymbol{x}-\boldsymbol{k}\boldsymbol{x})} + B_a e^{i(-\boldsymbol{k_a}\boldsymbol{x}-kx)}\right)e^{i(\boldsymbol{k}\boldsymbol{x}-\omega t)}$$

$$u_a(x, t) = (U_a)e^{i(\boldsymbol{k}\boldsymbol{x}-\omega t)}$$

Where $U_a = A_a e^{i(\boldsymbol{k_a}\boldsymbol{x}-\boldsymbol{k}\boldsymbol{x})} + B_a e^{i(-\boldsymbol{k_a}\boldsymbol{x}-kx)}$

Similarly,

$$u_b(x, t) = \left(A_b e^{i(\boldsymbol{k_b}\boldsymbol{x}-\boldsymbol{k}\boldsymbol{x})} + B_b e^{i(-\boldsymbol{k_b}\boldsymbol{x}-\boldsymbol{k}\boldsymbol{x})}\right)e^{i(\boldsymbol{k}\boldsymbol{x}-\omega t)}$$

$$u_b(x, t) = (U_b(x))e^{i(\boldsymbol{k}\boldsymbol{x}-\omega t)}$$

Where $U_b(x) = A_b e^{i(\boldsymbol{k_b}\boldsymbol{x}-\boldsymbol{k}\boldsymbol{x})} + B_b e^{i(-\boldsymbol{k_b}\boldsymbol{x}-\boldsymbol{k}\boldsymbol{x})}$

$$U_a(0) = U_b(h2)$$

$$A_a e^{i(\boldsymbol{k_a}0-\boldsymbol{k}0)} + B_a e^{i(-\boldsymbol{k_a}0-\boldsymbol{k}0)} = A_b e^{i(\boldsymbol{k_b}h2-\boldsymbol{k}h2)} + B_b e^{i(-\boldsymbol{k_b}h2-\boldsymbol{k}h2)}$$

$$A_a + B_a = A_b e^{i(\boldsymbol{k_b}h2-\boldsymbol{k}h2)} + B_b e^{i(-\boldsymbol{k_b}h2-\boldsymbol{k}h2)}$$

$$A_a + B_a - A_b e^{i(\boldsymbol{k_b}h2-\boldsymbol{k}h2)} - B_b e^{i(-\boldsymbol{k_b}h2-\boldsymbol{k}h2)} = 0$$

From Bloch-Flouqet Theorem

$$\sigma_{12_a}(x,t) = \mu_a\left(A_a i\boldsymbol{k_a} e^{i(\boldsymbol{k_a}x-\omega t)} + B_a i\boldsymbol{k_a} e^{i(-\boldsymbol{k_a}x-\omega t)}\right)$$

$$\sigma_{12_a}(x,t) = \mu_a\left(A_a i\boldsymbol{k_a} e^{i(\boldsymbol{k_a}x-\boldsymbol{k}x)} + B_a i\boldsymbol{k_a} e^{i(-\boldsymbol{k_a}x-\boldsymbol{k}x)}\right) e^{i(\boldsymbol{k}x-\omega t)}$$

$$\sigma_{12_a}(x,t) = T_{12_a} e^{i(\boldsymbol{k}x-\omega t)}$$

$$T_{12_a} = \mu_a\left(A_a i\boldsymbol{k_a} e^{i(\boldsymbol{k_a}x-\boldsymbol{k}x)} + B_a i\boldsymbol{k_a} e^{i(-\boldsymbol{k_a}x-\boldsymbol{k}x)}\right)$$

Similarly,

$$\sigma_{12_b}(x,t) = \mu_b\left(A_b i\boldsymbol{k_b} e^{i(\boldsymbol{k_b}x-\boldsymbol{k}x)} + B_b i\boldsymbol{k_b} e^{i(-\boldsymbol{k_b}x-\boldsymbol{k}x)}\right) e^{i(\boldsymbol{k}x-\omega t)}$$

$$T_{12_b} = \mu_b\left(A_b i\boldsymbol{k_b} e^{i(\boldsymbol{k_b}x-\boldsymbol{k}x)} + B_b i\boldsymbol{k_b} e^{i(-\boldsymbol{k_b}x-\boldsymbol{k}x)}\right)$$

$$T_{12_a}(0) = T_{12_b}(h2)$$

$$\mu_a\left(A_a i\boldsymbol{k_a} e^{i(\boldsymbol{k_a}0-\boldsymbol{k}0)} + B_a i\boldsymbol{k_a} e^{i(-\boldsymbol{k_a}0-\boldsymbol{k}0)}\right) = \mu_b\left(A_b i\boldsymbol{k_b} e^{i(\boldsymbol{k_b}h2-\boldsymbol{k}h2)} + B_b i\boldsymbol{k_b} e^{i(-\boldsymbol{k_b}h2-\boldsymbol{k}h2)}\right)$$

$$\mu_a(A_a i\boldsymbol{k_a} + B_a i\boldsymbol{k_a}) = \mu_b\left(A_b i\boldsymbol{k_b} e^{i(\boldsymbol{k_b}h2-\boldsymbol{k}h2)} + B_b i\boldsymbol{k_b} e^{i(-\boldsymbol{k_b}h2-\boldsymbol{k}h2)}\right)$$

$$\mu_a A_a\boldsymbol{k_a} + \mu_a B_a\boldsymbol{k_a} - \mu_b A_b\boldsymbol{k_b} e^{i(\boldsymbol{k_b}h2-\boldsymbol{k}h2)} - \mu_b B_b\boldsymbol{k_b} e^{i(-\boldsymbol{k_b}h2-\boldsymbol{k}h2)} = 0$$

Grouping equations,

$$A_a e^{i(\boldsymbol{k_a}h1)} + B_a e^{i(-\boldsymbol{k_a}h1)} - A_b - B_b = 0$$

$$\mu_a A_a\boldsymbol{k_a} e^{i(\boldsymbol{k_a}h1)} + \mu_a B_a\boldsymbol{k_a} e^{i(-\boldsymbol{k_a}h1)} - \mu_b A_b\boldsymbol{k_b} - \mu_b B_b\boldsymbol{k_b} = 0$$

$$A_a + B_a - A_b e^{i(\boldsymbol{k_b}h2-\boldsymbol{k}h2)} - B_b e^{i(-\boldsymbol{k_b}h2-\boldsymbol{k}h2)} = 0$$

$$\mu_a A_a \boldsymbol{k_a} + \mu_a B_a \boldsymbol{k_a} - \mu_b A_b \boldsymbol{k_b} e^{i(\boldsymbol{k_b} h2 - \boldsymbol{k} h2)} - \mu_b B_b \boldsymbol{k_b} e^{i(-\boldsymbol{k_b} h2 - \boldsymbol{k} h2)} = 0$$

$$\begin{bmatrix} e^{i(\boldsymbol{k_a} h1)} & e^{i(-\boldsymbol{k_a} h1)} & -1 & -1 \\ \mu_a \boldsymbol{k_a} e^{i(\boldsymbol{k_a} h1)} & \mu_a \boldsymbol{k_a} e^{i(-\boldsymbol{k_a} h1)} & -\mu_b \boldsymbol{k_b} & -\mu_b \boldsymbol{k_b} \\ 1 & 1 & -e^{i(\boldsymbol{k_b} h2 - \boldsymbol{k} h2)} & -e^{i(-\boldsymbol{k_b} h2 - \boldsymbol{k} h2)} \\ \mu_a \boldsymbol{k_a} & \mu_{a\boldsymbol{k_a}} & -\mu_b \boldsymbol{k_b} e^{i(\boldsymbol{k_b} h2 - \boldsymbol{k} h2)} & -\mu_b \boldsymbol{k_b} e^{i(-\boldsymbol{k_b} h2 - \boldsymbol{k} h2)} \end{bmatrix} \begin{bmatrix} A_a \\ B_a \\ A_b \\ B_b \end{bmatrix} = \begin{bmatrix} 0 \\ 0 \\ 0 \\ 0 \end{bmatrix}$$

The dispersion relation for longitudinal waves is,

$$\cos(k.h) = \cos\left(\frac{\omega h1}{C_{la}}\right)\cos\left(\frac{\omega h2}{C_{lb}}\right) - \frac{1}{2}\left(\frac{\rho_a C_{la}}{\rho_b C_{lb}} + \frac{\rho_b C_{lb}}{\rho_a C_{la}}\right)\sin\left(\frac{\omega h1}{C_{la}}\right)\sin\left(\frac{\omega h2}{C_{lb}}\right) \quad \text{3.36 eq}$$

The dispersion relation for transverse waves is,

$$\cos(k.h) = \cos\left(\frac{\omega h1}{C_{ta}}\right)\cos\left(\frac{\omega h2}{C_{tb}}\right) - \frac{1}{2}\left(\frac{\rho_a C_{ta}}{\rho_b C_{tb}} + \frac{\rho_b C_{tb}}{\rho_a C_{ta}}\right)\sin\left(\frac{\omega h1}{C_{ta}}\right)\sin\left(\frac{\omega h2}{C_{tb}}\right) \quad \text{3.37 eq}$$

3.5 BAND GAP CALCULATION FOR A 1D EPOXY-CNT PHONONIC CRYSTAL

In this section the frequency band gap calculations for an hypothesized Epoxy-CNT PhnC shown in Figure 3.8 are calculated using the derived dispersion relation of 3.38 eq. It is understood that the composite with such extreme properties is not physically realizable, but is presented to illustrate how the method can be used to analyze composites with very large property mismatch and impedance mismatch.

$$\cos(k.h) = \cos\left(\frac{\omega h1}{C_{la}}\right)\cos\left(\frac{\omega h2}{C_{lb}}\right) - \frac{1}{2}\left(\frac{\rho_a C_{la}}{\rho_b C_{lb}} + \frac{\rho_b C_{lb}}{\rho_a C_{la}}\right)\sin\left(\frac{\omega h1}{C_{la}}\right)\sin\left(\frac{\omega h2}{C_{lb}}\right)$$

For band gap calculations, this problems is split into three parts, First, is calculating the Left Hand Side (LHS) of the dispersion relation values for all possible **k** wave vectors. Second, is calculating the Right Hand Side (RHS) of the dispersion relation for all the

possible frequency values. Third, is selecting the set of frequency values that actually satisfy the LHS of the dispersion relation from the RHS. Using this condition, the frequency band gaps for the transverse and longitudinal wave types are calculated. A Matlab code was written to acheive results for the geometry shown in Figure 3.8. Matlab generated figures are shown as part of the solution process.

Figure 3.8 Geometry of the Epoxy-CNT PhnC

The thickness of each layer is 10mm and unit cell is 20mm.

Table 3.1 Material properties

	E (Gpa)	ρ(kg/m3)	ν
Epoxy	7.4	1142	0.35
CNT	1000	2000	0.30

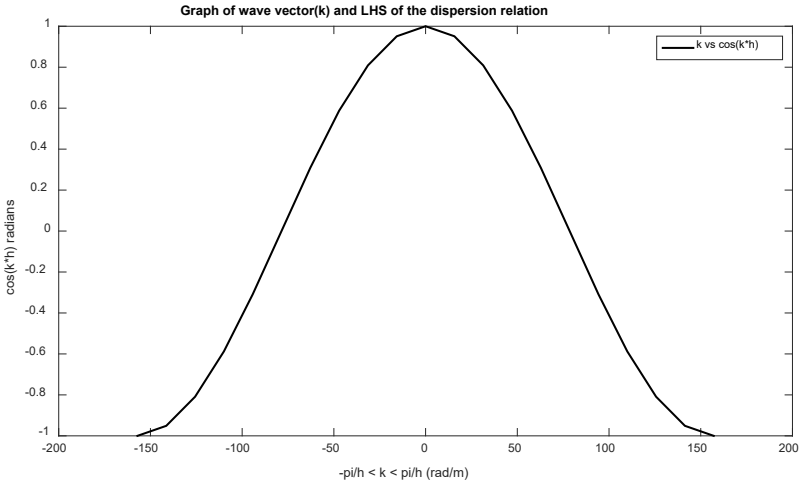

Figure 3.9 Wave vector vs Left Hand Side of the dispersion relation

As can be seen from Figure 3.9, the solution for the LHS of the dispersion relation i.e $\cos(k.h)$ spans from 1 to -1. This condition is checked for the RHS of the dispersion relation in the following figures.

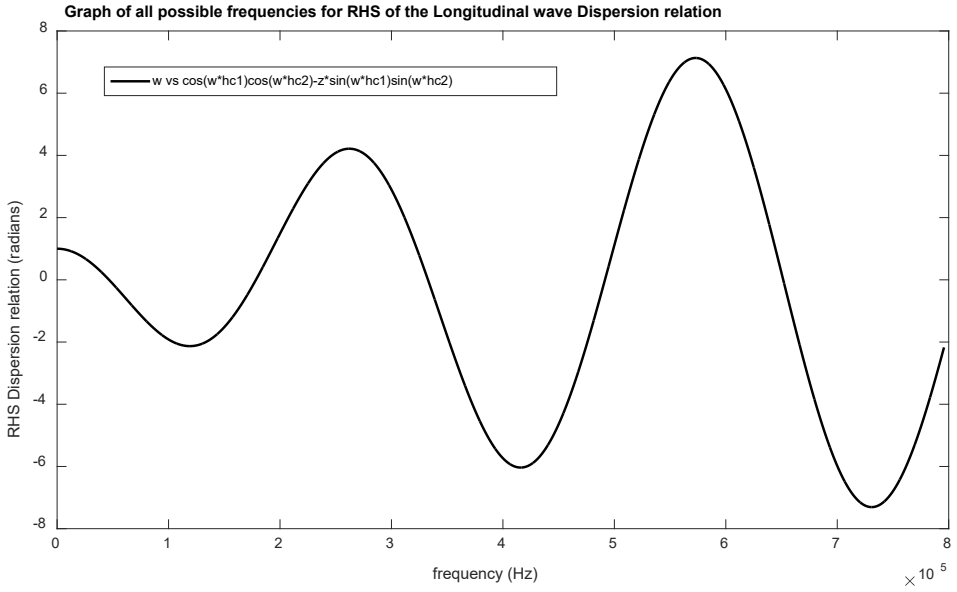

Figure 3.10 Figure of all possible frequencies satisfying the Right Hand Side of Longitudinal wave dispersion relation. (Note that values are x10^5)

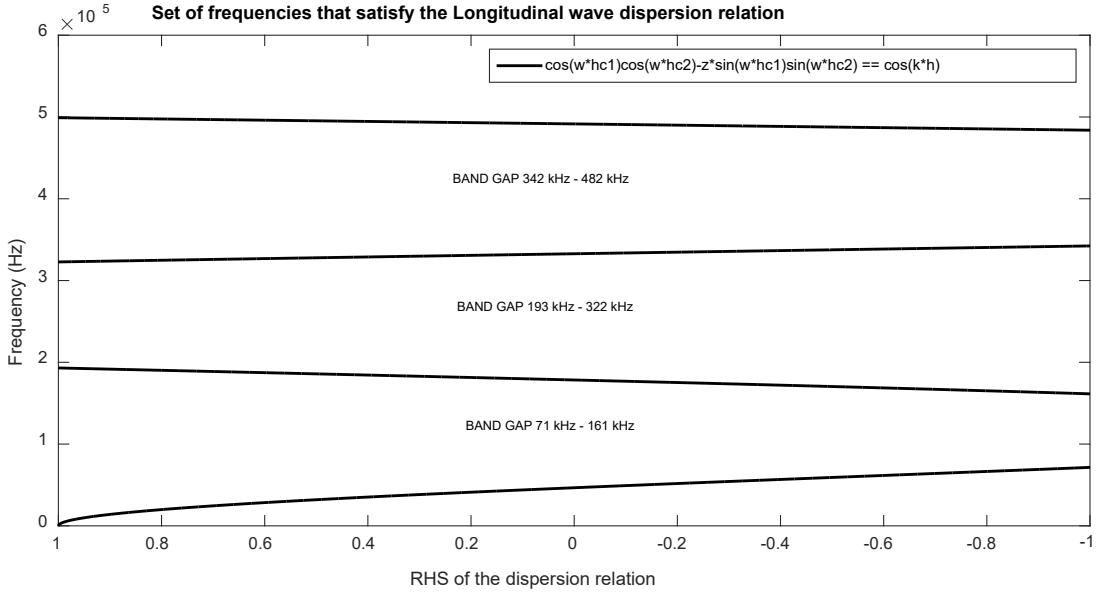

Figure 3.11 Set of frequencies that satisfy the longitudinal dispersion relation (frequency is x10^5)

As seen from Figure 3.10 , The solutions for RHS of the dispersion solution range within the limits of 8 to -8 radians . However, from this figure only the values ranging from 1 to -1 radians actually sastisfy the dispersion relation.The Figure 3.11 shows the range of frequencies that actually satisfy the dispersion relation.

As seen from the Figure 3.11, the frequency band gaps for the longitudinal wave type range from 71kHz – 161 kHz, 193 kHz-322 kHz and 342 kHz-482 kHz, etc. Longitudinal waves propagating within these frequencies are completely blocked by the Epoxy-CNT Phononic crystal. It can be further concluded that this crystal can block most of the frequencies lying in the ultrasonic range. This crystal can be used effectively for ultrasonic wave attenuation applications.

The transverse wave frequency band gaps are computed in the same way and the following figures show that the same solution process is followed to ensure that the transverse wave dispersion relation is satisfied. If any set of frequencies tend to fall in both the longitudinal and transverse band gaps, the PhnC would present a complete band gap reflecting both wave types. Therefore, a full band gap must be checked to build an effective vibration attenuator.

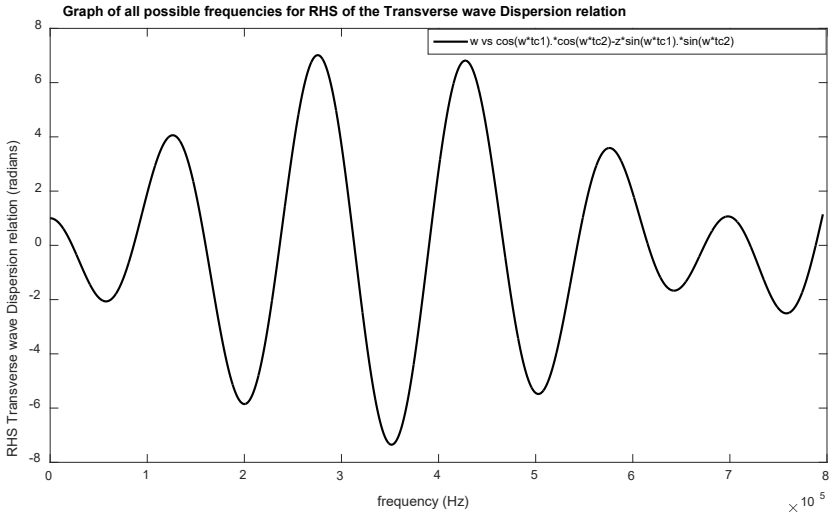

Figure 3.12 Set of all possible frequencies for RHS of Transverse wave dispersion relation (frequency is x10^5)

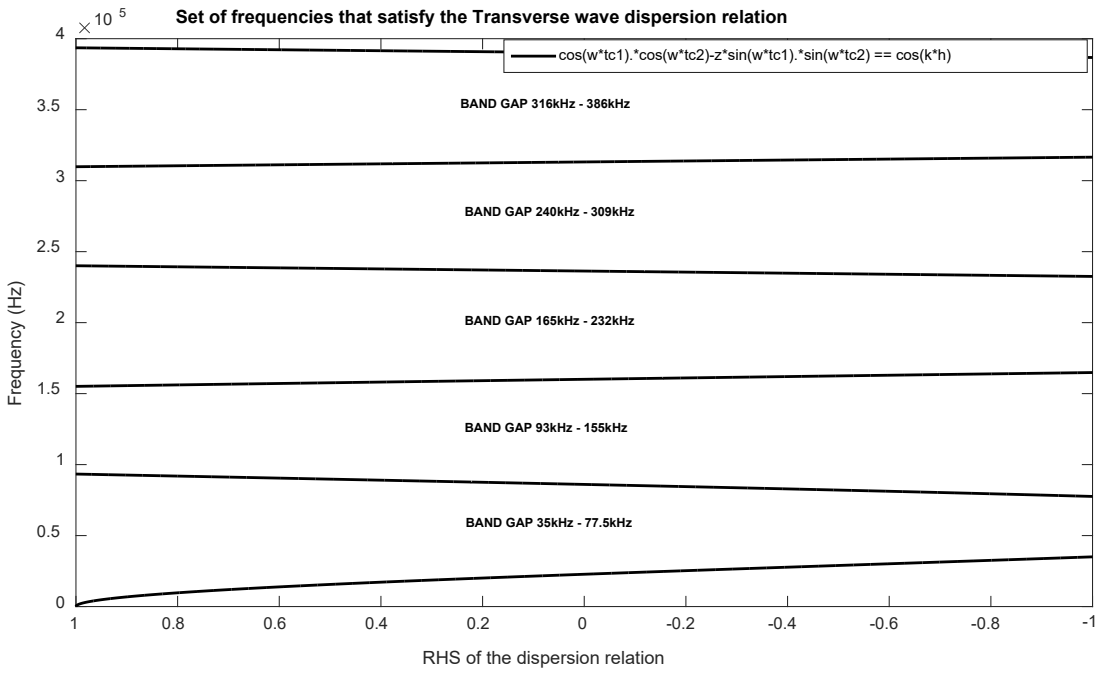

Figure 3.13 Set of frequencies that satisfy the Transverse wave dispersion relation

As seen from Figures 3.12 and 3.13, the frequency band gaps for the transverse wave range from 35kHz – 77.5 kHz, 93 kHz-155 kHz, 165 kHz- 232 kHz, 240kHz – 309kHz and 316kHz-386kHz, etc. Transverse waves propagating within these frequencies are completely blocked by the Epoxy-CNT Phononic crystal. It can be further concluded that this crystal can block most of the transverse wave frequencies within the ultrasonic range. This crystal can be used effectively for ultrasonic wave attenuation applications. However, only the overlapping frequencies from the longitudinal and transverse wave types can be concluded to be full a band gap. As can be seen from the figures, there are multiple ranges of frequencies that are common to the transverse and longitudinal band gaps. Therefore Epoxy-CNT crystals can act as wave reflectors for a large ultrasonic frequency range.

The band structure figures are further correlated with the frequency response and stress attenuation analysis using ABAQUS finite element code. The amplitude drops in frequency response analysis are correlated with band structure figures and a wave attenuation analysis is performed to study the attenuation properties. Also, ultrasonic frequency wave guides and vibration absorbers are designed and analyzed as part of the study for building suitable ultrasonic applications.

3.6 FREQUENCY RESPONSE ANALYSIS USING ABAQUS FINITE ELEMENT CODE

In this section the frequency response of a 1D Epoxy-CNT Phononic crystal is calculated using ABAQUS finite element explicit code. The PhnC of length 100 mm, with 5 alternating epoxy and 5 CNT layers is considered for the FEM analysis. The thickness of each layer is 10mm and the unit cell length is 20mm. The top and bottom edges of the FEM model are constrained in the Y direction in order to prevent the PhnC from moving up and down. A 1-micron displacement input in the longitudinal and transverse direction for a frequency range of 0 kHz to 400 kHz is applied at the left edge. The displacement at the right edge is measured in dB-scale in order to measure the relative response attenuation in the frequency range. CPE4R Plane strain quadrilateral elements are used to calculate the frequency response of the finite element model. A frequency sweep is performed with the specified displacement with LANCZOS Eigen matrix solver. The sampling is done at 1 kHz interval in order to better capture the dips in amplitudes. Figures 3.14 and 3.15 shows the FEM model of the 1D PhnC used for frequency response analysis.

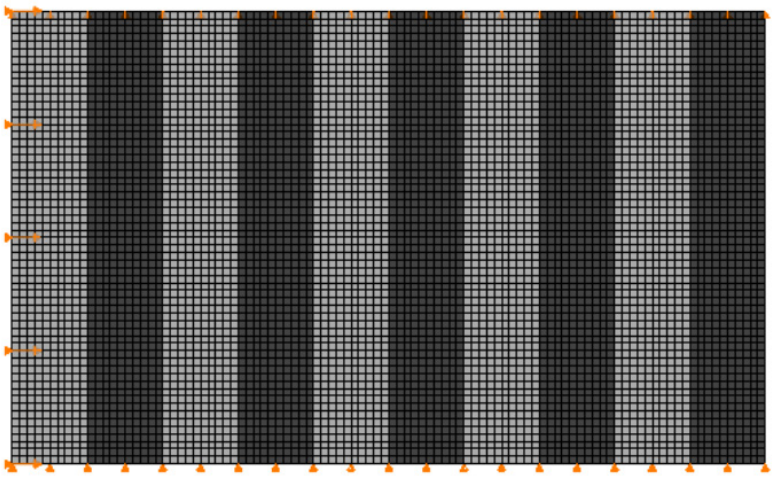

Figure 3.14 Frequency response boundary conditions for longitudinal loading

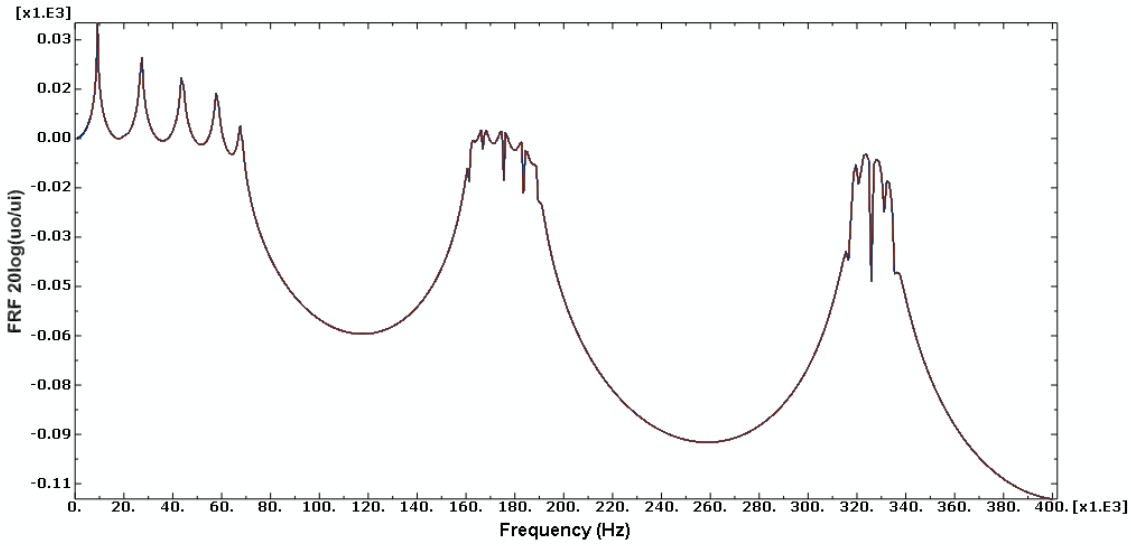

Figure 3.15 Frequency response for longitudinal loading (x10^3)

Drop in response correlates well with the calculated longitudinal wave band gaps

A 20dB log scale is used to measure the relative response at the right end of the PhnC. As seen from the frequency response figure 3.15, the response starts to drop right at calculated longitudinal band gaps of 71kHz – 161 kHz, 193 kHz-322 kHz and 342 kHz- 482 kHz. This response drop continues and reaches as low as -110dB on a 20dB log scale. This band gap data aligns well with the frequency response figures showing that a strong attenuation can be achieved by this idealized Epoxy-CNT Phononic crystal. This presents the Epoxy-CNT Phononic crystal or a similar design with large mismatch as an effective vibration absorber.

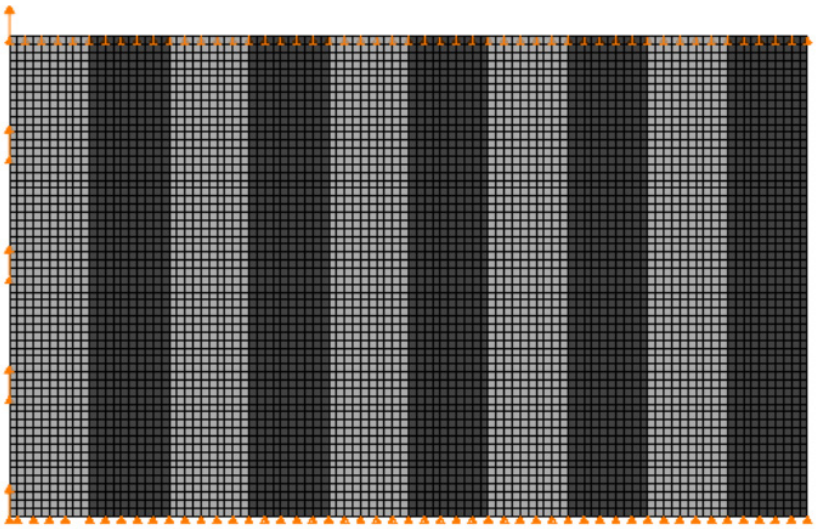

Figure 3.16 Frequency response boundary conditions for transverse loading

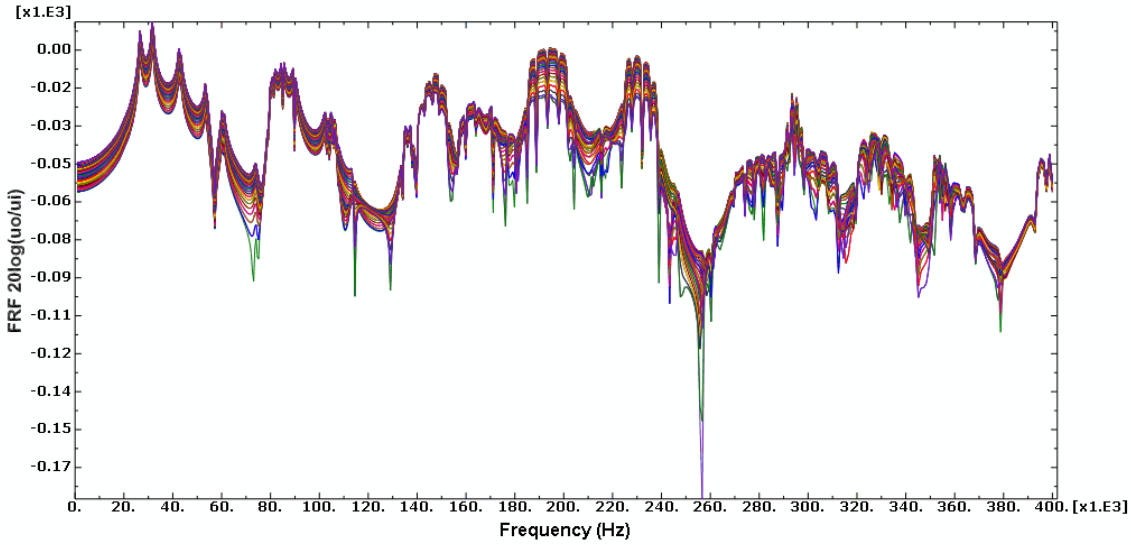

Figure 3.17 Frequency response for transverse loading (x10^3)

As seen from the frequency response figures 3.16 and 3.17, the response starts to drop right at the calculated transverse band gaps of 35kHz – 77.5 kHz, 93 kHz-155 kHz, 165 kHz-232 kHz, 240kHz – 309kHz and 316kHz-386kHz etc.This response drop continues and reaches as low as -90dB on a 20dB log scale. This band gap data aligns well with the frequency response figures showing that a strong attenuation can be achieved.

3.7 WAVE ATTENUATION ANALYSIS

In this section the wave attenuation in a 1D Epoxy-CNT PhnC is calculated using ABAQUS finite element explicit code. A 120 kHz frequency is chosen as the input, as this frequency falls in both the longitudinal and transverse band gap. The PhnC of length 100 mm, with 5 alternating epoxy and 5 CNT layers, is considered for the FEM analysis. The thickness of each layer is 10mm and the unit cell length is 20mm. The top and bottom edges of the FEM model are constrained in the Y direction in order to prevent the PhnC from moving up and down. The right edge is fixed and a 1MPa normal and transverse pressure of frequency 120 kHz is applied at the left edge. The Von Mises stress for the whole length of the PhnC is measured for stress attenuation characteristics. CPE4R plane strain quadrilateral elements are used to calculate the stress attenuation of the finite element model. The analysis is performed for 1 cycle in order to better capture the decay as the wave progresses through the PhnC. The Figure 3.18 shows the geometry of the 2D PhnC used for wave attenuation analysis.

3.7.1 Normal pressure periodic loading

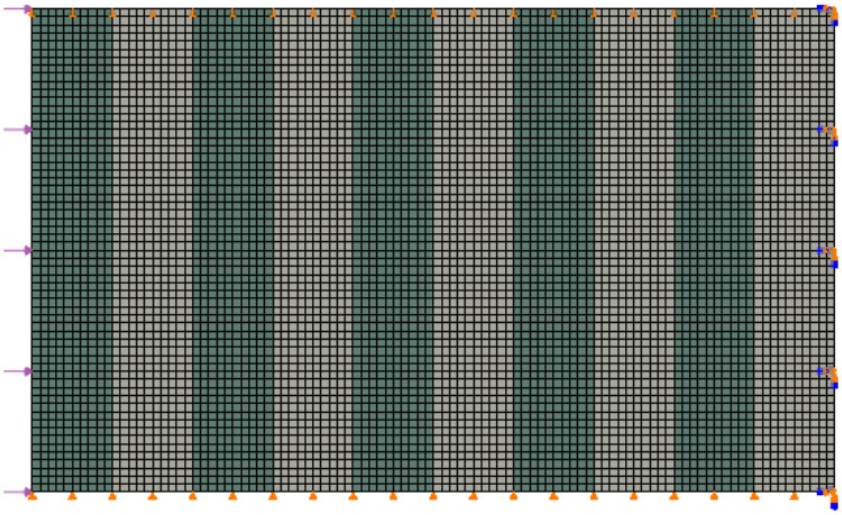

Figure 3.18. FEM model for wave attenuation analysis for normal loading

Loading: Periodic Loading of 120 KHz frequency subjected to 1MPa Longitudinal Pressure for **1** Cycle (8.333μ s)

Table 3.2 Material properties for materials

	E (GPa)	ρ(kg/m3)	ν
Epoxy	7.4	1142	0.35
CNT	1000	2000	0.30

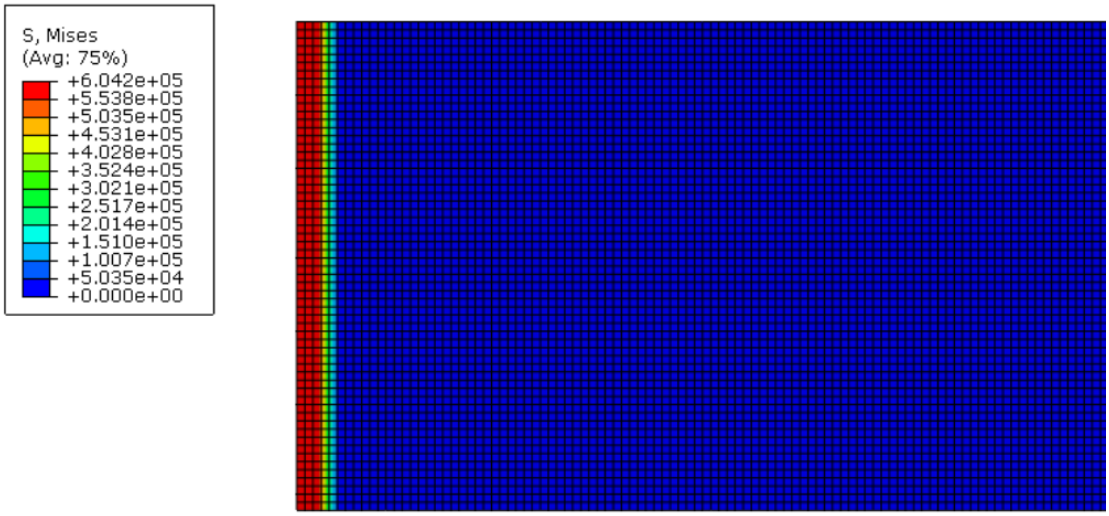

Figure 3.19 Longitudinal Stress attenuation in the PhnC (First frame of analysis, Stress is in Pa)

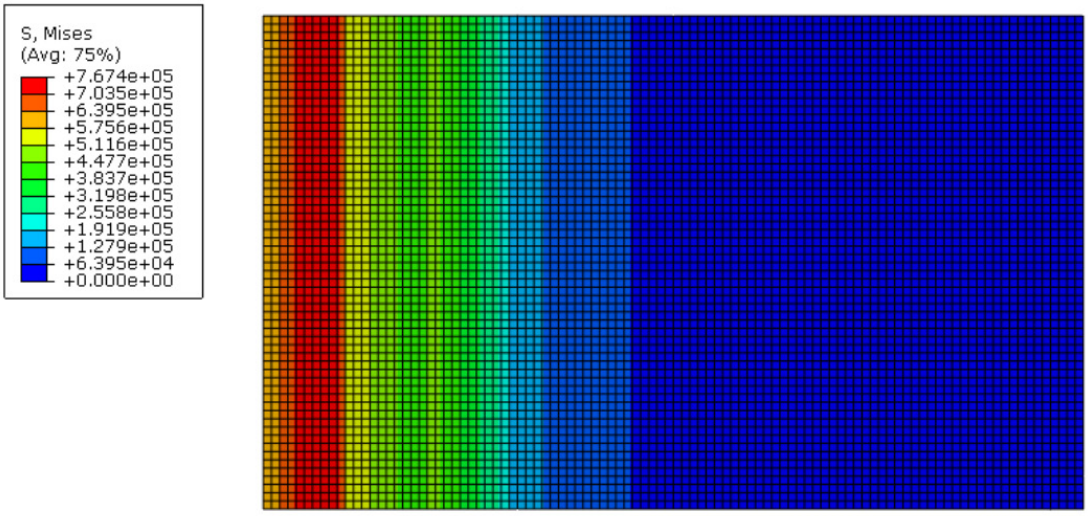

Figure 3.20 Longitudinal Stress attenuation in the PhnC (Last frame of analysis, Stress is in Pa)

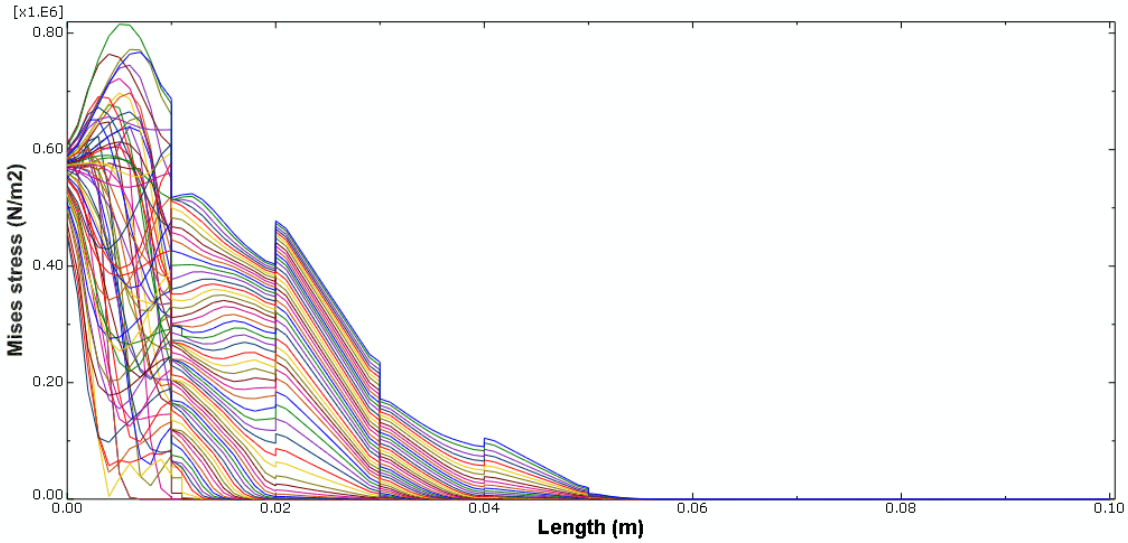

Figure 3.21 Longitudinal Stress attenuation (x10^6) in the PhnC (All frames of the analysis)

Analysis of attenuation characteristics of the PhnC are critical for sound and vibration isolation. As seen from the figures 3.19-3.21, the applied normal stress decays exponentially and correlates well with the band gap and frequency response data. Reflections from normal stress can be seen to occur at the interface between CNT and Epoxy layers. These reflections develop interfacial stresses and can lead to delamination of the PhnC. The highest interfacial stress developed is about 70% of the applied normal stress. Interfacial stresses could be even higher when the PhnC is subjected to multiple cycles of loading. Therefore, it is important that the interfacial stresses developed in the PhnC lie well below the interface bond strength. Attenuation properties of a real specimen can differ slightly since the finite element code assumes a perfect interface. Strong bonding between CNT and Epoxy layers is crucial for the performance of phononic crystals. A weak interface would delaminate and not transfer strains effectively between the layers and thereby reduce the acoustic properties. From the results, Von Mises stress is less than the amplitude of the largest input wave. Based on the results, adding more layers is suggested to attenuate the input pulse from propagating through the whole length of the composite.

Many layers ensure that the traveling wave encounters as many impedance mismatches as possible to reduce the transfer of acoustic energy. 1D Epoxy-CNT PhnCs can be used as effective acoustic mirrors and vibration absorbers in the ultrasonic range.

3.7.2 Transverse pressure periodic loading

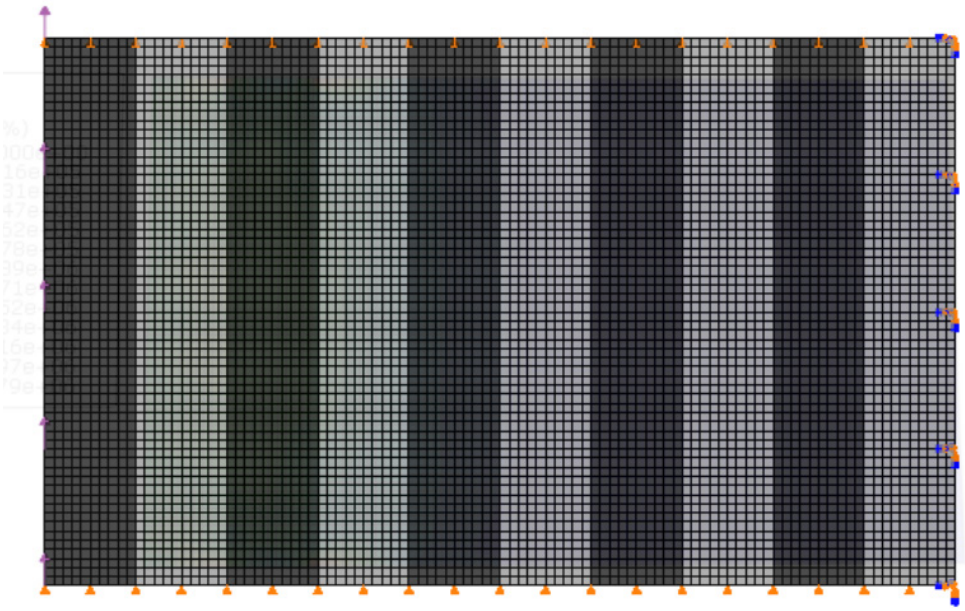

Figure 3.22 FEM model for wave attenuation analysis for transverse loading

Loading: Periodic Loading of 120 KHz frequency and 1MPa Transverse Pressure for **1** Cycle (8.333μ s)

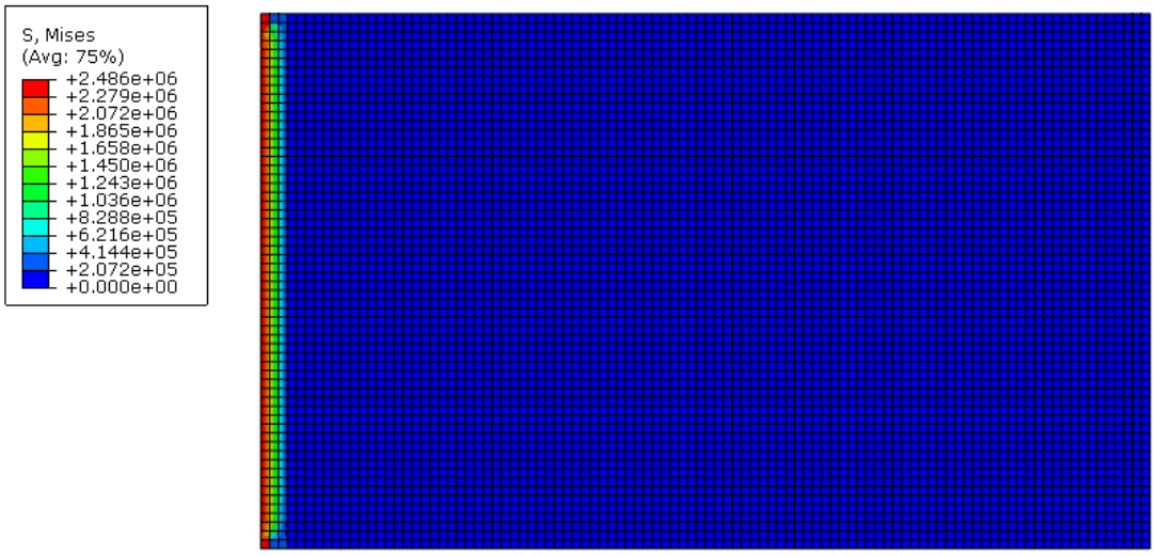

Figure 3.23 Transverse stress attenuation in the PhnC (First frame of analysis) (Stress in Pa)

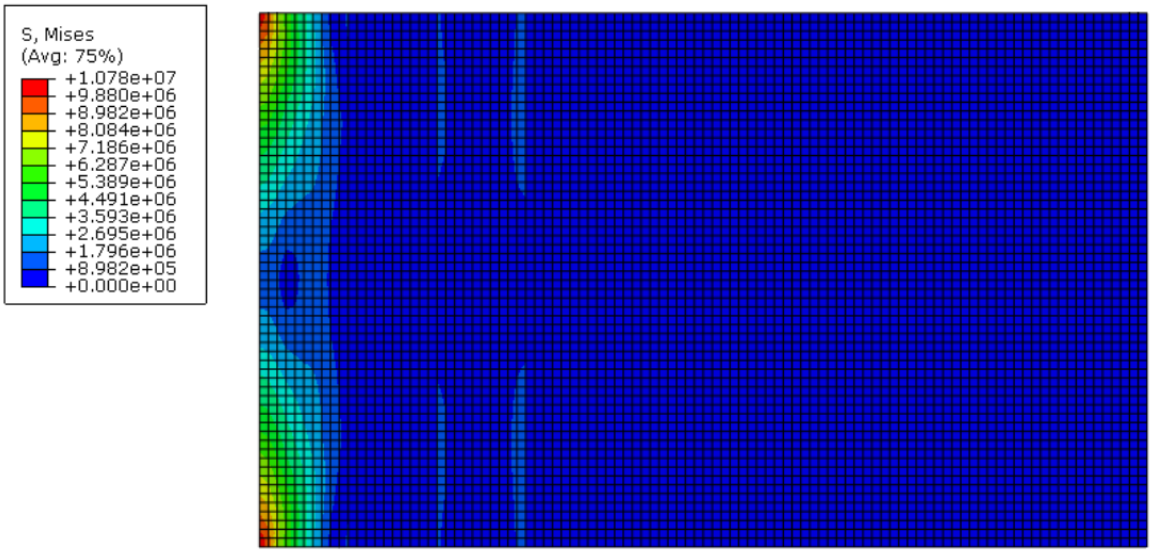

Figure 3.24 Transverse stress attenuation in the PhnC (Last frame of analysis) (Stress in Pa)

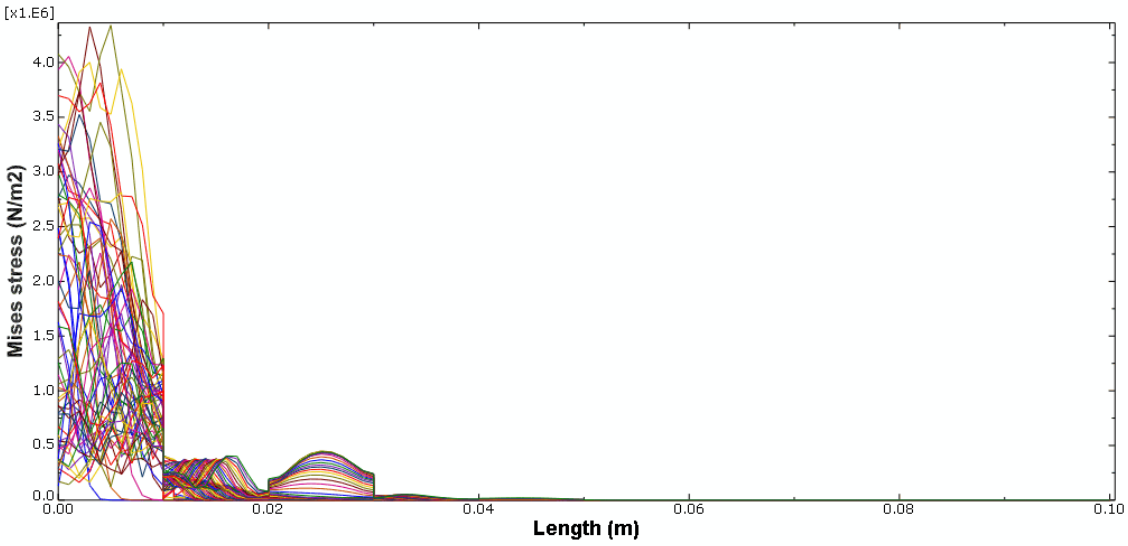

Figure 3.25 Stress attenuation for transverse loading (All frames of the analysis) (Stress is x10^6)

As seen from figure 3.25, the applied transverse stress decays exponentially as it progresses through the PhnC and correlates well with the band gap and frequency response data. It can be observed that transverse wave type attenuates more than the normal wave type. Reflections from transverse stress can be seen to occur at the interface between CNT and Epoxy layers. These reflections develop interfacial stresses and can lead to delamination of the PhnC. It is important that the interfacial stresses developed in the PhnC lie well below the bond shear strength.

3.8 CONCLUSION

As seen from the results, Epoxy-CNT Phononic crystals have potential to be used as vibration absorbers and sound attenuators in the ultrasonic frequency range. They have a very large band gap capability with multiple frequency band gaps spanning the ultrasonic frequency range. For vibration and sound isolation these PhnCs can cause a large drop in response, as low as 110dB on 20dB log scale in an idealized design. Although these results are from an idealized design, a lowering of as little as 3dB-6dB correlates with a reduction of 0.5 which for a physical system can be significant. These Phononic crystals can also be

used for stress attenuation and mitigation applications causing an exponential decay of the applied stress wave.

4 WAVE GUIDING IN NANOTUBE LAYERED MATERIALS

4.1 INTRODUCTION

Wave guides direct and steer incoming acoustic energy. They can be designed to guide energy around or away from an object in order to protect it from absorbing severe blast and shock energies. Energy can be carried away from the impact site quickly by incoroporating materials with high speed of sound . For example, these materials can be incorporated into body armors, to carry energy away from the area of impact. Incorporating these materials in soldier helmets could also guide blast energy around the helmets which could reduce the severity of the trauma injury. Military equipment and armored vehicles could also make use of these materials to dissipate energy from blasts from the impact site.

4.2 MODELING

In this section wave guiding properties of an idealized aluminum-bornon nitride nanotube layered material is studied using finite element method. The geometry of the composite considered for finite element analysis is as shown in Figure 4.1. The model is subjected to 60kHz normal pressure. The darker area represents nanotube material, the lighter area represents aluminum material and the striped area represents aluminum-boron nitride nanotube layered composite. The composite has a length of 1m and width of 0.08m. The spacing between aluminum and nanotube layers is 0.0143 m. The material properties are shown in Table 4.1.

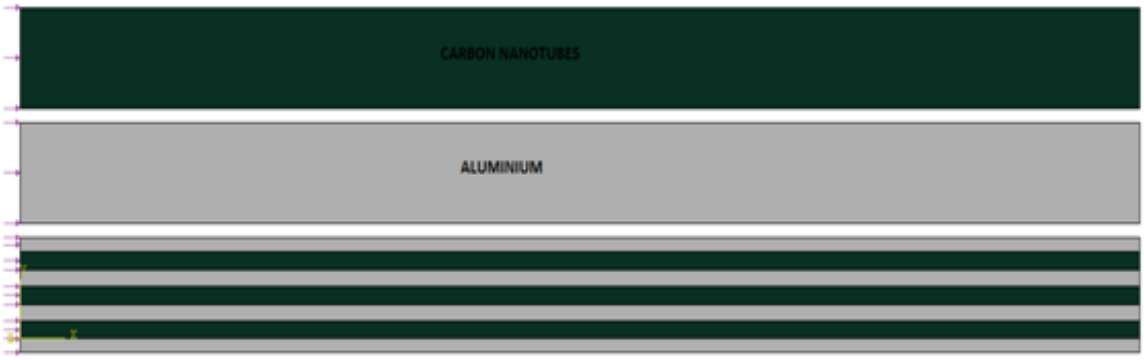

Figure 4.1 Geometry of the aluminum-bornon nitride nanotube wave guide

Table 4.1 Material Properties for the wave guide

Materials	Elastic Modulus (N/m2)	Density (kg/m3)	Poisson Ratio	Shear Modulus (N/m2)	Longitudinal sound speed (m/s)	Transverse sound speed (m/s)
Aluminum	7E+10	2700	0.3	2.632E+10	5092	3122
Nanotube	1E+12	1300	0.3	3.759E+11	27735	17005

4.3 ANALYSIS

In this section, FEA of acoustic waveguides in composite materials is presented. If acoustic waves can be confined to specific constituents in a metamaterial composite, then the direction of the acoustic wave can be controlled by the microstructure of the material. Figure 4.1 shows homogenous boron nitride nanotube yarns (process developed by NASA) and aluminum along with the corresponding composite material. Some high stiffness materials, such as boron nitride nanotubes, have high-temperature resistance and can be cast directly into aluminum. Figure 4.2 shows the results of a pressure wave applied to the left-side of the model at the moment that the pressure is applied. Figure 4.2 shows the Mises stresses after 33 microseconds (20 time steps). The high-intensity stresses can be confined to the stiffest component(s) of the composite enabling a waveguide effect.

Figure 4.2 Wave guiding - Stress wave propagation inside aluminum-boron nitride nanotubes. First of 20 time steps of 2 cycles of 60kHz normalized pressure to capture transients. Blue is lowest stress, red is highest.

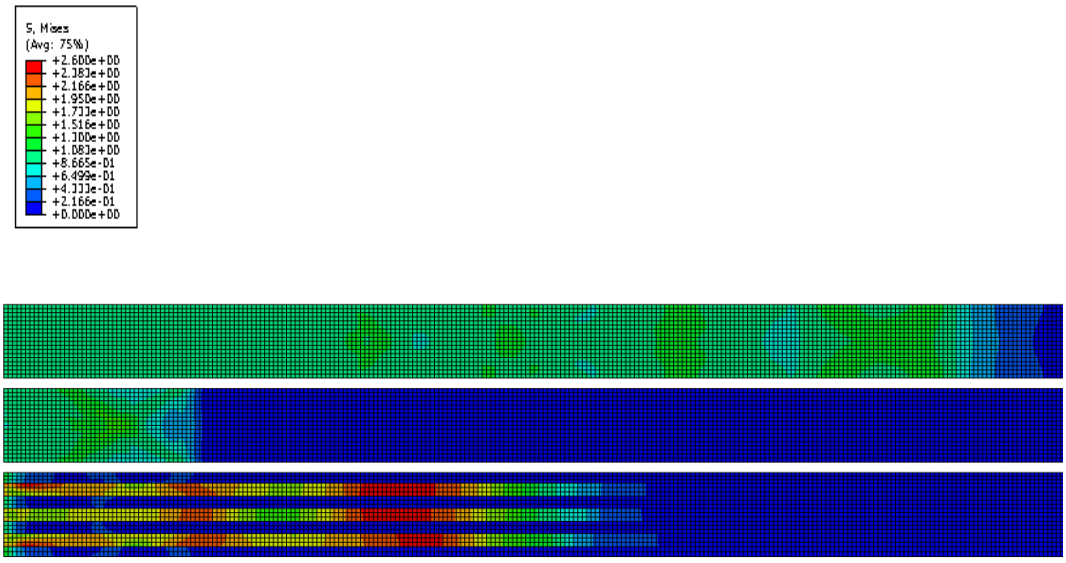

Figure 4.3 Wave guiding - Stress wave propagation inside aluminum-boron nitride nanotubes. (20th time step of 2 cycles of 60kHz normalized pressure to capture transients. Blue is lowest stress, red is highest. Bottom panel composite shows method for constraining energy to the very stiff constituent giving wave guiding effect. Total time is 33 microseconds)

Figure 4.3 shows the Mises stresses along the transverse direction of the composite strip for each of the 20 time intervals. The highest stresses are contained in the stiff inclusions and discontinuities exist at the interfaces. These models will enable the efficient design and analysis of waveguide materials and the prediction of their interfacial properties as shown in Figure 4.4.

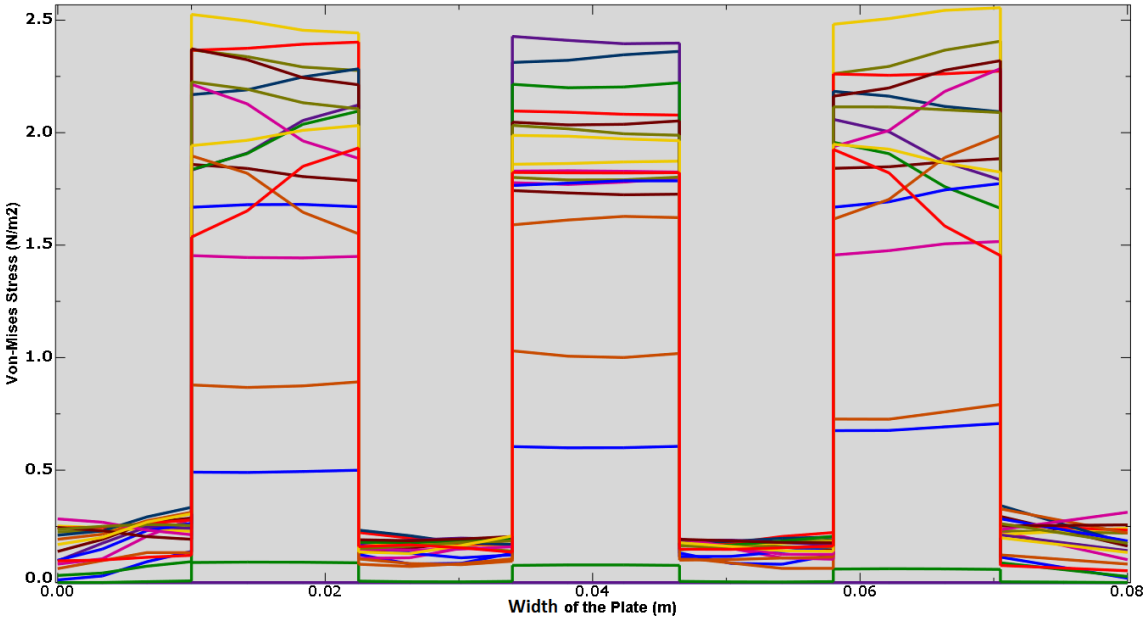

Figure 4.4 Interfacial Stresses developed in aluminum-boron nitride nanotube material

Stress measured along the width of the Composite. Vertical cross-section ~1/4 along the waveguide composite showing stress discontinuities at interfaces on both sides of the three waveguides. All 20 time steps are shown.

Analysis of wave guiding characteristics of the nanotube yarn wave guides are critical for blast and shock energy dissipation. As seen from the figures 4.2 and 4.3, the applied normal stress is carried well by the wave guides. In Figure 4.4 stress can be seen to occur at the interface between boron nitride nanotube and aluminum layers and these interfacial stresses can lead to delamination of the composite. The highest interfacial stress developed is about 250% of the applied normal stress. Interfacial stresses could be even more higher when the composite is subjected to multiple cycles of loading. Therefore, it is important that the interfacial stresses developed in the composite lie well below the interface bond strength. Wave guiding properties of a real specimen can differ slightly since the finite element code

assumes a perfect interface and linear properties. Displacement at the interface is assumed to be equal in the finite element code. This displacement boundary condition ensures that strains and stresses are effectively transferred from one layer to another and no discontinuity is present. Strong bonding between boron nitride nanotube and Aluminum layers is crucial for the performance of the composite. A weak interface would undergo delamination of the layers and thereby reduces the wave guiding properties.

4.4 BLAST LOADING

In this section wave guiding properties of aluminum-boron nitride nanotube layered helmet is studied under blast conditions using finite element method. The helmet is subjected to an air blast pressure of 0.6 MPa for 0.5 milliseconds.

The top part of the helmet is coated with an aluminum-boron nitride nanotube layer and the bottom part is with rubber material as shown in Figure 4.5. The geometry and finite element model of of the helemet considered for blast analysis is as shown in Figure 4.6. The model is subjected to normal pressure. The red striped area represents oriented nanotube material, grey striped area represents aluminum material and the blue area represents the rubber layer. The material properties are shown in Table 4.2

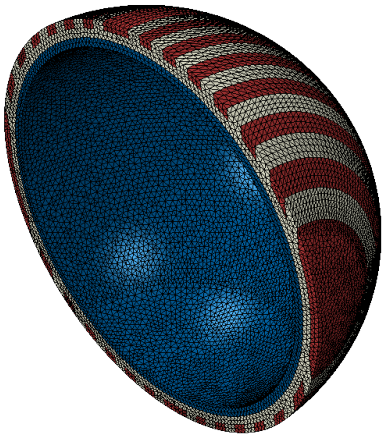

Figure 4.5 Finite element model of Aluminum-Boron nitride nanotube helmet

Table 4.2 Material properties of Helmet

Material	Elastic Modulus (N/m2)	Density (kg/m3)	Poisson Ratio
Aluminum	7E+10	2700	0.3
Boron nitride nanotube	1E+12	1300	0.3
Rubber	1E+7	1100	0.47

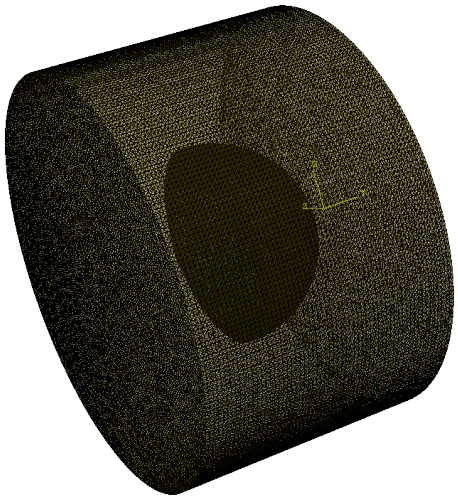

Figure 4.6 Finite element mesh of air and helmet

Fig 4.6 shows the helmet placed inside an air mesh. A blast load is applied at one end of the air mesh and the wave guiding characteristics of the helmet are studied as shown in Figure 4.7.

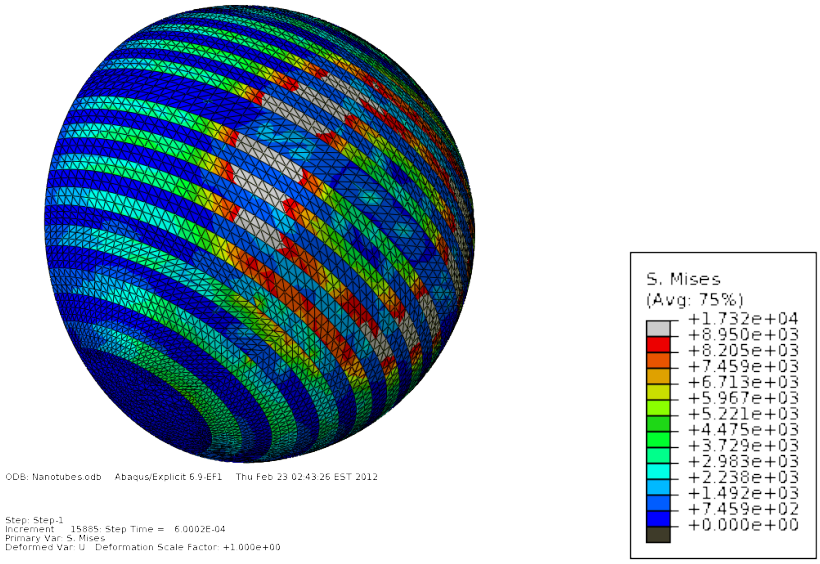

Figure 4.7 Blast Loading on Helmet

Figure 4.7 shows the Mises stresses after the blast load is applied. The high-intensity stresses can be confined to the stiffest component(s) of the composite enabling a waveguide effect to rapidly disperse the blast energy. As seen from the results the stiffest components act as stress and strain carriers dissipating the energy away from the area of impact. This energy from the stiff components can be further guided to a portion of the helmet equipped with energy absorbing materials. By dispersing the energy to the sides of the helmet, this wave guide effect can reduce the severity of trauma injury.

4.5 WAVE GUIDING IN SERPENTINE SHAPED NANOTUBES

In the previous sections wave guiding in straight nanotube yarns was analyzed. In this section wave guiding properties for serpentine shaped nanotubes are analyzed using finite element method. For this analysis, serpentine shaped nanotubes are embedded in epoxy matrix is modeled in ABAQUS FEA software. The geometry is as shown in Fig 4.8. One face is subjected to pressure loading and wave guiding in serpentine nanotubes are studied.

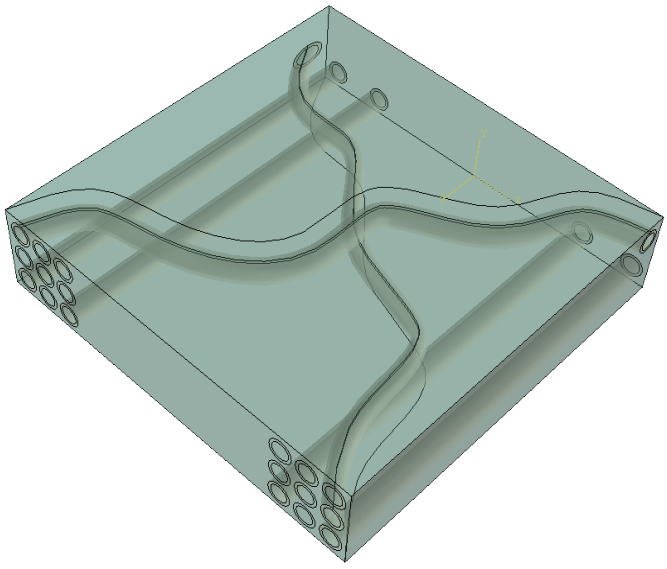

Figure 4.8 Serpentine Nanotubes embedded in epoxy matrix

A cut section of the finite element model is shown in Figure 4.9 . Blue indicates low stress, green indicates medium, grey and red indicating high stress. The pressure applied on the face is effectively carried away by the nanotubes then the epoxy matrix and this is indicated by grey and red color . While epoxy matrix shows low stress which is indicated by green and blue color. Leakage of stress around the tubes also seem to be very low which is indicated by blue color in the vicinity of the tubes. The pressure follows along the serpentine pattern of the tubes . This result presents nanotubes with a possibility of carrying strain and stress carriers in serpentine pattern.

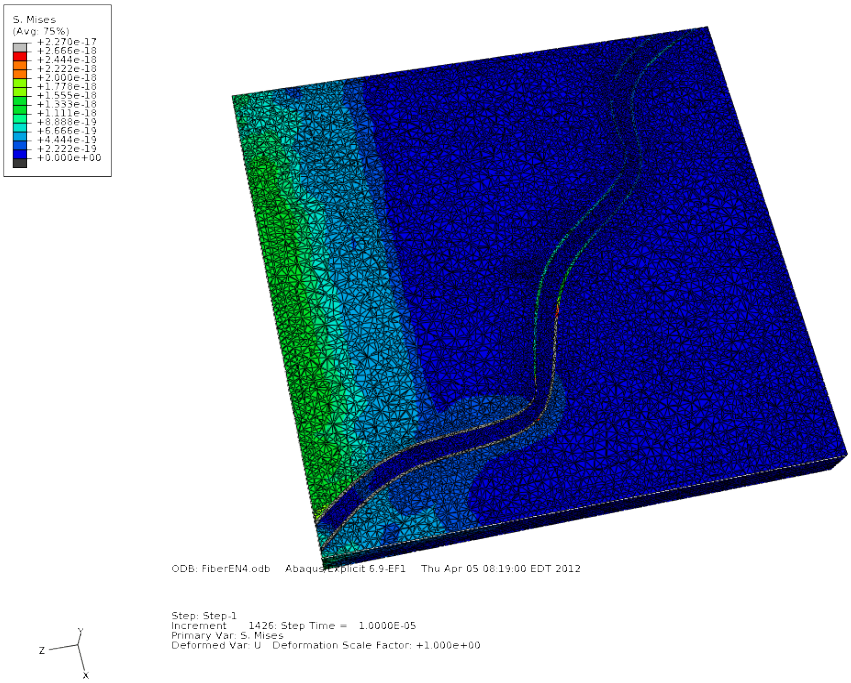

Figure 4.9 Serpentine wave guides

4.6 WAVE GUIDING FOR IMPACT

In this section analysis is performed to find wave dissipation properties under high velocity impact. Wave guiding properties of kevlar with epoxy carbon nanotube composite is compared. For this analysis a bullet impact on a 1 cm thick 10X10 cm^2 plates made of kevlar and epoxy-cnt composite is analysed using ABAQUS finite element program. These

plates are modeled using hex elements with orthotropic properties shown below in Table 4.3 & 4.4. For epoxy carbon nanotube composite , plain weave is assumed for calculating composite properties.

Table 4.3 Orthotropic properties of Kevlar[45]

E11 = 17.9 GPa	E22=17.9 GPa	E33=1.94 GPa
v12 = 0.08	v23 = 0.69	v31 = 0.0756
G12 = 1.85 GPa	G23 = 0.22 GPa	G31 = 0.22 GPa

Table 4.4 Orthotropic properties of Epoxy-CNT plain weave composite[46-48]

E11 = 131 GPa	E22=131 GPa	E33=11 GPa
v12 = 0.03	v23 = 0.03	v31 = 0.03
G12 = 3.82 GPa	G23 = 3.82 GPa	G31 = 3.82 GPa

A rigid bullet of mass 11.5 g traveling at a speed of 100 m/s is made to impact the kevlar and epoxy carbon nanotube composite plate . The bullet has a diameter of 5 mm and simulation time is 0.5 ms. The wave dissipation patterns for Kevlar and the nanotube composite are shown Figure 4.10 and Fig 4.11. Blue indicates low stress, green indicates medium, grey and red indicating high stress. Very little of impact stress is carried away from the point of impact by the Kevlar plate as shown in Figures 4.10, 4.12 and this is indicated by green and blue color. The impact stress from the bullet is effectively carried away from the point of impact by the Epoxy-nanotube composite as showin in Figures 4.11, 4.13 and this is indicated by grey and red color . This result presents nanotube embedded composites as a candidate for better impact dissipation than Kevlar for soldier helmets and body armors.

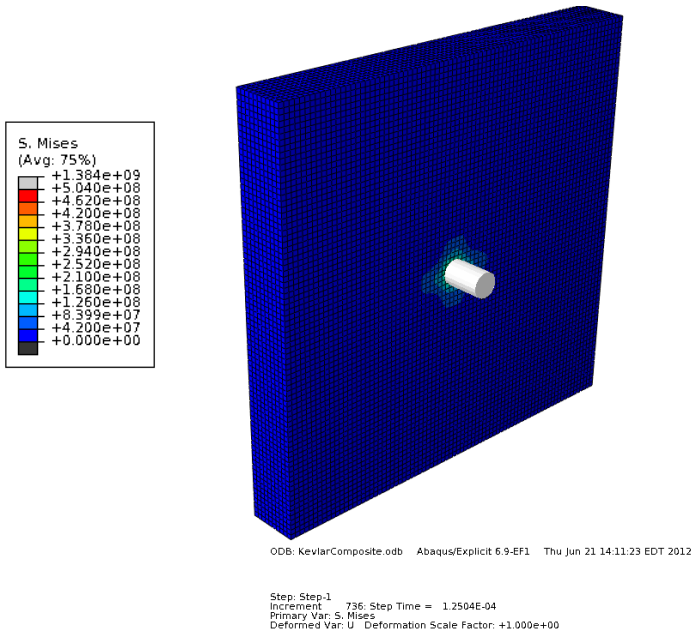

Figure 4.10 Bullet Impact on Kevlar Plate at initial contact

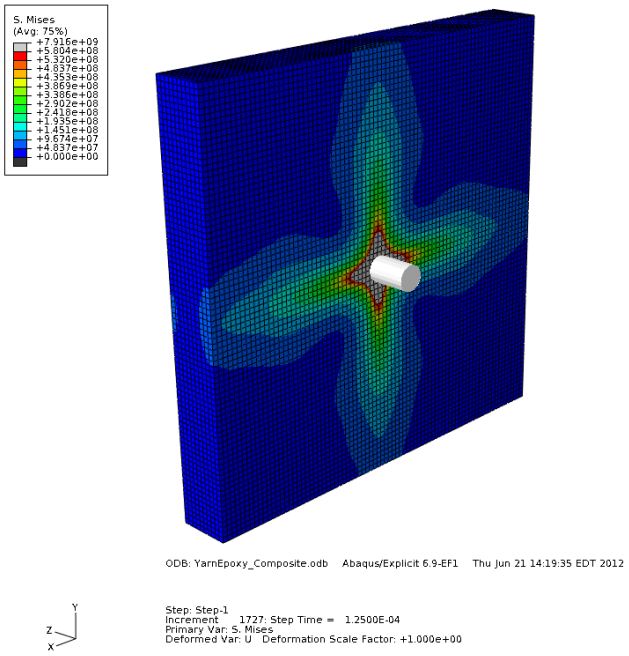

Figure 4.11 Bullet impact on Epoxy- Carbon nanotube composite plate at initial contact

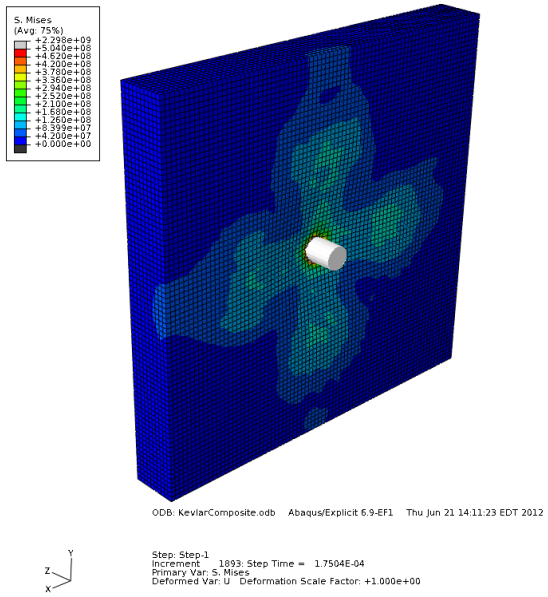

Figure 4.12 Bullet Impact on Kevlar Plate after full contact

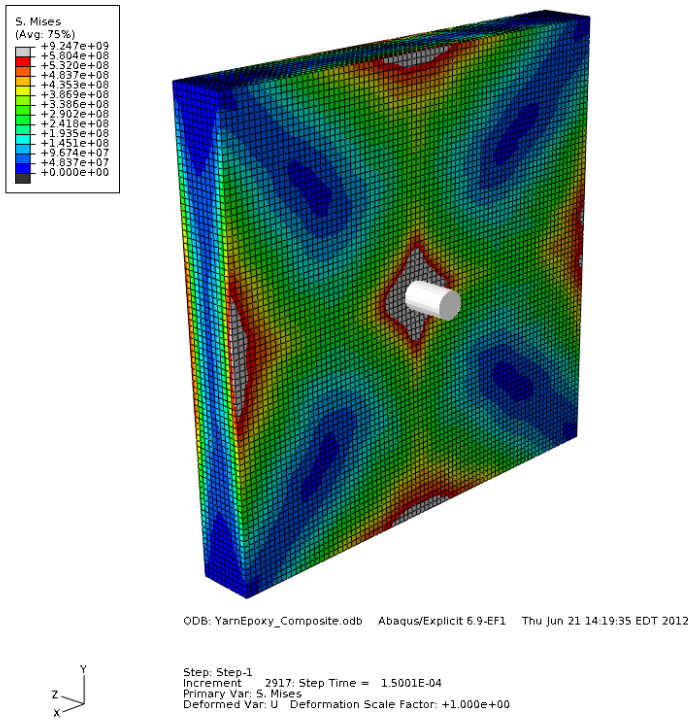

Figure 4.13 Bullet impact on Epoxy- Carbon nanotube composite plate after full contact

4.7 CONCLUSION

As seen from the results, nanotube embedded materials have a potential for wave guiding, impact and energy dissipation. These materials have a potential to be incorporated into body armors to carry energy away from the area of impact. Incorporating these materials in soldier helmets could also guide blast energy around the helmets which could reduce the severity of the trauma injury. Military equipment and armored vehicles could also make use of these materials to dissipate blast energy away from the impact site.

5 TWO-DIMENSIONAL EPOXY-CNT PHONONIC CRYSTAL

5.1 INTRODUCTION

Two-dimensional Phononic crystal are PhnCs that are periodic in two orthogonal directions. In this section we will look at “CNT cylinders” embedded in epoxy matrix is to again demonstrate the analysis technique when there is a very large mismatch in material properties. These cylinders are assumed to be of infinite length and represent a plane strain condition. Unlike 1D Phononic crystals, in which longitudinal and transverse waves exist independently and present no problem in finding an exact solution, in 2D Phononic crystals, longitudinal and transverse waves can couple and present a problem in arriving at an exact solution. Therefore, numerical methods must be relied upon to solve the governing equations and to find the existing Eigen modes. These Phononic crystals can either block or guide incoming waves not only in one direction but two directions. The wave vector components can assume any value in the in-plane directions and a complete band gap must also be searched for in the diagonal direction. To better understand the 2D Phononic crystal, basic concepts related to 2D lattice vibrations are presented and mass spring dynamic equations are solved. The frequency and wave vector dependence for the in-plane directions are obtained and concepts related to 2D Brillouin zone and reciprocal lattice vectors are presented.

Subsequently Eigen relations for the actual Phononic crystal are derived using finite element method with plane strain assumptions. Bloch-Fouquet boundary conditions are used to reflect the periodicity of the Phononic crystal. The band gap diagrams for 2D Phononic crystal are calculated and plotted using the parametric FEM solver COMSOL. To correlate the band gap data, frequency response and stress attenuation analysis is performed in ABAQUS. Based on the correlated results, a conclusion is arrived about the transmission properties of the two-dimensional Epoxy-CNT Phononic crystal.

5.2 2D LATTICE VIBRATIONS

5.2.1 2D single mass lattice vibrations

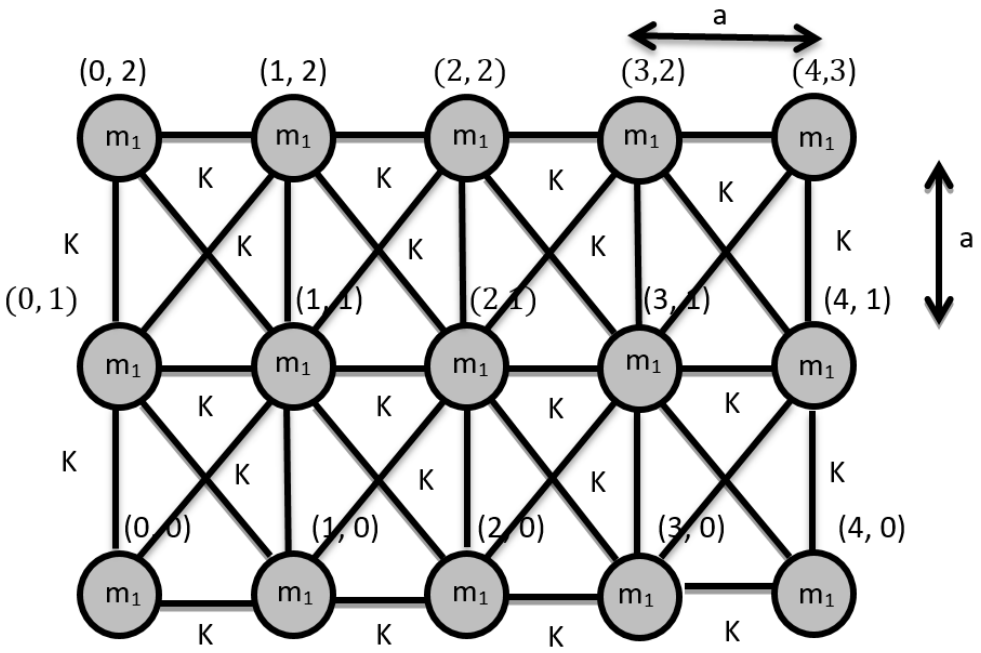

Figure 5.1 Two dimensional single-mass square lattice

In this section, the two dimensional lattice dynamic equations are derived and solved for Eigen modes. As shown in Figure 5.1, consider masses m_1 connected with springs having stiffness K in the horizontal, vertical and diagonal directions. The springs oppose the displacement of the masses in the x and y plane. The Newtonian equations of motion are solved considering opposing forces only from the neighboring masses. The mass displacement **u** is assumed to be in the form of a traveling wave with wave vector **k** and circular frequency $\boldsymbol{\omega}$. The wave vector has components $\mathbf{k}_x$, $\mathbf{k}_y$ and the displacement has components $\mathbf{u}_x$ and $\mathbf{u}_y$. The equations of motion are derived for the mass located at position coordinates (2, 1) and forces due to neighboring masses are taken into account. After substituting the displacement position coordinates in the equation of motion, the Eigen problem has the form of $\mathbf{M}\boldsymbol{\omega}^2=\mathbf{K}$ with **M** being the mass matrix and **K** being the Stiffness matrix. The stiffness matrix **K** contains $\mathbf{k}_x$ and $\mathbf{k}_y$ terms and while solving for Eigen modes,

these wave vector components must be swept in the boundaries of the 2D Brillouin zone to obtain the band diagrams for waves traveling in the horizontal, vertical, and diagonal directions.

Considering,

u_n = displacement of mass from equilibrium position

m_1 = mass

K = spring stiffness

n = position

a = lattice distance or distance between mass centers

k= wave vector

Considering only opposing forces due to neighboring masses,

$$m_1 \frac{d^2 \boldsymbol{u_x}(\boldsymbol{k}) e^{i\left((k_x \boldsymbol{x}+k_y \boldsymbol{y}).(2a\boldsymbol{x}+1a\boldsymbol{y})-\omega t\right)}}{dt^2} = K(u_x(\boldsymbol{k}) e^{i\left((k_x \boldsymbol{x}+k_y \boldsymbol{y}).(3a\boldsymbol{x}+1a\boldsymbol{y})-\omega t\right)} - u_x(\boldsymbol{k}) e^{i\left((k_x \boldsymbol{x}+k_y \boldsymbol{y}).(2a\boldsymbol{x}+1a\boldsymbol{y})-\omega t\right)}) + K\left(u_x(\boldsymbol{k}) e^{i\left((k_x \boldsymbol{x}+k_y \boldsymbol{y}).(1a\boldsymbol{x}+1a\boldsymbol{y})-\omega t\right)} - u_x(\boldsymbol{k}) e^{i\left((k_x \boldsymbol{x}+k_y \boldsymbol{y}).(2a\boldsymbol{x}+1a\boldsymbol{y})-\omega t\right)}\right) + \left[\frac{K}{2}\left(u_x(\boldsymbol{k}) e^{i\left((k_x \boldsymbol{x}+k_y \boldsymbol{y}).(3a\boldsymbol{x}+2a\boldsymbol{y})-\omega t\right)} - u_x(\boldsymbol{k}) e^{i\left((k_x \boldsymbol{x}+k_y \boldsymbol{y}).(2a\boldsymbol{x}+1a\boldsymbol{y})-\omega t\right)}\right) + \frac{K}{2}\left(u_y(\boldsymbol{k}) e^{i\left((k_x \boldsymbol{x}+k_y \boldsymbol{y}).(3a\boldsymbol{x}+2a\boldsymbol{y})-\omega t\right)} - u_y(\boldsymbol{k}) e^{i\left((k_x \boldsymbol{x}+k_y \boldsymbol{y}).(2a\boldsymbol{x}+1a\boldsymbol{y})-\omega t\right)}\right)\right] + \left[\frac{K}{2}\left(u_x(\boldsymbol{k}) e^{i\left((k_x \boldsymbol{x}+k_y \boldsymbol{y}).(1a\boldsymbol{x}+2a\boldsymbol{y})-\omega t\right)} - u_x(\boldsymbol{k}) e^{i\left((k_x \boldsymbol{x}+k_y \boldsymbol{y}).(2a\boldsymbol{x}+1a\boldsymbol{y})-\omega t\right)}\right) - \frac{K}{2}\left(u_y(\boldsymbol{k}) e^{i\left((k_x \boldsymbol{x}+k_y \boldsymbol{y}).(1a\boldsymbol{x}+2a\boldsymbol{y})-\omega t\right)} - u_y(\boldsymbol{k}) e^{i\left((k_x \boldsymbol{x}+k_y \boldsymbol{y}).(2a\boldsymbol{x}+1a\boldsymbol{y})-\omega t\right)}\right)\right] + \left[\frac{K}{2}\left(u_x(\boldsymbol{k}) e^{i\left((k_x \boldsymbol{x}+k_y \boldsymbol{y}).(1a\boldsymbol{x}+0a\boldsymbol{y})-\omega t\right)} - u_x(\boldsymbol{k}) e^{i\left((k_x \boldsymbol{x}+k_y \boldsymbol{y}).(2a\boldsymbol{x}+1a\boldsymbol{y})-\omega t\right)}\right) + \frac{K}{2}\left(u_y(\boldsymbol{k}) e^{i\left((k_x \boldsymbol{x}+k_y \boldsymbol{y}).(1a\boldsymbol{x}+0a\boldsymbol{y})-\omega t\right)} - u_y(\boldsymbol{k}) e^{i\left((k_x \boldsymbol{x}+k_y \boldsymbol{y}).(2a\boldsymbol{x}+1a\boldsymbol{y})-\omega t\right)}\right)\right] + \left[\frac{K}{2}\left(u_x(\boldsymbol{k}) e^{i\left((k_x \boldsymbol{x}+k_y \boldsymbol{y}).(3a\boldsymbol{x}+0a\boldsymbol{y})-\omega t\right)} - u_x(\boldsymbol{k}) e^{i\left((k_x \boldsymbol{x}+k_y \boldsymbol{y}).(2a\boldsymbol{x}+1a\boldsymbol{y})-\omega t\right)}\right) - \frac{K}{2}\left(u_y(\boldsymbol{k}) e^{i\left((k_x \boldsymbol{x}+k_y \boldsymbol{y}).(3a\boldsymbol{x}+0a\boldsymbol{y})-\omega t\right)} - u_y(\boldsymbol{k}) e^{i\left((k_x \boldsymbol{x}+k_y \boldsymbol{y}).(2a\boldsymbol{x}+1a\boldsymbol{y})-\omega t\right)}\right)\right]$$

$$m_1 \frac{d^2 \boldsymbol{u}_y(2a\boldsymbol{x} + 1a\boldsymbol{y})}{dt^2}$$

$$= K(u_y(\boldsymbol{k})e^{i\left((k_x\boldsymbol{x}+k_y\boldsymbol{y}).(2a\boldsymbol{x}+2a\boldsymbol{y})-\omega t\right)} - u_y(\boldsymbol{k})e^{i\left((k_x\boldsymbol{x}+k_y\boldsymbol{y}).(2a\boldsymbol{x}+1a\boldsymbol{y})-\omega t\right)})$$

$$+ K\left(u_y(\boldsymbol{k})e^{i\left((k_x\boldsymbol{x}+k_y\boldsymbol{y}).(2a\boldsymbol{x}+0a\boldsymbol{y})-\omega t\right)} - u_y(\boldsymbol{k})e^{i\left((k_x\boldsymbol{x}+k_y\boldsymbol{y}).(2a\boldsymbol{x}+1a\boldsymbol{y})-\omega t\right)}\right)$$

$$+ \left[\frac{K}{2}\left(u_y(\boldsymbol{k})e^{i\left((k_x\boldsymbol{x}+k_y\boldsymbol{y}).(3a\boldsymbol{x}+2a\boldsymbol{y})-\omega t\right)}\right.\right.$$

$$\left. - u_y(\boldsymbol{k})e^{i\left((k_x\boldsymbol{x}+k_y\boldsymbol{y}).(2a\boldsymbol{x}+1a\boldsymbol{y})-\omega t\right)}\right)$$

$$+ \frac{K}{2}\left(u_x(\boldsymbol{k})e^{i\left((k_x\boldsymbol{x}+k_y\boldsymbol{y}).(3a\boldsymbol{x}+2a\boldsymbol{y})-\omega t\right)}\right.$$

$$\left.\left. - u_x(\boldsymbol{k})e^{i\left((k_x\boldsymbol{x}+k_y\boldsymbol{y}).(2a\boldsymbol{x}+1a\boldsymbol{y})-\omega t\right)}\right)\right]$$

$$+ \left[\frac{K}{2}\left(u_y(\boldsymbol{k})e^{i\left((k_x\boldsymbol{x}+k_y\boldsymbol{y}).(1a\boldsymbol{x}+2a\boldsymbol{y})-\omega t\right)}\right.\right.$$

$$\left. - u_y(\boldsymbol{k})e^{i\left((k_x\boldsymbol{x}+k_y\boldsymbol{y}).(2a\boldsymbol{x}+1a\boldsymbol{y})-\omega t\right)}\right)$$

$$- \frac{K}{2}\left(u_x(\boldsymbol{k})e^{i\left((k_x\boldsymbol{x}+k_y\boldsymbol{y}).(1a\boldsymbol{x}+2a\boldsymbol{y})-\omega t\right)}\right.$$

$$\left.\left. - u_x(\boldsymbol{k})e^{i\left((k_x\boldsymbol{x}+k_y\boldsymbol{y}).(2a\boldsymbol{x}+1a\boldsymbol{y})-\omega t\right)}\right)\right]$$

$$+ \left[\frac{K}{2}\left(u_y(\boldsymbol{k})e^{i\left((k_x\boldsymbol{x}+k_y\boldsymbol{y}).(1a\boldsymbol{x}+0a\boldsymbol{y})-\omega t\right)}\right.\right.$$

$$\left. - u_y(\boldsymbol{k})e^{i\left((k_x\boldsymbol{x}+k_y\boldsymbol{y}).(2a\boldsymbol{x}+1a\boldsymbol{y})-\omega t\right)}\right)$$

$$+ \frac{K}{2}\left(u_x(\boldsymbol{k})e^{i\left((k_x\boldsymbol{x}+k_y\boldsymbol{y}).(1a\boldsymbol{x}+0a\boldsymbol{y})-\omega t\right)}\right.$$

$$\left.\left. - u_x(\boldsymbol{k})e^{i\left((k_x\boldsymbol{x}+k_y\boldsymbol{y}).(2a\boldsymbol{x}+1a\boldsymbol{y})-\omega t\right)}\right)\right]$$

$$+ \left[\frac{K}{2}\left(u_y(\boldsymbol{k})e^{i\left((k_x\boldsymbol{x}+k_y\boldsymbol{y}).(3a\boldsymbol{x}+0a\boldsymbol{y})-\omega t\right)}\right.\right.$$

$$\left. - u_y(\boldsymbol{k})e^{i\left((k_x\boldsymbol{x}+k_y\boldsymbol{y}).(2a\boldsymbol{x}+1a\boldsymbol{y})-\omega t\right)}\right)$$

$$- \frac{K}{2}\left(u_x(\boldsymbol{k})e^{i\left((k_x\boldsymbol{x}+k_y\boldsymbol{y}).(3a\boldsymbol{x}+0a\boldsymbol{y})-\omega t\right)}\right.$$

$$\left.\left. - u_x(\boldsymbol{k})e^{i\left((k_x\boldsymbol{x}+k_y\boldsymbol{y}).(2a\boldsymbol{x}+1a\boldsymbol{y})-\omega t\right)}\right)\right]$$

After substitution, we arrive at the following Eigen relation,

$$\omega^2 \begin{bmatrix} m_1 & 0 \\ 0 & m_1 \end{bmatrix} \begin{bmatrix} u_x(\boldsymbol{k}) \\ u_y(\boldsymbol{k}) \end{bmatrix} = \begin{bmatrix} 4K \sin^2\left[\frac{k_x a}{2}\right] + 2K\left[1 - \cos(k_x a)\cos(k_y a)\right] & 2K \sin k_x a \sin k_y a \\ 2K \sin k_x a \sin k_y a & 4K \sin^2\left[\frac{k_y a}{2}\right] + 2K\left[1 - \cos(k_x a)\cos(k_y a)\right] \end{bmatrix} \begin{bmatrix} u_x(\boldsymbol{k}) \\ u_y(\boldsymbol{k}) \end{bmatrix}$$

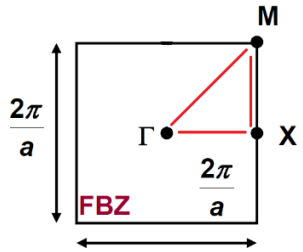

Figure 5.2 2D Brillouin zone for the single mass square lattice

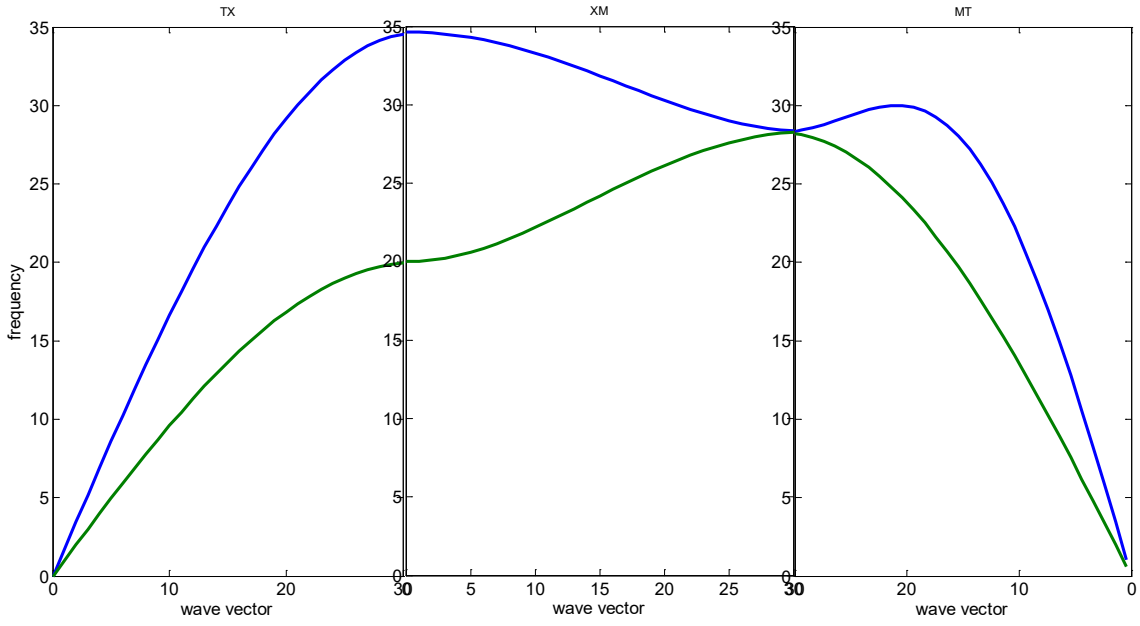

Figure 5.3 Band gap diagram for two dimensional single-mass square lattice (frequency is in Hz)

As see from Figure 5.3, no band gaps exist in the mono-atomic case. The band diagram for a mono atomic model is swept for a wave traveling in the horizontal **TX**, vertical **XM** and diagonal direction **MT** as shown. The horizontal traveling wave **TX** assumes wave vector components kx = 0 to pi/a and ky = 0, the vertical traveling wave **XM** assumes kx=pi/a and ky=0 to pi/a and the diagonal traveling wave **MT** assumes kx=pi/a to 0, ky = pi/a to 0. The components falling between the boundaries of the Brillouin zone are not needed and a density of states computation is not essential for a band gap diagram.

5.2.2 2D Double-mass lattice vibrations

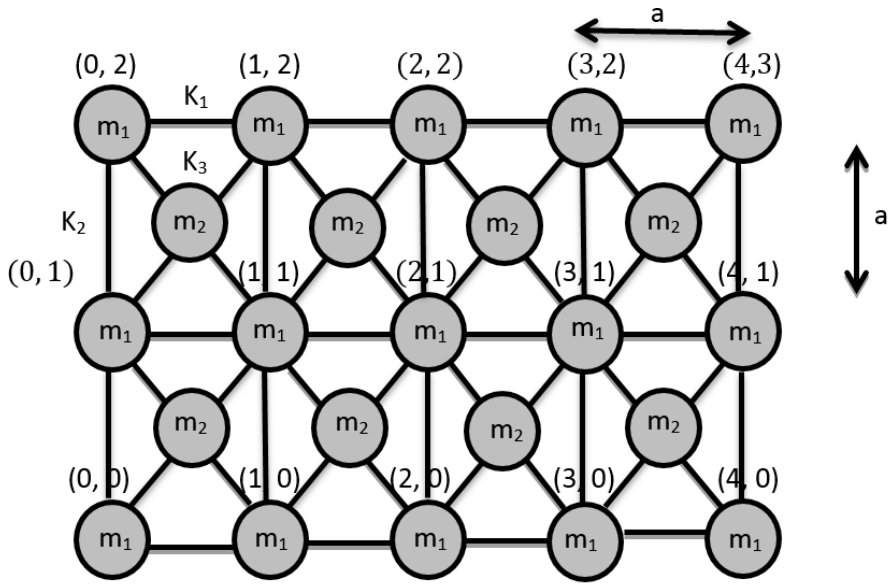

Figure 5.4 Two dimensional double-mass square lattice

This model is considered because it represents an idealized approximation of a CNT cylinders embedded in Epoxy matrix and the masses m_1 representing epoxy and masses m_2 representing CNT cylinders. We study this in order to better understand the band diagrams for the epoxy-CNT Phononic crystal using the finite element method. In this section we derive two dimensional lattice dynamic equations for a double mass square lattice and solve for Eigen vectors and frequencies. As shown in Figure 5.4, we consider masses m_1 and m_2 connected with springs having stiffness K_1 in the horizontal, K_2 in vertical, and K_3 in diagonal directions. The springs oppose the displacement of the masses in the in-plane

directions. The Newtonian equations of motion are solved considering opposing forces only from the neighboring masses. The mass displacement **u** is assumed to be in the form of a traveling wave with wave vector **k** and circular frequency $\boldsymbol{\omega}$. The wave vector has components $\mathbf{k}_x$, $\mathbf{k}_y$ and the displacement has components $\mathbf{u}_x$ and $\mathbf{u}_y$. The equations of motion are derived for the masses m_1 and m_2 and forces due to neighboring masses are taken into account. After substituting the displacement position coordinates in the equation of the motion, the Eigen problem is arrived in the form of $\mathbf{M}\boldsymbol{\omega}^2=\mathbf{K}$, with **M** being the mass matrix and **K** being the stiffness matrix. The stiffness matrix **K** contains $\mathbf{k}_x$ and $\mathbf{k}_y$ terms and while solving for Eigen modes, these wave vector components must be swept in the boundaries of the 2D Brillouin zone to obtain the band diagrams for waves traveling in horizontal, vertical and diagonal directions.

The equations of motion are not shown due to the length of equations. After substitution, we arrive at the Eigen relation,

$$\omega^2 \begin{bmatrix} m_1 & 0 & 0 & 0 \\ 0 & m_1 & 0 & 0 \\ 0 & 0 & m_2 & 0 \\ 0 & 0 & 0 & m_2 \end{bmatrix} \begin{bmatrix} u_{1x}(\boldsymbol{k}) \\ u_{1y}(\boldsymbol{k}) \\ u_{2x}(\boldsymbol{k}) \\ u_{2y}(\boldsymbol{k}) \end{bmatrix} = \lfloor A \rfloor \begin{bmatrix} u_{1x}(\boldsymbol{k}) \\ u_{1y}(\boldsymbol{k}) \\ u_{2x}(\boldsymbol{k}) \\ u_{2y}(\boldsymbol{k}) \end{bmatrix}$$

Where matrix A =

$2K_1 + 4K_1 \sin^2\left(\frac{k_x a}{2}\right) + 2K_2[1 - \cos(k_x a)\cos(k_y a)]$	$2K_2 \sin(k_x a)\sin(k_y a)$	$\left[-2K_1 \cos\left(\frac{k_x a}{2}\right)\cos\left(\frac{k_y a}{2}\right)\right]$	$2K_1 \sin\left(\frac{k_x a}{2}\right)\sin\left(\frac{k_y a}{2}\right)$
$2K_2 \sin(k_x a)\sin(k_y a)$	$2K_1 + 4K_1 \sin^2\left(\frac{k_y a}{2}\right) + 2K_2[1 - \cos(k_x a)\cos(k_y a)]$	$2K_1 \sin\left(\frac{k_x a}{2}\right)\sin\left(\frac{k_y a}{2}\right)$	$-2K_1 \cos\left(\frac{k_x a}{2}\right)\cos\left(\frac{k_y a}{2}\right)$

$-2K_1 \cos\left(\frac{k_x a}{2}\right)\cos\left(\frac{k_y a}{2}\right)$	$2K_1 \sin\left(\frac{k_x a}{2}\right)\sin\left(\frac{k_y a}{2}\right)$	$2K_1 + 4K_1 \sin^2\left(\frac{k_x a}{2}\right) + 2K_2[1 - \cos(k_x a)\cos(k_y a)]$	$2K_2 \sin(k_x a)\sin(k_y a)$
$2K_1 \sin\left(\frac{k_x a}{2}\right)\sin\left(\frac{k_y a}{2}\right)$	$-2K_1 \cos\left(\frac{k_x a}{2}\right)\cos\left(\frac{k_y a}{2}\right)$	$2K_2 \sin(k_x a)\sin(k_y a)$	$2K_1 + 4K_1 \sin^2\left(\frac{k_y a}{2}\right) + 2K_2[1 - \cos(k_x a)\cos(k_y a)]$

This Eigen relation is solved for a wave traveling in the horizontal **TX**, vertical **XM** and diagonal direction **MT** as shown in Figure 5.5. The horizontal traveling wave **TX** assumes wave vector components kx = 0 to pi/a and ky = 0, the vertical traveling wave **XM** assumes kx=pi/a and ky=0 to pi/a and the diagonal traveling wave **MT** assumes kx=pi/a to 0 , ky = pi/a to 0. The components falling between the boundaries of the Brillouin zone are not needed and a density of states computation is not essential for a band gap diagram.

Assuming for example the following values for illustration,

```
m1 = 2; % mass1 in kg
m2 = 1; % mass2 in kg
K1 = 300; % spring stiffness in N/m
K2 = 200; % spring stiffness in N/m
K3 = 100; % spring stiffness in N/m
a = 0.1; % lattice constant in m
```

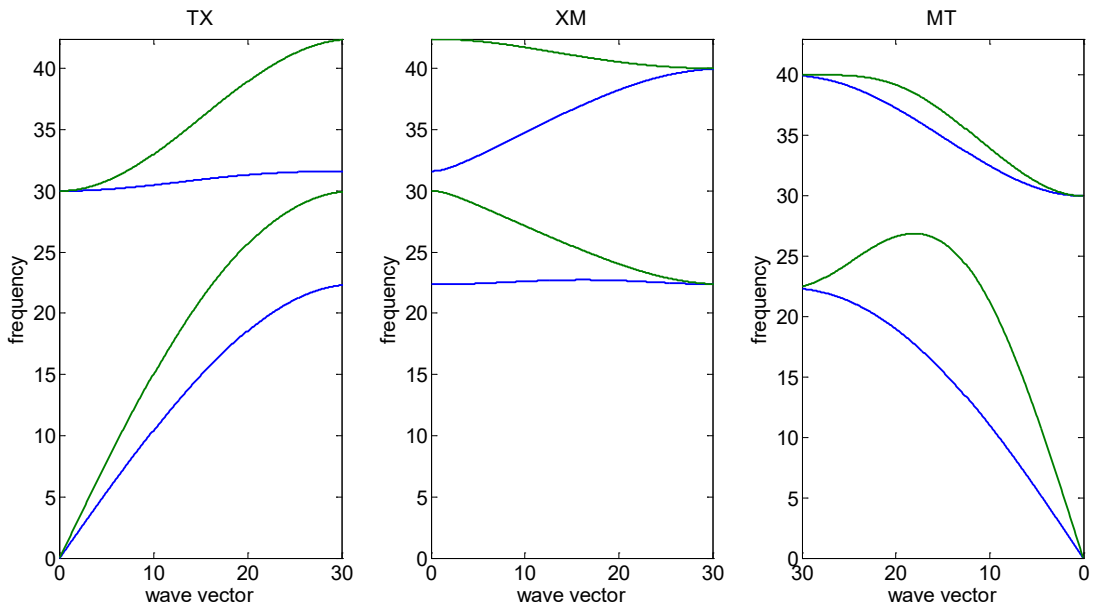

Figure 5.5 Band diagram for a 2D di-atomic square lattice

As shown in the Figure 5.5, a frequency band gap arises for the di-atomic model due to difference in the two masses and the width of this gap is dictated by this difference. The greater the difference, the wider the gap and vice versa. This model can be used to further interpret results given by the finite element method. However, in the continuum model, the width of the gap is controlled by the following parameters: density, elasticity, longitudinal and transverse speed of sound and impedance. Presenting a higher contrast in these parameters would present a wider gap for stress and displacement attenuation for incoming frequencies falling within the gap.

5.2.3 Dispersion using finite element method

In order to better understand the COMSOL FEM code, in this section the dispersion approximation for a 2D Phononic crystal using the finite element method is presented. First the goverinig 3D wave and constitutive equations for an isotropic material are derived and the mass and stiffness formulation for triangular plane strain elements is presented. The

Bloch periodic boundary conditions are applied and the dispersion relation via finite element method is developed.

Consider a unit cube solid isotropic body as shown in Figure 5.6,

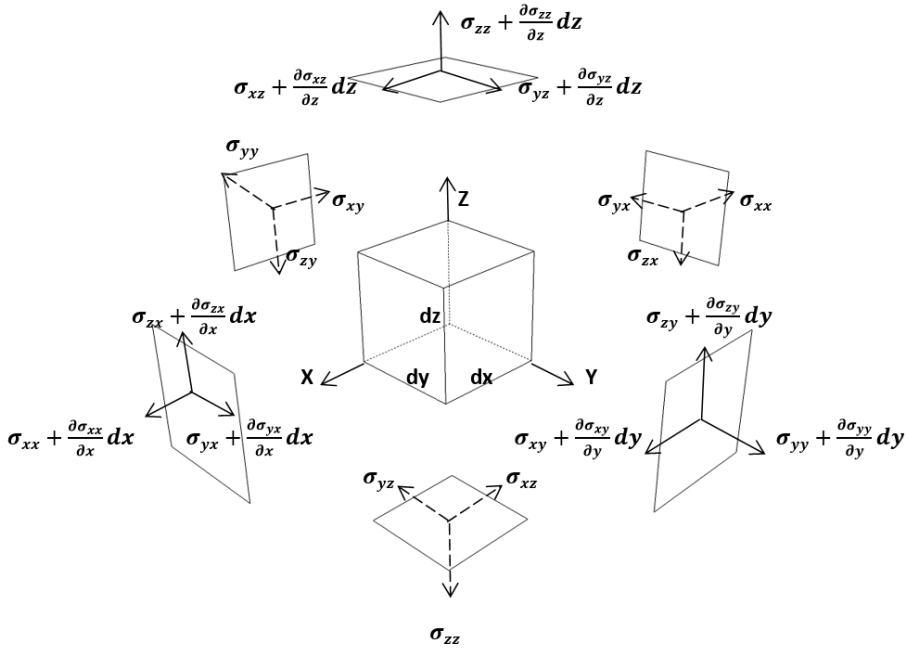

Figure 5.6 Stress components for wave propagation in an isotropic solid body

Neglecting body forces such as gravity, forces in x-direction are equal to,

$$\left(\sigma_{xx} + \frac{\partial \sigma_{xx}}{\partial x} dx\right) dydz - \sigma_{xx} dydz + \left(\sigma_{xy} + \frac{\partial \sigma_{xy}}{\partial y} dy\right) dxdz - \sigma_{xy} dydz + \left(\sigma_{xz} + \frac{\partial \sigma_{xz}}{\partial z} dz\right) dxdy - \sigma_{xz} dxdy = \rho dxdydz \frac{\partial^2 u}{\partial t^2}$$

Forces in y-direction are equal to,

$$\left(\sigma_{yy} + \frac{\partial \sigma_{yy}}{\partial y} dy\right) dxdz - \sigma_{yy} dxdz + \left(\sigma_{yx} + \frac{\partial \sigma_{yx}}{\partial x} dx\right) dydz - \sigma_{yx} dydz + \left(\sigma_{yz} + \frac{\partial \sigma_{yz}}{\partial z} dz\right) dxdy - \sigma_{yz} dxdy = \rho dxdydz \frac{\partial^2 v}{\partial t^2}$$

Forces in z-direction are equal to,

$\left(\sigma_{zz} + \frac{\partial \sigma_{zz}}{\partial z} dz\right) dxdy - \sigma_{zz} dxdy + \left(\sigma_{zx} + \frac{\partial \sigma_{zx}}{\partial x} dx\right) dydz - \sigma_{yx} dydz + \left(\sigma_{yz} + \frac{\partial \sigma_{zy}}{\partial y} dy\right) dxdz - \sigma_{yz} dxdz = \rho dxdydz \frac{\partial^2 w}{\partial t^2}$

This simplifies to,

$$\frac{\partial \sigma_{xx}}{\partial x} + \frac{\partial \sigma_{xy}}{\partial y} + \frac{\partial \sigma_{xz}}{\partial z} = \rho \frac{\partial^2 u}{\partial t^2}$$

$$\frac{\partial \sigma_{yx}}{\partial x} + \frac{\partial \sigma_{yy}}{\partial y} + \frac{\partial \sigma_{yz}}{\partial z} = \rho \frac{\partial^2 v}{\partial t^2}$$

$$\frac{\partial \sigma_{zx}}{\partial x} + \frac{\partial \sigma_{zy}}{\partial y} + \frac{\partial \sigma_{zz}}{\partial z} = \rho \frac{\partial^2 w}{\partial t^2}$$

For an isotropic material, a stress in the x-direction causes a strain in the x- direction of $\frac{\sigma_x}{E}$ and this σ_x also causes a strain in the y-direction $-\frac{\nu \sigma_x}{E}$

This situation can be summarized by the following matrix,

	Resulting strain in each direction		
Stress	x	y	z
σ_x	$\frac{\sigma_x}{E}$	$-\frac{\nu \sigma_x}{E}$	$-\frac{\nu \sigma_x}{E}$
σ_y	$-\frac{\nu \sigma_y}{E}$	$\frac{\sigma_y}{E}$	$-\frac{\nu \sigma_y}{E}$
σ_z	$-\frac{\nu \sigma_z}{E}$	$-\frac{\nu \sigma_z}{E}$	$\frac{\sigma_z}{E}$

Adding columns in this matrix to obtain the total strain in each direction gives the equations,

$$\varepsilon_x = \left(\frac{\sigma_x}{E} - \frac{\nu \sigma_y}{E} - \frac{\nu \sigma_z}{E}\right)$$

$$\varepsilon_y = \left(\frac{\sigma_y}{E} - \frac{\nu \sigma_x}{E} - \frac{\nu \sigma_z}{E}\right)$$

$$\varepsilon_z = \left(\frac{\sigma_z}{E} - \frac{\nu \sigma_x}{E} - \frac{\nu \sigma_y}{E}\right)$$

Similarly for shear strain

$$\gamma_{xy} = \frac{\tau_{xy}}{G} \text{ where } G = \frac{E}{2(1+\nu)}$$

$$\gamma_{yz} = \frac{\tau_{yz}}{G}$$

$$\gamma_{zx} = \frac{\tau_{zx}}{G}$$

Normal and shear stresses are given by,

$$\sigma_x = \frac{E}{(1+\nu)(1-2\nu)}\left[(1-\nu)\varepsilon_x + \nu\left(\varepsilon_y + \varepsilon_z\right)\right]$$

$$\sigma_y = \frac{E}{(1+\nu)(1-2\nu)}\left[(1-\nu)\varepsilon_y + \nu(\varepsilon_x + \varepsilon_z)\right]$$

$$\sigma_z = \frac{E}{(1+\nu)(1-2\nu)}\left[(1-\nu)\varepsilon_z + \nu\left(\varepsilon_x + \varepsilon_y\right)\right]$$

$$\tau_{xy} = \frac{E}{2(1+\nu)}\gamma_{xy}$$

$$\tau_{xz} = \frac{E}{2(1+\nu)}\gamma_{xz}$$

$$\tau_{yz} = \frac{E}{2(1+\nu)}\gamma_{yz}$$

$$\varepsilon_x = \frac{\partial u}{\partial x}, \quad \varepsilon_y = \frac{\partial v}{\partial x}, \quad \varepsilon_z = \frac{\partial w}{\partial z}$$

$$\gamma_{yz} = \frac{\partial w}{\partial y} + \frac{\partial v}{\partial z}, \quad \gamma_{zx} = \frac{\partial u}{\partial z} + \frac{\partial w}{\partial x}, \quad \gamma_{xy} = \frac{\partial u}{\partial y} + \frac{\partial v}{\partial x}$$

Where displacement $u = A_x e^{i(\boldsymbol{k_x}.\boldsymbol{x}-\omega t)}$, $v = A_y e^{i(\boldsymbol{k_y}.\boldsymbol{y}-\omega t)}$ and $w = A_z e^{i(\boldsymbol{k_z}.\boldsymbol{z}-\omega t)}$

A solid body is said to be in a state of plane strain if it satisfies all the assumptions of plane stress theory except that the body's thickness is large in comparison to the dimesion in the xy plane. Therfore,`

$$\sigma_x = \frac{E}{(1+v)(1-2v)}\left[(1-v)\varepsilon_x + v(\varepsilon_y)\right]$$

$$\sigma_y = \frac{E}{(1+v)(1-2v)}\left[(1-v)\varepsilon_y + v(\varepsilon_x)\right]$$

$$\tau_{xy} = \frac{E}{2(1+v)}\gamma_{xy}$$

For plane strain,

$$\varepsilon_z = \frac{\partial w}{\partial z} = 0, \gamma_{zx} = \frac{\partial u}{\partial z} + \frac{\partial w}{\partial x} = 0, \;\; \gamma_{xy} = \frac{\partial v}{\partial x} + \frac{\partial u}{\partial y} = 0, \sigma_z = 0 \; (negligible)$$

For finite element calculations, the displacement is given in terms of interpolation functions N_1, N_2 & N_3 ,

$$u(x,y) = N_1(x,y)u_1 + N_2(x,y)u_2 + N_3(x,y)u_3$$

$$v(x,y) = N_1(x,y)v_1 + N_2(x,y)v_2 + N_3(x,y)v_3$$

$$\varepsilon_x = \frac{\partial u}{\partial x} = \frac{\partial N_1}{\partial x}u_1 + \frac{\partial N_2}{\partial x}u_2 + \frac{\partial N_3}{\partial x}u_3$$

$$\varepsilon_y = \frac{\partial v}{\partial x} = \frac{\partial N_1}{\partial y}v_1 + \frac{\partial N_2}{\partial y}v_2 + \frac{\partial N_3}{\partial y}v_3$$

$$\gamma_{xy} = \frac{\partial u}{\partial y} + \frac{\partial v}{\partial x} = \frac{\partial N_1}{\partial y}u_1 + \frac{\partial N_2}{\partial y}u_2 + \frac{\partial N_3}{\partial y}u_3 + \frac{\partial N_1}{\partial x}v_1 + \frac{\partial N_2}{\partial x}v_2 + \frac{\partial N_3}{\partial x}v_3$$

$$\begin{bmatrix}\varepsilon_x \\ \varepsilon_y \\ \gamma_{xy}\end{bmatrix} = \begin{bmatrix} \frac{\partial N_1}{\partial x} & 0 & \frac{\partial N_2}{\partial x} & 0 & \frac{\partial N_3}{\partial x} & 0 \\ 0 & \frac{\partial N_1}{\partial y} & 0 & \frac{\partial N_2}{\partial y} & 0 & \frac{\partial N_3}{\partial y} \\ \frac{\partial N_1}{\partial y} & \frac{\partial N_1}{\partial x} & \frac{\partial N_2}{\partial y} & \frac{\partial N_2}{\partial x} & \frac{\partial N_3}{\partial y} & \frac{\partial N_3}{\partial x} \end{bmatrix} \begin{bmatrix} u_1 \\ v_1 \\ u_2 \\ v_2 \\ u_3 \\ v_3 \end{bmatrix} = [B][\delta^e]$$

The elastic strain energy is,

$$U_e{}^{(e)} = \frac{1}{2}\iiint \left(\sigma_x\varepsilon_x + \sigma_y\varepsilon_y + \tau_{xy}\gamma_{xy}\right) dV$$

$$U_e{}^{(e)} = \frac{1}{2}\iiint [\varepsilon_x \quad \varepsilon_y \quad \gamma_{xy}] \frac{E}{(1+v)(1-2v)} \begin{bmatrix} 1-v & v & 0 \\ v & 1-v & 0 \\ 0 & 0 & \frac{1-2v}{2} \end{bmatrix} \begin{bmatrix} \varepsilon_x \\ \varepsilon_y \\ \gamma_{xy} \end{bmatrix} dV$$

$$U_e{}^{(e)} = \frac{1}{2}[\delta^e]^T V^e [B]^T [D][B][\delta^e]$$

$$W = f_{1x}u_1 + f_{2x}u_2 + f_{3x}u_3 + f_{1y}v_1 + f_{2y}v_2 + f_{3y}v_3 = [\delta^e]^T[f]$$

The Potential Strain Energy is $\Pi = \frac{1}{2}[\delta]^T[k][\delta] - [\delta^T][f]$

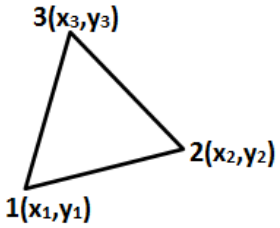

Field variable in the polynomial form

$$\phi(x,y) = a_0 + a_1 x + a_2 y$$

Applying nodal conditions,

$$\phi(x_1, y_1) = \phi_1$$

$$\phi(x_2, y_2) = \phi_2$$

$$\phi(x_3, y_3) = \phi_3$$

$$\begin{bmatrix} 1 & x_1 & y_1 \\ 1 & x_2 & y_2 \\ 1 & x_3 & y_3 \end{bmatrix} \begin{bmatrix} a_0 \\ a_1 \\ a_2 \end{bmatrix} = \begin{bmatrix} \phi_1 \\ \phi_2 \\ \phi_3 \end{bmatrix}$$

$$a_0 = \frac{1}{2A}[\phi_1(x_2y_3 - x_3y_2) + \phi_2(x_3y_1 - x_1y_3) + \phi_3(x_1y_2 - x_2y_1)]$$

$$a_1 = \frac{1}{2A}[\phi_1(y_2 - y_3) + \phi_2(y_3 - y_1) + \phi_3(y_1 - y_2)]$$

$$a_2 = \frac{1}{2A}[\phi_1(x_3 - x_2) + \phi_2(x_1 - x_3) + \phi_3(x_2 - x_1)]$$

$$\begin{aligned}\phi(x,y) = \frac{1}{2A}([(x_2y_3 - x_3y_2) + (y_2 - y_3)x + (x_3 - x_2)y]\phi_1 \\ + [(x_3y_1 - x_1y_3) + (y_3 - y_1)x + (x_1 - x_3)y]\phi_2 \\ + [(x_1y_2 - x_2y_1) + (y_1 - y_2)x + (x_2 - x_1)y]\phi_3)\end{aligned}$$

$$N_1(x,y) = \frac{1}{2A}[(x_2y_3 - x_3y_2) + (y_2 - y_3)x + (x_3 - x_2)y] = \frac{1}{2A}(\alpha_1 + \beta_1 x + \gamma_1 y)$$

$$N_2(x,y) = \frac{1}{2A}[(x_3y_1 - x_1y_3) + (y_3 - y_1)x + (x_1 - x_3)y] = \frac{1}{2A}(\alpha_2 + \beta_2 x + \gamma_2 y)$$

$$N_3(x,y) = \frac{1}{2A}[(x_1y_2 - x_2y_1) + (y_1 - y_2)x + (x_2 - x_1)y] = \frac{1}{2A}(\alpha_3 + \beta_3 x + \gamma_3 y)$$

$$N = [N_1(x,y) \quad N_2(x,y) \quad N_3(x,y)]$$

$$N = \frac{1}{2A}[(\alpha_1 + \beta_1 x + \gamma_1 y) \quad (\alpha_2 + \beta_2 x + \gamma_2 y) \quad (\alpha_3 + \beta_3 x + \gamma_3 y)]$$

Where $A = det\begin{bmatrix}1 & x_1 & y_1\\ 1 & x_2 & y_2\\ 1 & x_3 & y_3\end{bmatrix}$

And the required partial derivatives are,

$$\frac{\partial N_1}{\partial x} = \frac{1}{2A}(y_2 - y_3) = \frac{\beta_1}{2A}$$

$$\frac{\partial N_2}{\partial x} = \frac{1}{2A}(y_3 - y_1) = \frac{\beta_2}{2A}$$

$$\frac{\partial N_3}{\partial x} = \frac{1}{2A}(y_1 - y_2) = \frac{\beta_3}{2A}$$

$$\frac{\partial N_1}{\partial y} = \frac{1}{2A}(x_3 - x_2) = \frac{\gamma_1}{2A}$$

$$\frac{\partial N_2}{\partial y} = \frac{1}{2A}(x_1 - x_3) = \frac{\gamma_2}{2A}$$

$$\frac{\partial N_3}{\partial y} = \frac{1}{2A}(x_2 - x_1) = \frac{\gamma_3}{2A}$$

The strain displacement matrix is,

$$B = \begin{bmatrix} \frac{\partial N_1}{\partial x} & 0 & \frac{\partial N_2}{\partial x} & 0 & \frac{\partial N_3}{\partial x} & 0 \\ 0 & \frac{\partial N_1}{\partial y} & 0 & \frac{\partial N_2}{\partial y} & 0 & \frac{\partial N_3}{\partial y} \\ \frac{\partial N_1}{\partial y} & \frac{\partial N_1}{\partial x} & \frac{\partial N_2}{\partial y} & \frac{\partial N_2}{\partial x} & \frac{\partial N_3}{\partial y} & \frac{\partial N_3}{\partial x} \end{bmatrix}$$

B

$$= \frac{1}{2A}\begin{bmatrix} (y_2 - y_3) & 0 & (y_3 - y_1) & 0 & (y_1 - y_2) & 0 \\ 0 & (x_3 - x_2) & 0 & (x_1 - x_3) & 0 & (x_2 - x_1) \\ (x_3 - x_2) & (y_2 - y_3) & (x_1 - x_3) & (y_3 - y_1) & (x_2 - x_1) & (y_1 - y_2) \end{bmatrix}$$

$$B = \frac{1}{2A}\begin{bmatrix} \beta_1 & 0 & \beta_2 & 0 & \beta_3 & 0 \\ 0 & \gamma_1 & 0 & \gamma_2 & 0 & \gamma_3 \\ \gamma_1 & \beta_1 & \gamma_2 & \beta_2 & \gamma_3 & \beta_3 \end{bmatrix}$$

Material constants matrix is,

$$D = \frac{E}{(1+v)(1-2v)}\begin{bmatrix} 1-v & v & 0 \\ v & 1-v & 0 \\ 0 & 0 & \frac{1-2v}{2} \end{bmatrix}$$

$$\text{Element stiffness matrix } k^{(e)} = V^e[B]^T[D][B]$$

Where $k^{(e)} =$

$$At(\tfrac{1}{2A})\begin{bmatrix} \beta_1 & 0 & \gamma_1 \\ 0 & \gamma_1 & \beta_1 \\ \beta_2 & 0 & \gamma_2 \\ 0 & \gamma_2 & \beta_2 \\ \beta_3 & 0 & \gamma_3 \\ 0 & \gamma_3 & \beta_3 \end{bmatrix}\frac{E}{(1+v)(1-2v)}\begin{bmatrix} 1-v & v & 0 \\ v & 1-v & 0 \\ 0 & 0 & \frac{1-2v}{2} \end{bmatrix}\frac{1}{2A}\begin{bmatrix} \beta_1 & 0 & \beta_2 & 0 & \beta_3 & 0 \\ 0 & \gamma_1 & 0 & \gamma_2 & 0 & \gamma_3 \\ \gamma_1 & \beta_1 & \gamma_2 & \beta_2 & \gamma_3 & \beta_3 \end{bmatrix}$$

Element mass matrix $m_e = \int_{A_e} \rho t [N]^T [N] dA = \frac{\rho t A}{12} \begin{bmatrix} 2 & 0 & 1 & 0 & 1 & 0 \\ 0 & 2 & 0 & 1 & 0 & 1 \\ 1 & 0 & 2 & 0 & 1 & 0 \\ 0 & 1 & 0 & 2 & 0 & 1 \\ 1 & 0 & 1 & 0 & 2 & 0 \\ 0 & 1 & 0 & 1 & 0 & 2 \end{bmatrix}$

And the assembly matrix is,

$$[M]\left[\ddot{U}\right] + [K][U] = 0$$

$$|[K] - \omega^2[M]| = 0$$

Where $U = A_x e^{i(\boldsymbol{k_x}.\boldsymbol{x} - \omega t)} + A_y e^{i(\boldsymbol{k_y}.\boldsymbol{y} - \omega t)}$

The above modal equations are solved by COMSOL to predict all the possible mode shapes present in the PhnC in terms of frequency and wave vector. The equations presented in this section are referenced from textbooks [49, 50].

5.3 FREQUENCY BAND STRUCTURE ANALYSIS

In this section the frequency band structure of a 2D Epoxy-CNT Phononic crystal is calculated using COMSOL FEM code. The crystal has a unit cell of size 10X10 mm^2 and cylinder radius of 4.6 mm adding up to 67% volume fraction. This volume fraction was found to be the optimum to achieve the widest band gap and was calculated by back calculations using the band structure figures. Bloch-Floquet periodic boundary conditions are applied on the external edges of the unit cell to reflect periodicity. Plane strain quadrilateral elements are used to calculate the band structure of the finite element model. A parametric sweep is performed for the Bloch wave vector components in the boundaries of the Brillouin zone with PARADISO Eigen matrix solver. Up to 40 Eigen frequencies are requested for each wave vector iteration and the frequency bands are calculated.

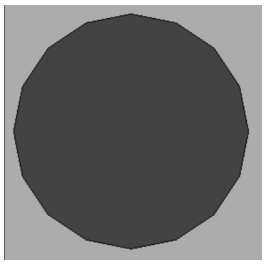

Figure 5.7 Unit cell of 2D Epoxy-CNT Phononic crystal

Figure 5.7 shows the geometry of a single unit cell of 2D Phononic crystal. The grey area represents Epoxy matrix and the darker area represents idealized CNT cylinder inclusions. The cylindrical inclusions are assumed to be of infinite length in the out-of-plane direction.

Table 5.1 Material properties of 2D Epoxy-CNT Phononic crystal

Material	Elastic Modulus (GPa)	Density (kg/m3)	Poisson ratio
Epoxy	7.4	1142	0.35
CNT	1000	2000	0.30

Table 5.1 shows the material properties of Epoxy and carbon nanotube cylinders. These material properties are sufficient for linear finite element calculations and are used to demonstrate the analysis technique for vastly different material properties.

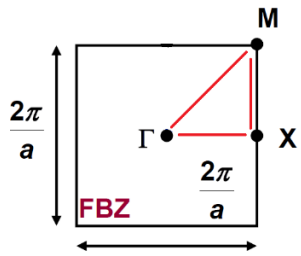

Figure 5.8 First irreducible Brillouin zone of a 2D square lattice

For 2D Phononinc crystals, the wave vector can assume any angle between 0^o to 360^o in the plane of the PhC. Because of symmetry and repetition of the Eigen modes, it is enough to sweep the wave vector along the boundary of first irreducible Brillouin zone. This is represented by the red triangle TXM in Figure 5.8 and the wave vector is swept along the boundaries TX, XM and TM. Density of states can also be obtained by scanning the entire area of the triangle but only the boundaries are enough for frequency band gap calculations. For boundary TX, the x-component of the wave vector assumes a value between 0 to π/a and the y-component assumes a value of 0. For boundary XM the x-component of the wave vector assumes a value of π/a and the y-component assumes a value of 0 to π/a. For boundary TM the x-component of the wave vector assumes a value between 0 to π/a and the y-component assumes a value between 0 to π/a. Scanning along all these boundaries generates a frequency band structure.

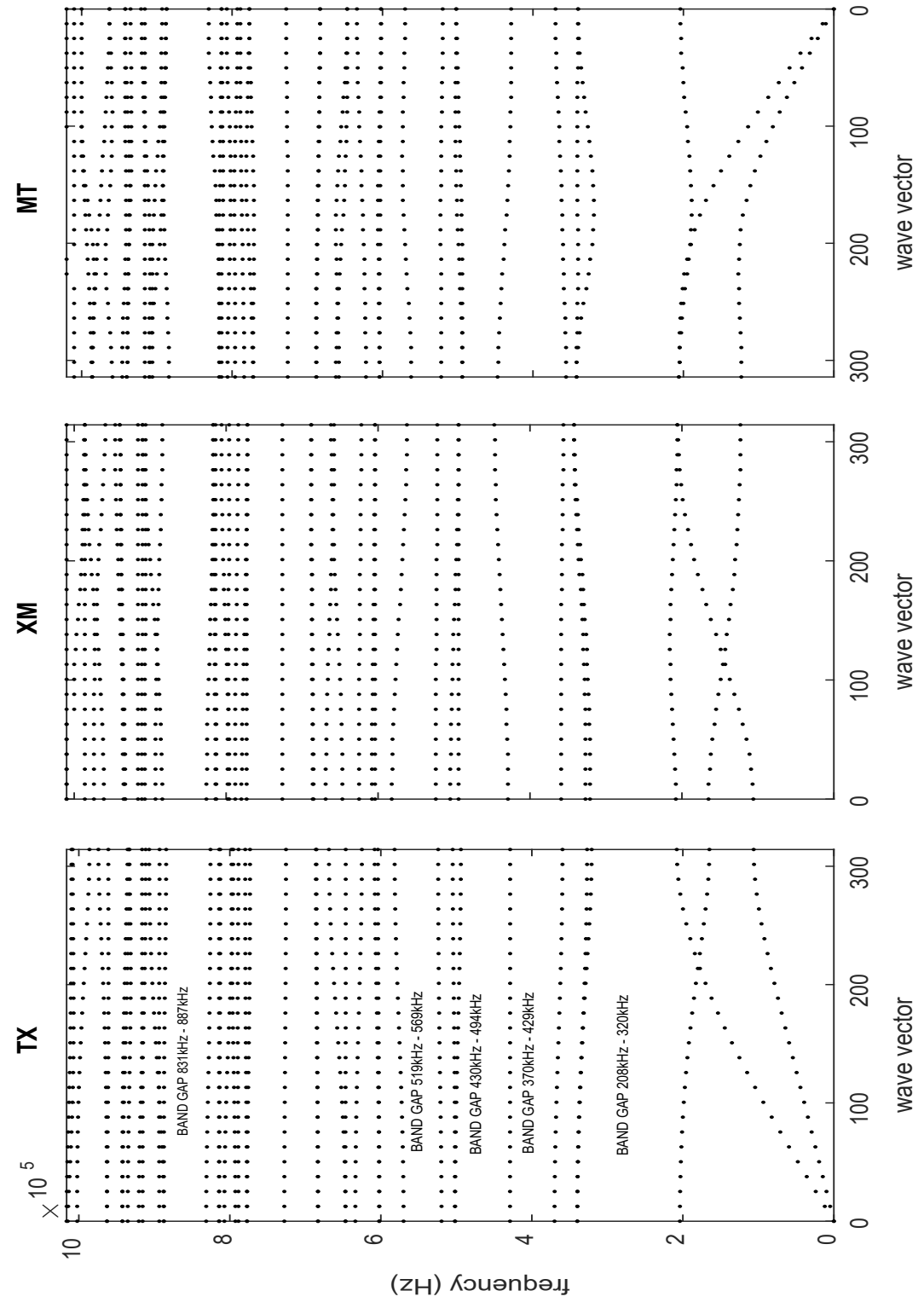

Figure 5.9 Frequency band structure of 2D Epoxy-CNT Phononic crystal

As seen from Figure 5.9, there are multiple complete band gaps in the Epoxy-CNT Phononic crystal and the widest gap is in the range of 208kHz to 320kHz. In this complete frequency band gap , the periodic structure acts as an effective mirror for the incoming wave frequencies. Further complete band gaps occur in the range of 370kHz - 429kHz, 430kHz - 494kHz, 519kHz - 569kHz and 831kHz - 887kHz. These multiple frequency band gaps present the epoxy-CNT Phononic crystal as a potential candidate for 2D ultrasonic wave attentuation and guiding applications. This range can further be tuned for specific ultrasonic applications as desired by changing the size of the unit cell as shown in Figure 5.10.

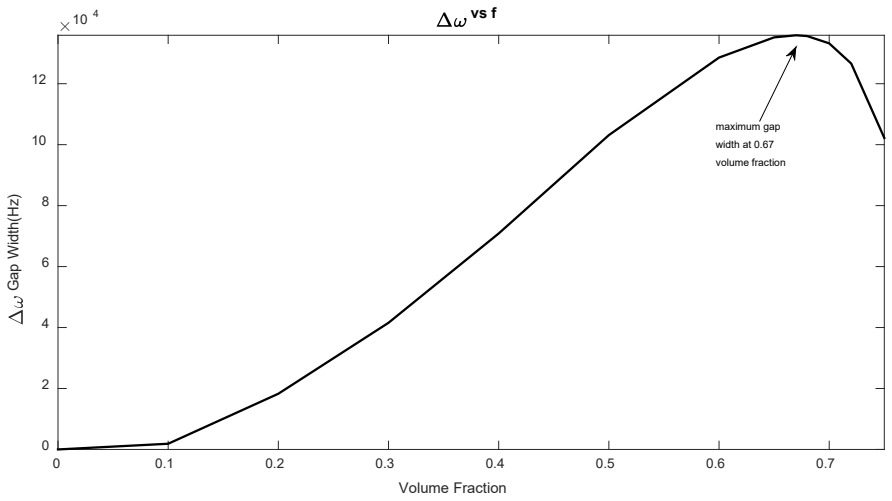

Figure 5.10 Optimum CNT cylinder volume fraction for achieving widest single band gap ($x10^4$)

Figure 5.10 shows the optimum volume fraction to achieve the widest band gap and was back calculated using the multiple band structure figures. As can be seen from the figure, at 10% volume fraction, the band gap starts to open up and constantly increases up to 67% volume fraction and drops down after further increase. At 67% the width of the band gap reaches its maximum and decreases after further increasing volume fraction.

The band gap figures are further correlated with the frequency response and stress attenuation analysis using ABAQUS finite element code. The amplitude drops in frequency response analysis are correlated with band structure figures and a wave attenuation analysis is performed to study the attenuation properties. Also, ultrasonic frequency wave guides and vibration absorbers are designed and analyzed as part of the study for building suitable ultrasonic applications.

The previous results tell us what frequencies and wave vectors the Phononic crystal can allow or block, but does not give any physical insight into the mode shapes. It is important to know the mode shapes associated with these frequencies and wave vectors at which it will vibrate. Figure 5.11 gives us a physical insight into how the structure vibrates at the predicted frequencies and wave vectors.

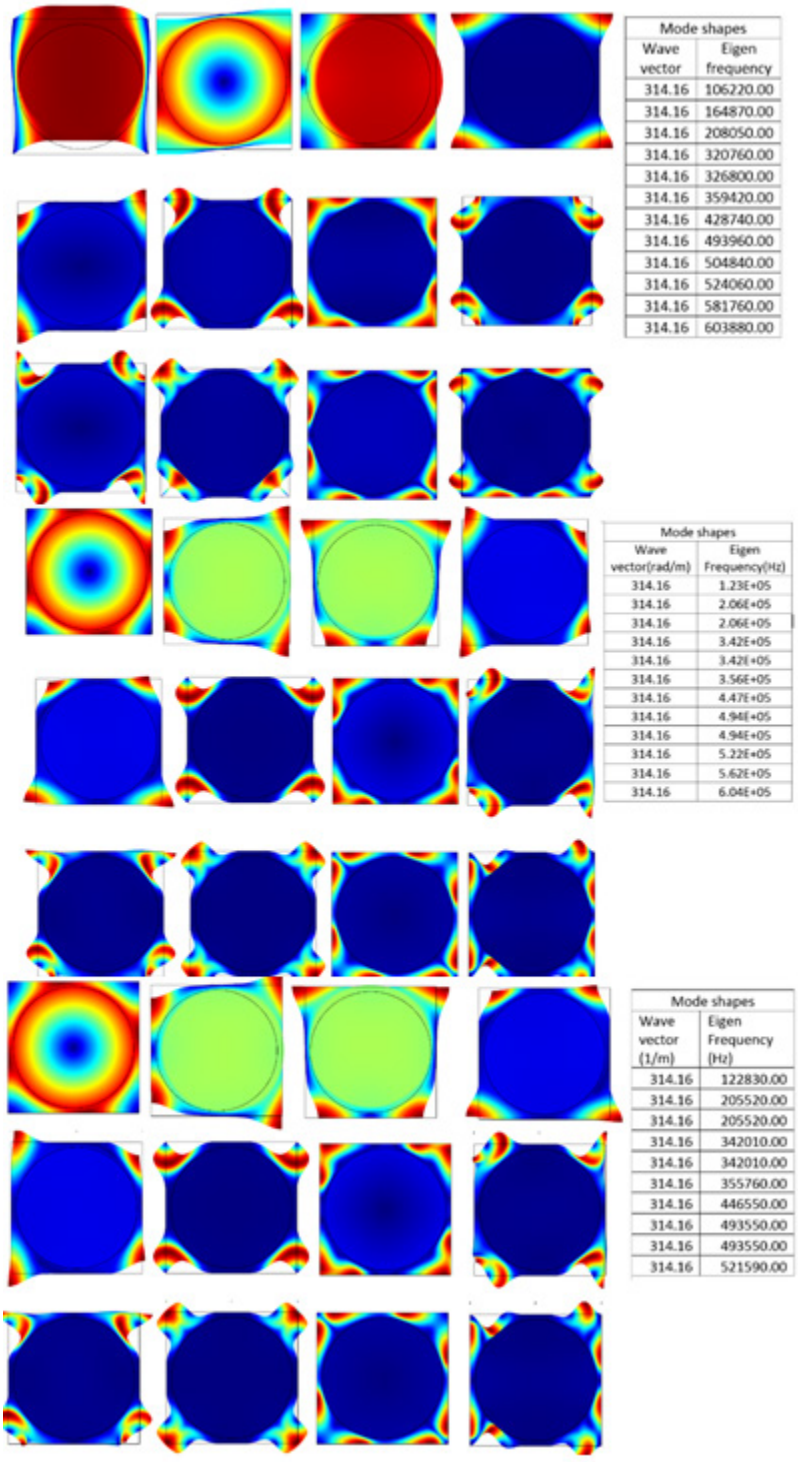

Mode shapes	
Wave vector	Eigen frequency
314.16	106220.00
314.16	164870.00
314.16	208050.00
314.16	320760.00
314.16	326800.00
314.16	359420.00
314.16	428740.00
314.16	493960.00
314.16	504840.00
314.16	524060.00
314.16	581760.00
314.16	603880.00

Mode shapes	
Wave vector(rad/m)	Eigen Frequency(Hz)
314.16	1.23E+05
314.16	2.06E+05
314.16	2.06E+05
314.16	3.42E+05
314.16	3.42E+05
314.16	3.56E+05
314.16	4.47E+05
314.16	4.94E+05
314.16	4.94E+05
314.16	5.22E+05
314.16	5.62E+05
314.16	6.04E+05

Mode shapes	
Wave vector (1/m)	Eigen Frequency (Hz)
314.16	122830.00
314.16	205520.00
314.16	205520.00
314.16	342010.00
314.16	342010.00
314.16	355760.00
314.16	446550.00
314.16	493550.00
314.16	493550.00
314.16	521590.00

Figure 5.11 Mode shapes for band structure calculations

5.4 FREQUENCY RESPONSE ANALYSIS

In this section the frequency response of a 2D Epoxy-CNT Phononic crystal is calculated using ABAQUS's finite element explicit code. The PhnC of size 60X50 mm^2 with 6X5 array of CNT cylinders was considered for the FEM analysis. The same unit cell size of 10X10 mm^2 and CNT volume fraction of 67% are used. The top and bottom edges of the FEM model are constrained in the Y direction in order to prevent the PhnC from moving up and down. A 1-micron displacement input in the X direction for a frequency range of 100 kHz to 1000 kHz is applied at the left edge. The displacement at the right edge is measured in dB scale in order to measure the relative response attenuation in the frequency range. CPE4R Plane strain quadrilateral elements are used to calculate the frequency response of the finite element model. A frequency sweep is performed with the specified displacement with LANCZOS Eigen matrix solver. The sampling is done at 1 kHz interval in order to better capture the dips in amplitudes. Figures 5.12 and 5.13 show the geometry of the 2D PhnC used for frequency response analysis.

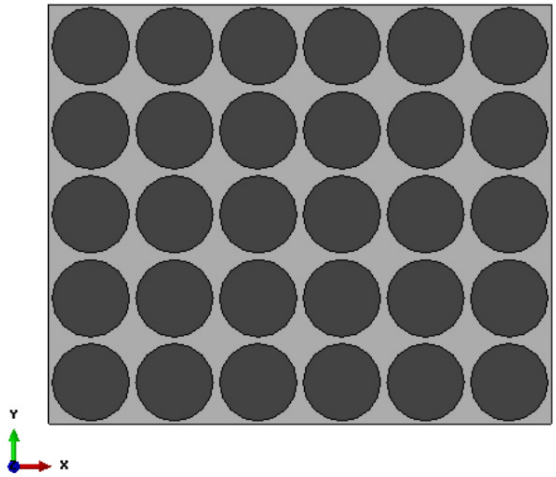

Figure 5.12 Array of CNT cylinders embedded in Epoxy matrix

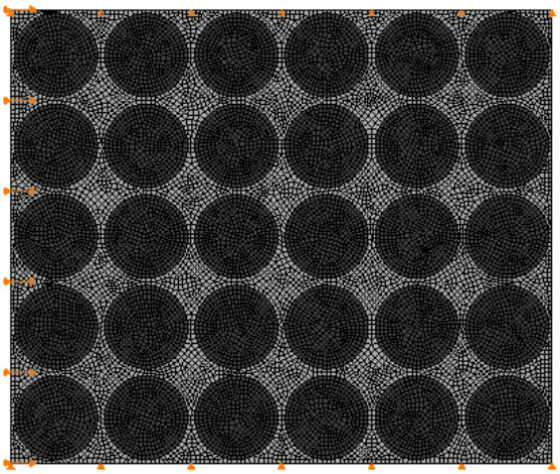

Figure 5.13 FEM boundary conditions for the finite element model

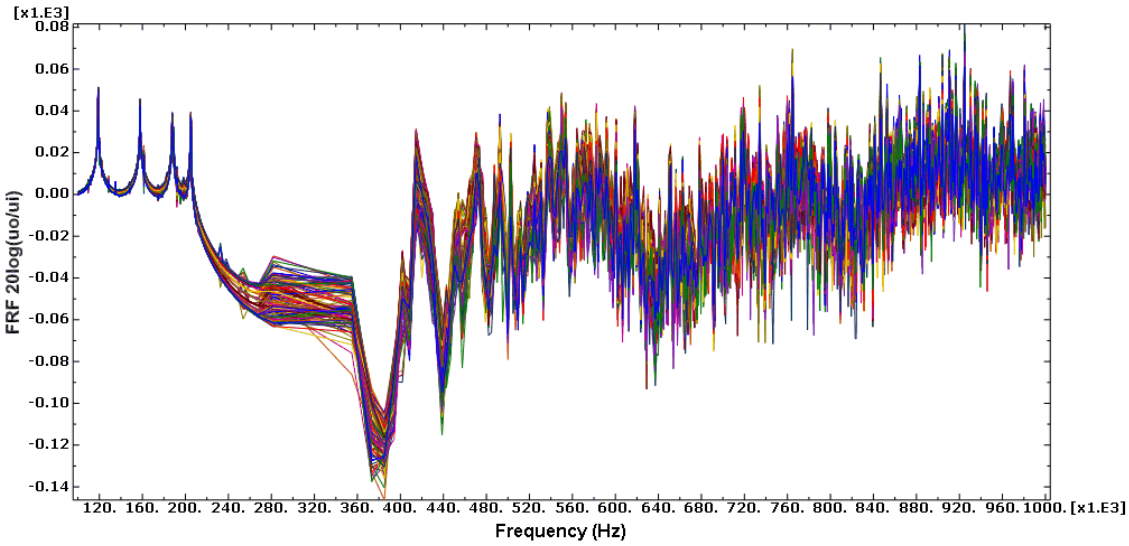

Figure 5.14 Frequency response for Epoxy-CNT PhnC (x10^3)

A 20dB log scale is used to measure the relative response at the right end of the PhnC. As seen from the frequency response Figure 5.14, the response starts to drop right at 208kHz and continues decreasing as predicted by band structure calculations. This response drop continues and reaches its lowest at -140 dB on a 20dB log scale. The band gaps calculated are in the range of 208kHz- 320kHz, 370kHz - 429kHz, 430kHz – 494kHz, 519kHz-569kHz and 831kHz – 887kHz. This band gap data aligns well with the frequency response figures showing that attenuation can be achieved by the idealized Epoxy-CNT Phononic crystal. This presents the Epoxy-CNT Phononic crystal as an effective vibration absorber.

5.5 WAVE ATTENUATION ANALYSIS

In this section the wave attenuation in a 2D Epoxy-CNT PhnC is calculated using ABAQUS's finite element explicit code. A 270 kHz frequency is chosen as the input, as this frequency falls right in the center of the widest band gap predicted by band structure calculations. The PhnC of size 60X60 mm^2 with 6X5 array of idealized CNT cylinders was considered for the wave attenuation analysis. The same unit cell size of 10X10 mm^2 and CNT volume fraction of 67% are used. The top and bottom edges of the FEM model are constrained in the Y direction in order to prevent the PhnC from moving up and down. The right edge is fixed and a 1MPa normal and transverse pressure of frequency 270 kHz is applied at the left edge. The Von Mises stress for the whole length of the PhnC is measured for stress attenuation characteristics. CPE4R plane strain quadrilateral elements are used to calculate the stress attenuation of the finite element model. The analysis is performed for 1cycle in order to better capture the decay as the wave progresses through the PhnC. Figure 5.15 below shows the geometry of the 2D PhnC used for wave attenuation analysis with material properties shown in Table 5.2.

5.5.1 Normal pressure periodic loading

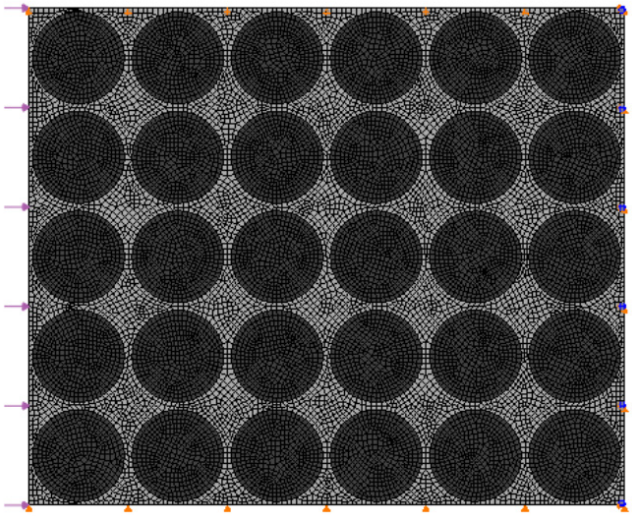

Figure 5.15. FEM model for wave attenuation analysis

Geometry: Length = 0.06 m Phononic crystal Spacing= 0.001 m

Loading: Periodic Loading of 270 KHz frequency and to 1MPa Normal Pressure for **1** Cycle (3.703μ s)

Table 5.2 Material properties for materials

	E (Gpa)	ρ(kg/m3)	ν
Epoxy	7.4	1142	0.35
CNT	1000	2000	0.30

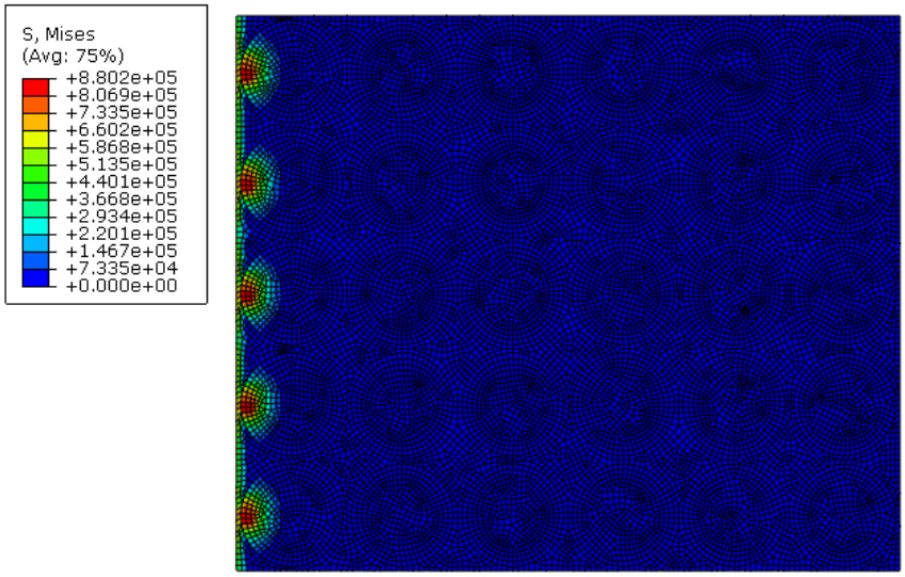

Figure 5.16 Stress propagation in the Phononic crystal (First frame of analysis)

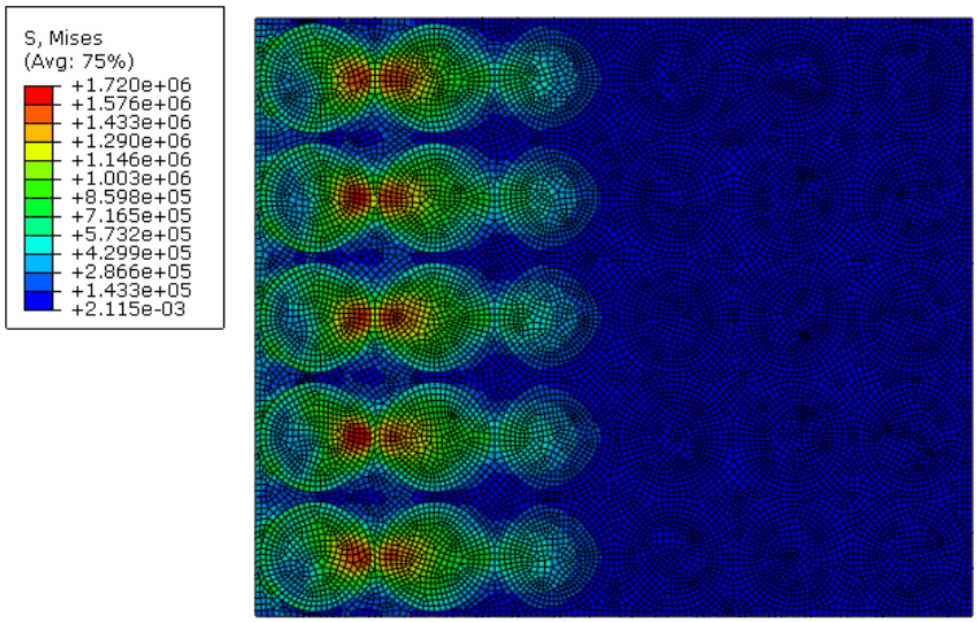

Figure 5.17 Stress propagation in the Phononic crystal (Last frame of analysis 3.703µs)

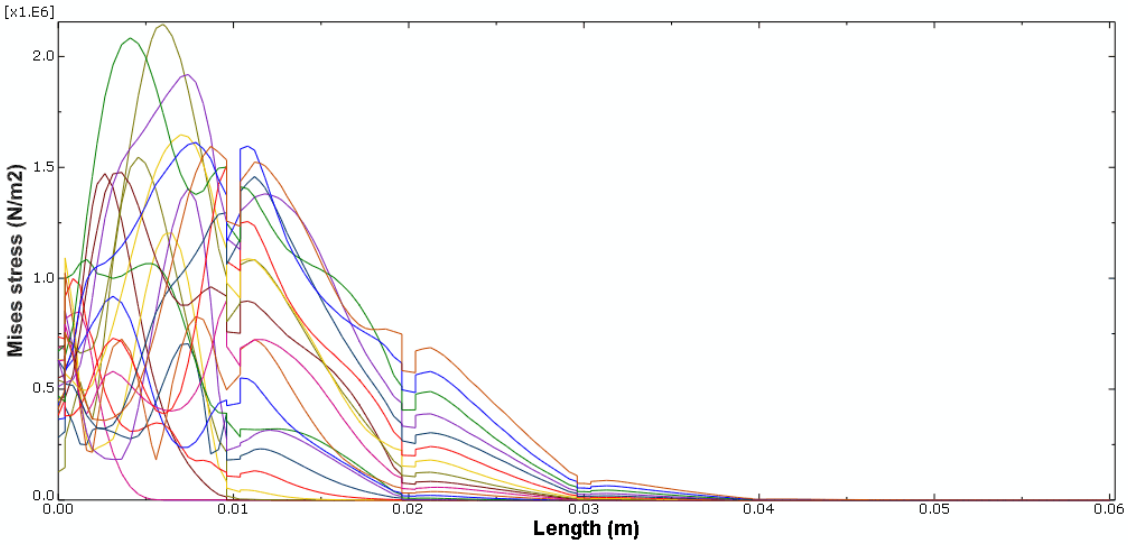

Figure 5.18 Applied Normal stress attenuation in the Phononic crystal (All frames of the analysis)

Analysis of attenuation characteristics of 2D PhnC are critical for sound and vibration isolation. As seen from Figures 5.16-5.18, the applied normal stress decays exponentially and correlates well with the band gap and frequency response data. Reflections from

normal stress can be seen to occur at the interface between Epoxy and CNT cylinders. These reflections develop interfacial stresses and can lead to delamination of the PhnC. The highest interfacial stress developed is about 150% of the applied normal stress. Interfacial stresses could be even more higher when the PhnC is subjected to multiple cycles of loading. It is important that the interfacial stresses developed in the PhnC lie well below the interface bond strength. Attenuation properties of a real specimen can differ slightly since the finite element code assumes a perfect interface. Strong bonding between Epoxy and CNT cylinders is crucial for the performance of phononic crystals. A weak interface would not transfer strains effectively between the layers and thereby reduces the acoustic properties. Based on the results, adding more layers is suggested to attenuate the input pulse from propagating through the whole length of the composite. Many layers ensure that the traveling wave encounters as many impedance mismatches as possible to reduce the transfer of acoustic energy. 2D Epoxy-CNT PhnCs can be used as effective acoustic mirrors and vibration absorbers in the ultrasonic range.

5.5.2 Transverse pressure periodic loading

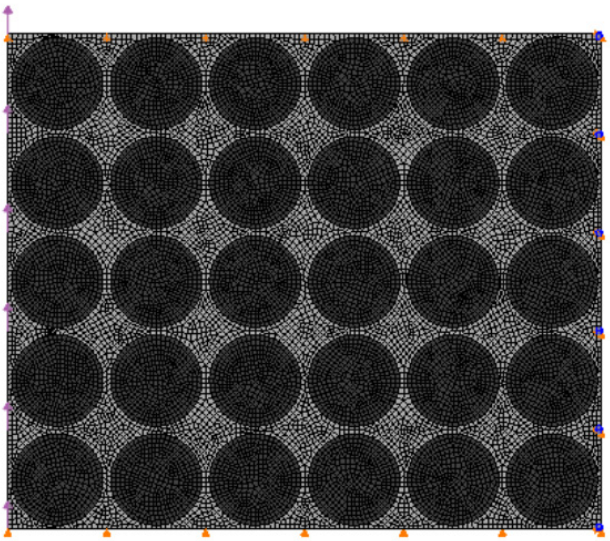

Figure 5.19. Geometry of a 1D periodic Phononic crystal

Geometry: Length = 0.06 m Phononic crystal gap spacing= 0.001 m

Loading: Periodic Loading of 270 KHz frequency subjected to 1MPa Transverse Pressure for **1** Cycle (3.703µs)

Table 5.3 Material properties for materials

	E (GPa)	ρ(kg/m3)	ν
Epoxy	7.4	1142	0.35
CNT	1000	2000	0.30

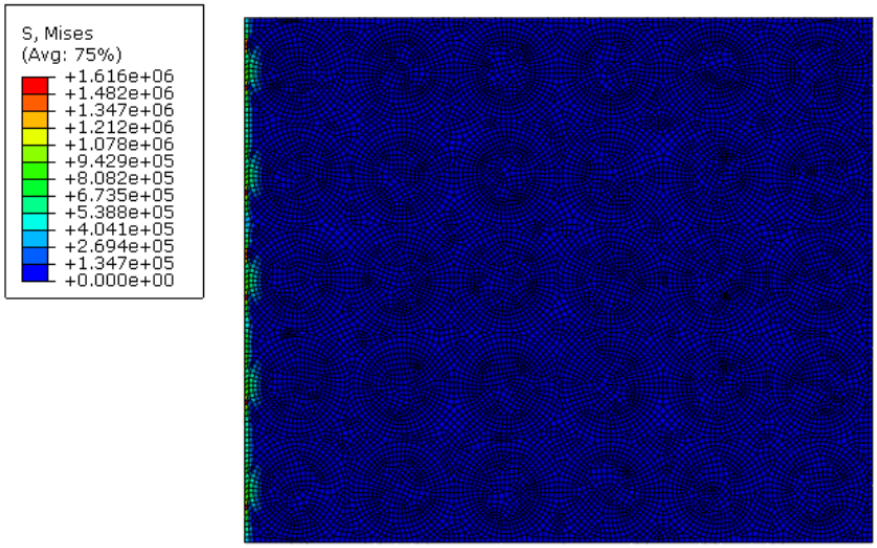

Figure 5.20 Stress propagation in the Phononic crystal (First frame of analysis)

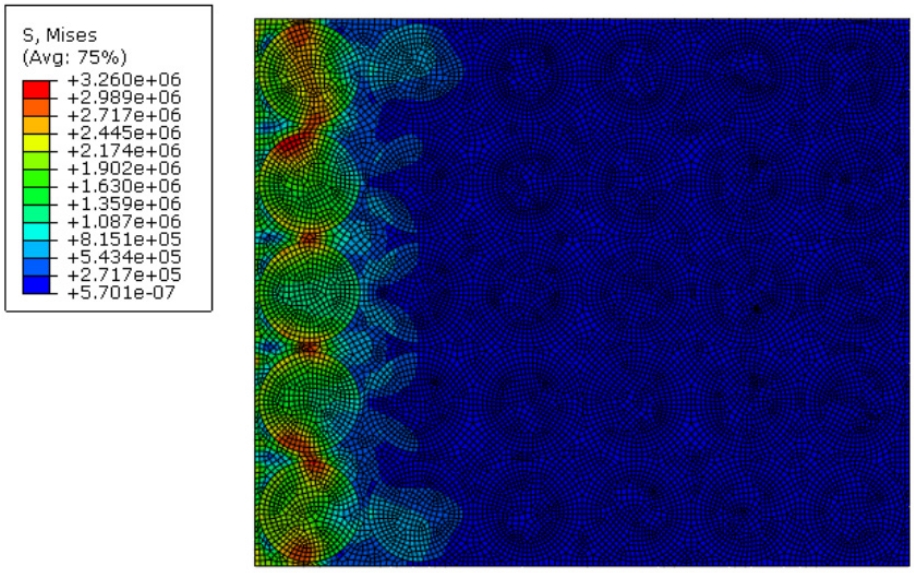

Figure 5.21 Stress propagation in the Phononic crystal (Last frame of analysis 3.703µs)

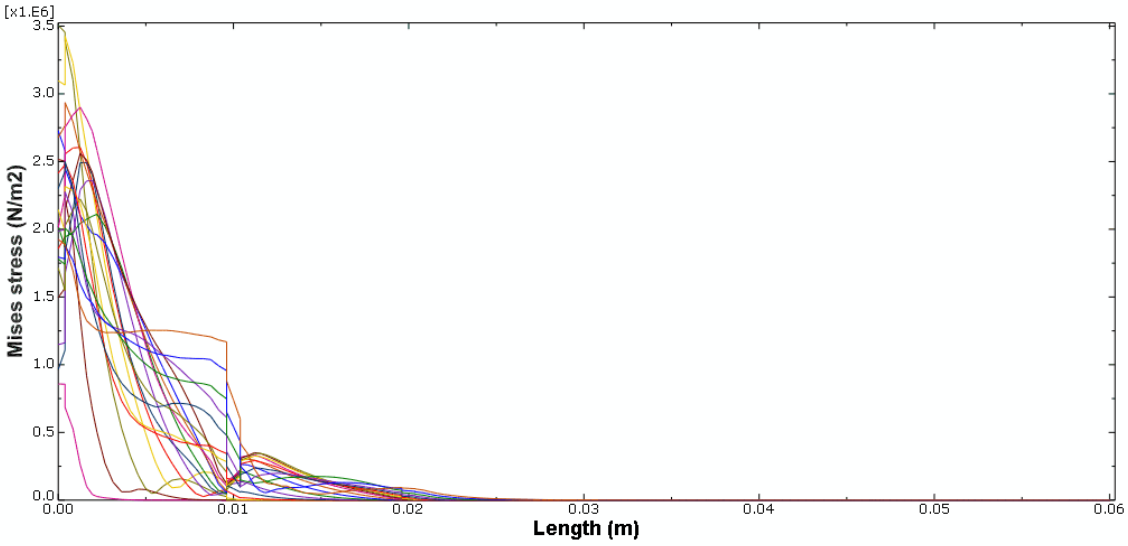

Figure 5.22 Applied transverse stress attenuation in the Phononic crystal (All frames of the analysis)

As seen from Figures 5.20-5.22, the applied transverse stress decays exponentially as it progresses through the PhnC and correlates well with the band gap and frequency response data. It can be observed that transverse wave type attenuates more than the normal wave type. Reflections from transverse stress can be seen to occur at the interface between CNT and Epoxy layers. These reflections develop interfacial stresses and can lead to delamination of the PhnC. It is important that the interfacial stresses developed in the PhnC lie well below the bond shear strength.

5.6 CONCLUSION

As seen from the results, the Epoxy-CNT Phononic crystals have the potential to be used as frequency filters, vibration absorbers, sound isolators and wave guides in the ultrasonic frequency range. They have very large band gap capabilities with multiple frequency band gaps spanning the ultrasonic frequency range. For vibration and sound isolation these idealized PhnCs can register a large drop in response, to as low as -140dB on 20dB log scale. These Phononic crystals can also be used for stress attenuation and mitigation applications causing an exponential decay of the applied stress wave.

6 THREE DIMENSIONAL EPOXY-CNT PHONONIC CRYSTAL

6.1 INTRODUCTION

Three dimensional Phononic crystals are periodic in three directions. In this section, idealized CNT spheres embedded in epoxy matrix will be analyzed. Unlike 1D and 2D Phononic crystals, in which a complete band gap is easier to exist. In 3D Phononic crystals, it is rather hard to find a complete Phononic band gap. The main reason being Eigen modes can occur in unidirectional and coupled mode shapes. Nevertheless, as shown partial band gaps do exist in these crystals. If a complete Phononic band gap exists, these Phononic crystals can either block or guide incoming waves not only in one direction but in all the directions, thus representing a complete wave isolator i.e. an acoustic black hole. The wave vector components can assume any value in the three directions and a complete band gap must also be searched in all the directions. Bloch Floquet boundary conditions are used to reflect the periodicity of the Phononic crystal. The band gap diagrams for 3D Phononic crystals are calculated using parametric FEM solver COMSOL. To correlate the band gap data, frequency response analysis is performed in ABAQUS.

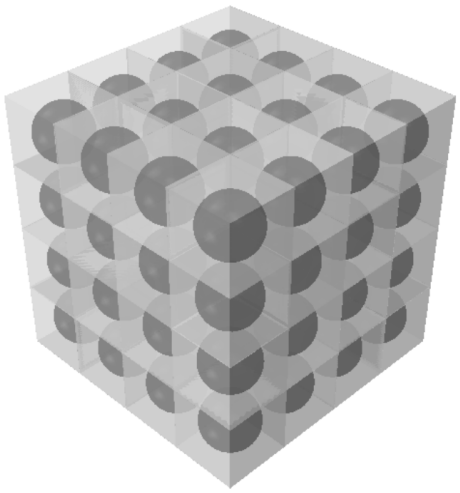

Figure 6.1 3D Epoxy-CNT Phononic crystal

Figure 6.1 shows the “carbon nanotube spheres” embedded in epoxy matrix. Epoxy-CNT unit cell is of size 10X10X10 mm^3 and CNT spheres of radius 4.85 mm with a 27% volume fraction. A 40X40X40 mm^3 cube is shown.

6.2 BAND STRUCTURE ANALYSIS

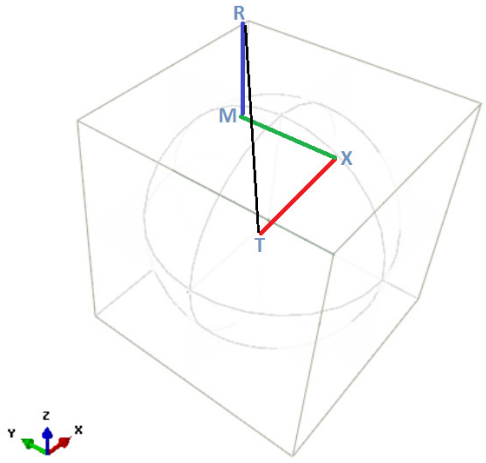

Figure 6.2 Brillouin zone of a simple cubic lattice

For 3D Phononinc crystals, the wave can travel in all three directions. Because of symmetry and repetition of the Eigen modes, it is enough to sweep the wave vector along the boundary of the first irreducible Brillouin zone as depicted in Figure 6.2. This is represented by the lines TXMR and the wave vector is swept along the boundaries TX, XM,MR and TR. Density of states can also be obtained by scanning the entire volume but only the boundaries are enough for frequency band gap calculations. For boundary TX, the x-component of the wave vector assumes a value between 0 to π/a , the y-component assumes a value of 0 and the z-component assumes a value of 0 . For boundary XM the x-component of the wave vector assumes a value of π/a , y-component assumes a value between 0 to π/a and the z-component assumes a value of 0. For boundary MR the x-component of the wave vector assumes a value of π/a , y-component assumes a value of π/a and and the z-component assumes a value of between 0 to π/a . Scanning the wave vector along all these boundaries generates a frequency band diagram.

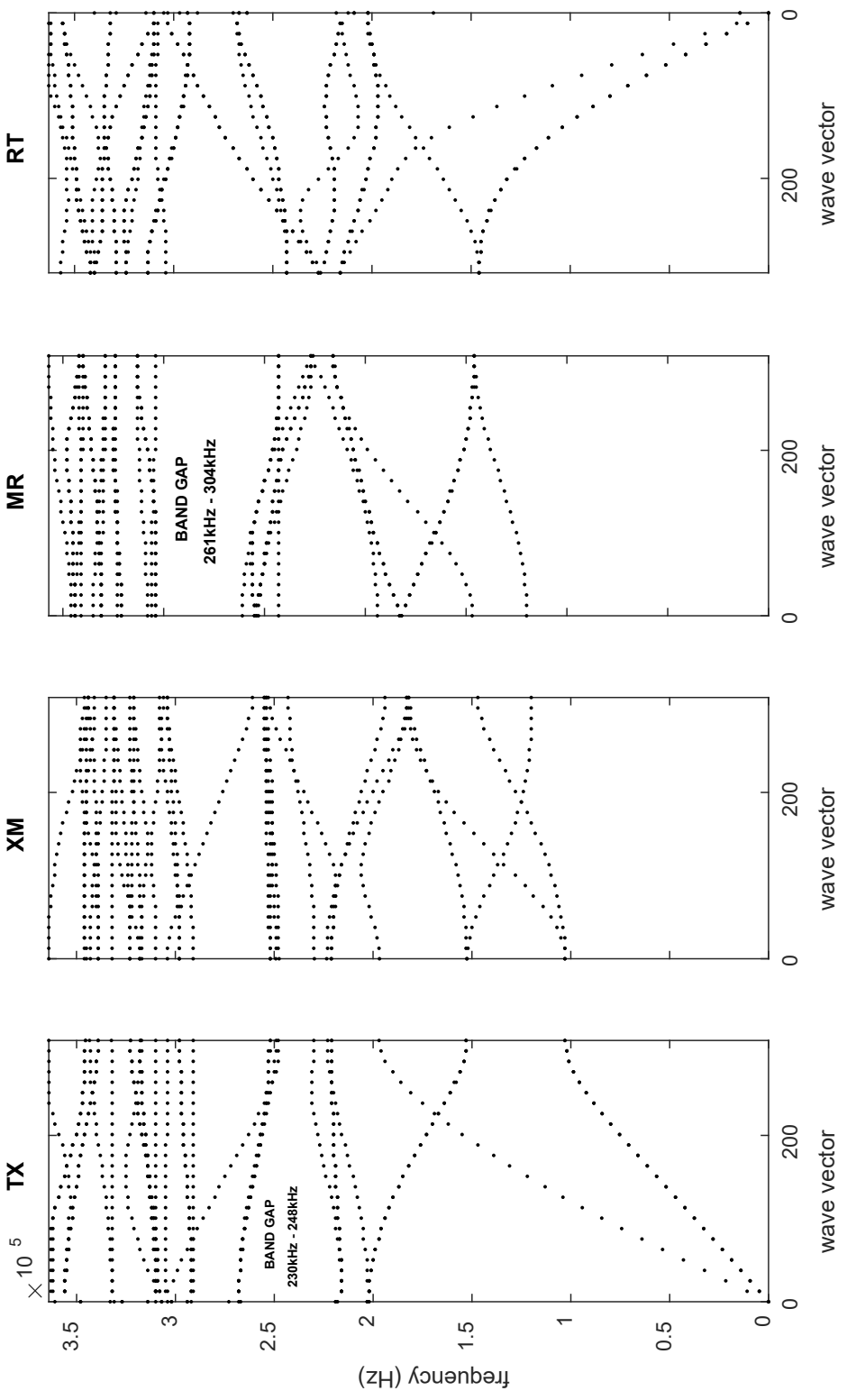

Figure 6.3 Frequency band structure of 3D Epoxy-CNT Phononic crystal

As seen from Figure 6.3, there are no complete band gaps in the 3D Epoxy-CNT Phononic crystal but there are two partial band gaps in the range of 230kHz - 248kHz and 261kHz - 304 kHz. In these partial band gaps , the periodic structure would attenuate incoming wave frequencies in the TX and MR directions. Further there are no partial band gaps in the XM and RT directions. These partial band gaps could be used to block waves for TX and MR directions for ultrasonic wave attentuation and guiding applications. This range can further be tuned for specific ultrasonic applications as desired by changing the size of the unit cell.

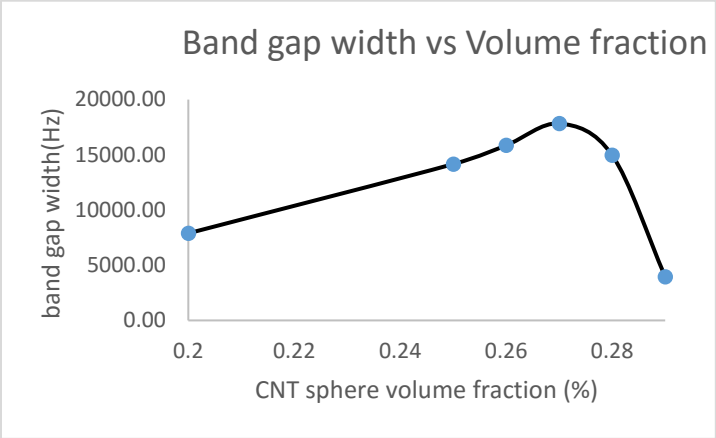

Figure 6.4 Optimum CNT sphere volume fraction for achieving widest band gap

Figure 6.4 shows the optimum volume fraction to achieve the widest band gap in the TX direction and was back calculated using multiple band structure figures. As seen from the figure, the band gap constantly increases from 20% volume fraction to 27% volume fraction and drops after further increase.

The Band structure plot shown in Figure 6.3 tell us what frequencies and wave vectors the Phononic crystal can allow or block, but does not give any physical insight into the mode shapes. It is important to know the mode shapes associated with these frequencies and wave vectors at which it will vibrate. Figures 6.5 and 6.6 gives us a physical insight into how the structure vibrates at the predicted frequencies and wave vectors.

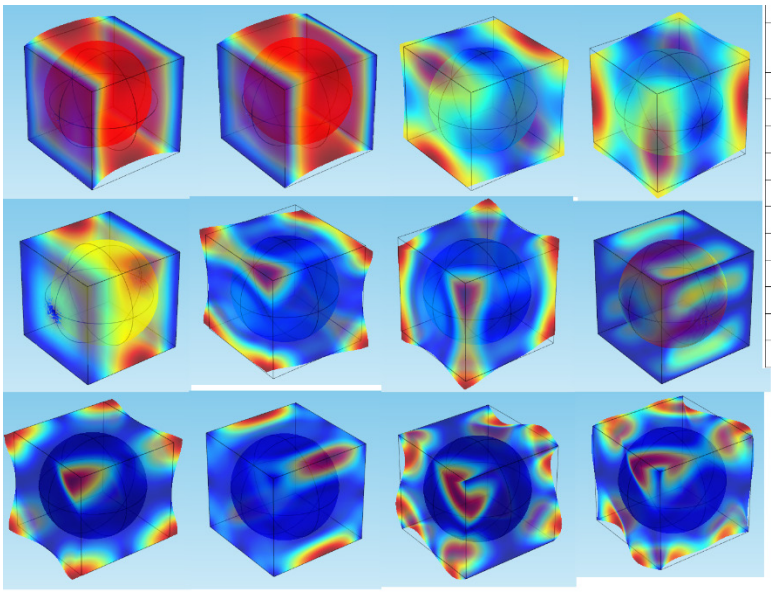

Mode shapes	
Wave vector (1/m)	Eigen Frequency (Hz)
314.16	102990.00
314.16	102990.00
314.16	152500.00
314.16	152560.00
314.16	196760.00
314.16	221100.00
314.16	221130.00
314.16	223460.00
314.16	229690.00
314.16	247520.00
314.16	249180.00

Figure 6.5 Mode shapes of a 3D Epoxy-CNT Phononic crystal

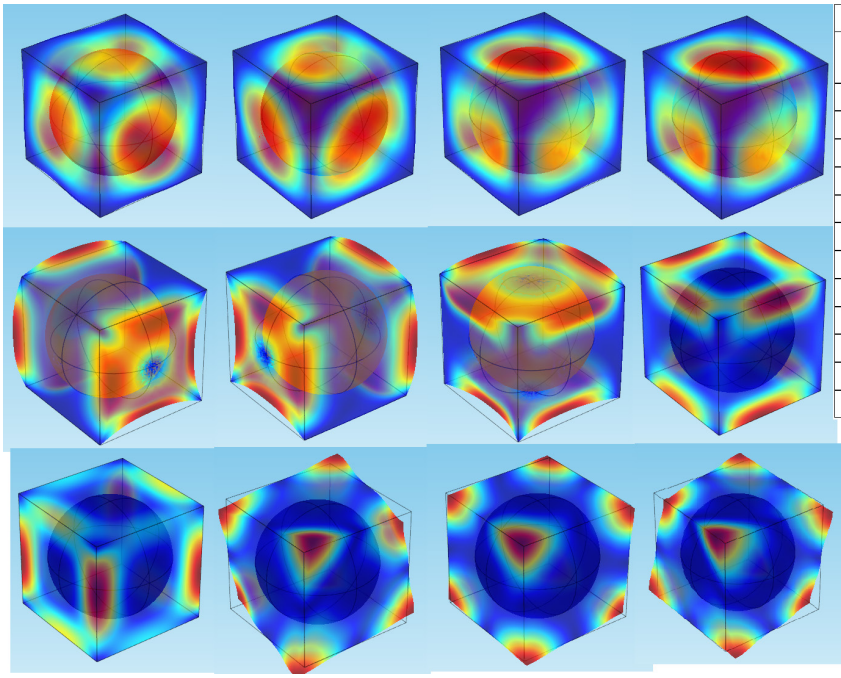

Mode shapes	
Wave vector(1/m)	Eigen frequency(Hz)
314.16	317140.00
314.16	317720.00
314.16	317730.00
314.16	322700.00
314.16	322710.00
314.16	332400.00
314.16	339070.00
314.16	339100.00
314.16	343460.00
314.16	345470.00
314.16	345500.00
314.16	364060.00

Figure 6.6 Mode shapes of a 3D Epoxy-CNT Phononic crystal

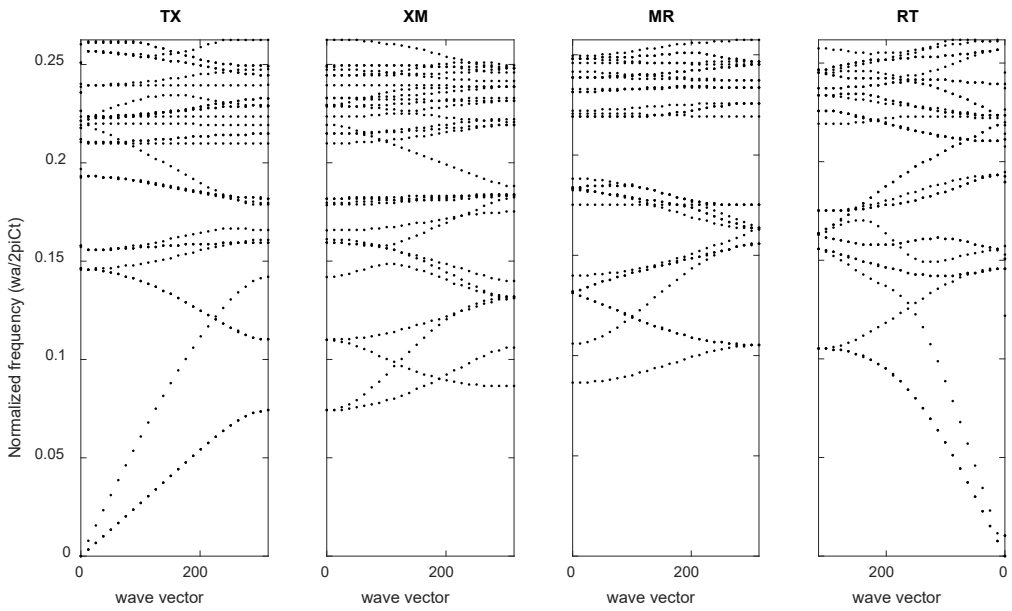

Figure 6.7 Reduced frequency band structure of 3D Epoxy-CNT Phononic crystal

Standard literature use normalized frquency for band structure plots. Figure 6.7 shows the normalized frequency band structure.

6.3 FREQUENCY RESPONSE ANALYSIS

In this section the frequency response of a 3D Epoxy-CNT Phononic crystal is calculated using ABAQUS finite element explicit code. The PhnC of size 30X30X60 mm^3 with 3X3X6 array of CNT spheres was considered for the FEM analysis. The same unit cell size of 10X10X10 mm^3 and CNT sphere volume fraction of 27% are used. The top and bottom faces of the FEM model are constrained in the Y direction and the front and back faces are constrained in the X-direction in order to prevent the PhnC from moving up, down and sideways. A 1-micron displacement input in the Z direction for a frequency range of 150 kHz to 400 kHz is applied at the right face. The displacement at the left face is measured in dB scale in order to measure the relative response attenuation in the frequency range. CHEX8 first order 3D Hex elements are used to calculate the frequency response of the

finite element model. A frequency sweep is performed with the specified displacement with LANCZOS Eigen matrix solver. The sampling is done at 1 kHz interval in order to better capture the dips in amplitudes. Figures 6.8 and 6.9 shows the geometry of the 3D PhnC used for frequency response analysis.

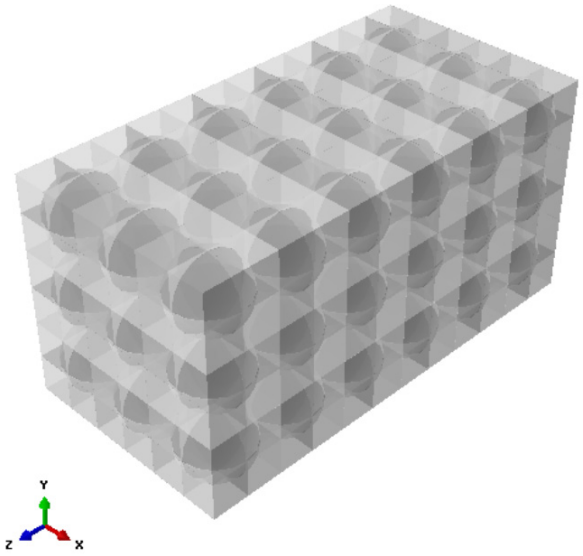

Figure 6.8 Array of CNT spheres embedded in Epoxy matrix

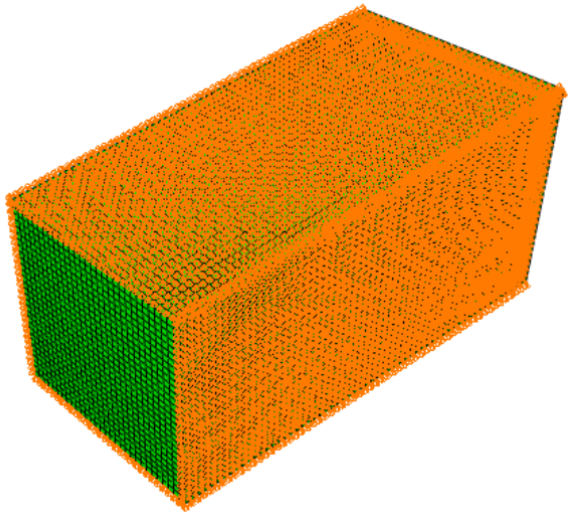

Figure 6.9 FEM boundary conditions for the finite element model

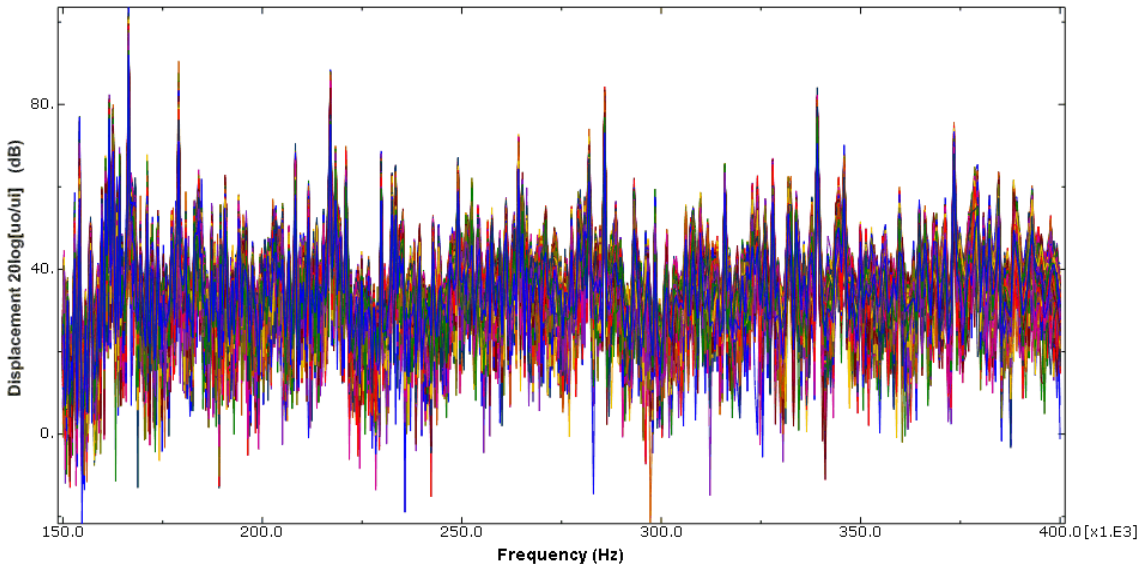

Figure 6.10 Frequency response for 3D Epoxy-CNT Phononic crystal(x10^3)

A 20dB log scale is used to measure the relative response at the right end of the PhnC. As seen from the frequency response in Figure 6.10, the PhnC presents no drop in response for the applied laoding direction. However frequency response analsyses must be performed in all the directions in order to confirm the band structure calcuclations.

7 VIBRATION ISOLATION AND SOUND GUIDING WITH EPOXY-CNT PHONONIC CRYSTALS

7.1 INTRODUCTION

In this section the 2D Epoxy-CNT Phononic crystals are studied for vibration isolation and sound guiding applications. To conduct this study, a vibrating object is placed inside the idealized Epoxy-CNT array by removing one of the cylinders. This object is let to vibrate at a frequency that falls within the band gap and the PhnCs guiding and attenuation properties are studied.

7.2 VIBRATION ISOLATION

In this section, vibration isolation in a 2D Epoxy-CNT PhnC is studied using ABAQUS finite element explicit code. A 270 kHz frequency is chosen as the input, as this frequency falls right in the center of the widest band gap predicted by band structure calculations. The PhnC of size 100X100 mm^2 with 10X10 array of CNT cylinders was considered for the vibration isolation analysis as shown in Figure 7.1. The same unit cell size of 10X10 mm^2 and CNT cylinder volume fraction of 67% and of radius 4.6 mm are used. All the external edges of the FEM model are constrained in order to prevent the PhnC from moving. A vibrating object is simulated by applying a 270 kHz periodic displacement of 1 micron at the center hole of the PhnC with a sensor location as shown in Figure 7.2 to analyze the internal response. This loading is applied for 10 cycles and the displacement at the farther end of the PhnC is measured for vibration isolation characteristics. CPE4R plane strain quadrilateral elements are used to calculate the displacement attenuation of the finite element model. The analysis is performed for 10 cycles in order to better capture the decay as the wave progresses through the PhnC. The figure below shows the geometry of the 2D PhnC used for wave attenuation analysis.

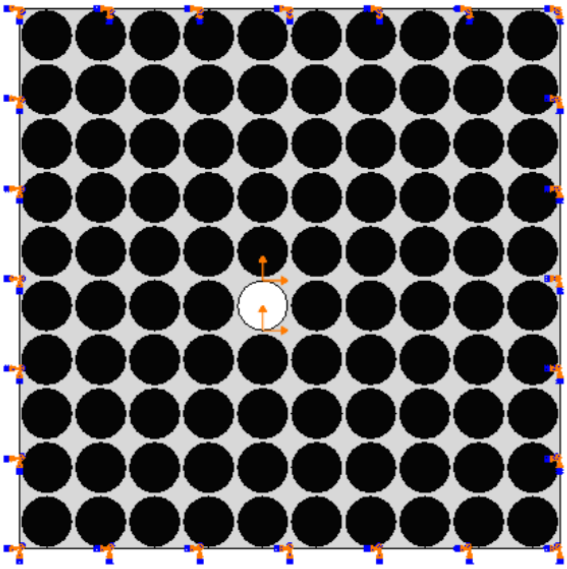

Figure 7.1 Geometry of the PhnC designed for vibration isolation

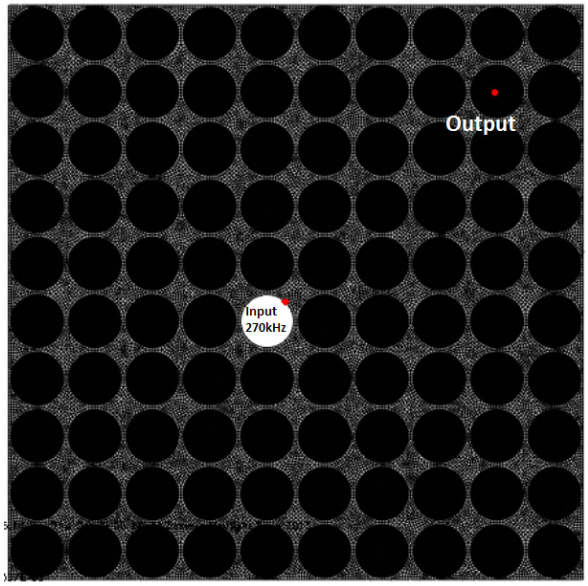

Figure 7.2 FEM model showing the sensor locations

Displacement magnitude at the input and output of the 2D PhnC are compared as shown in Figure 7.3. Displacement magnitude measured at the output is about 10% of the applied input displacement magnitude. This shows that PhnC effectively attenuates the internally generated input displacement.

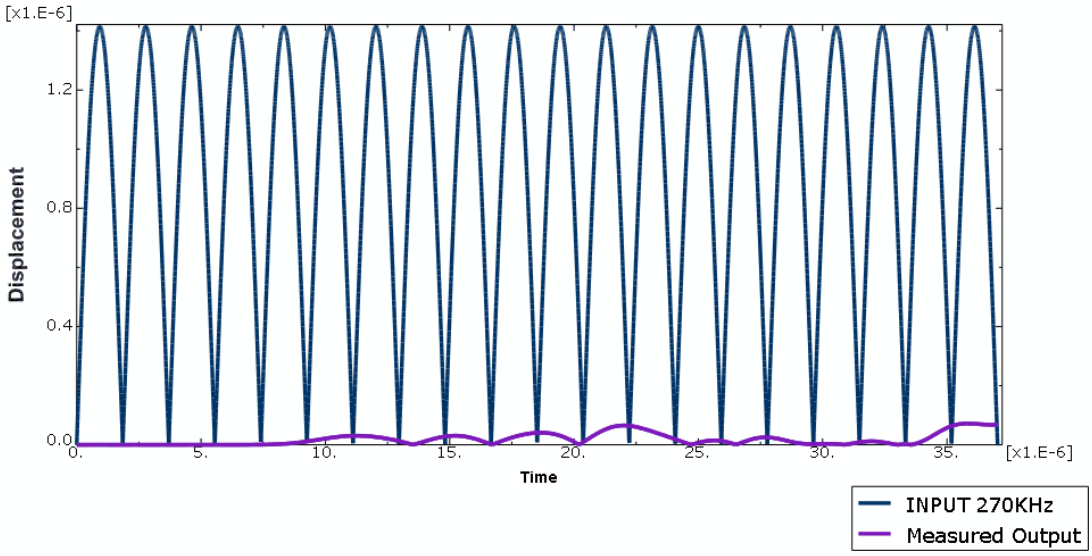

Figure 7.3 Displacement magnitude measured at the input and output (time and displacement x10^{-6})

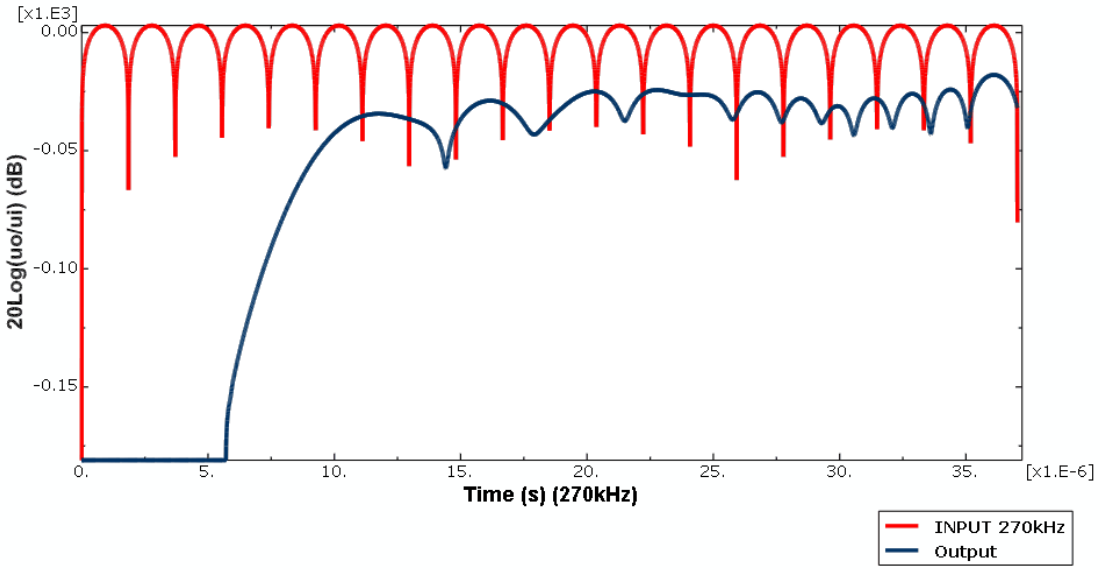

Figure 7.4 Relative response measured at the input and output

Relative response at the input and output of the 2D PhnC are compared as shown in Figure 7.4. Response measured at the output is negative showing that only attenuation of the signal occurs.

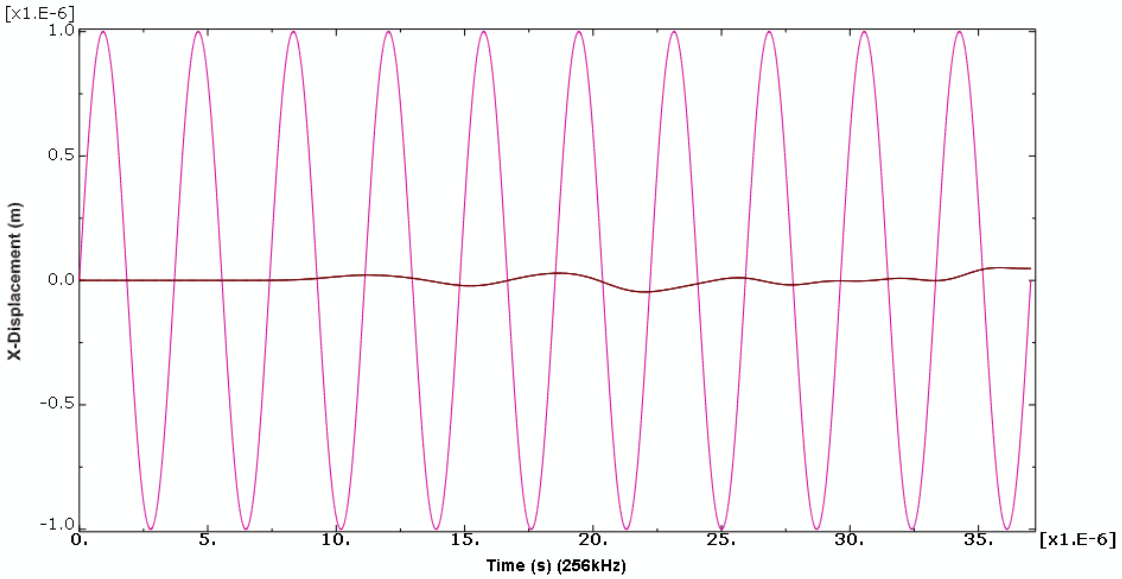

Figure 7.5 X-Displacement measured at the input and output

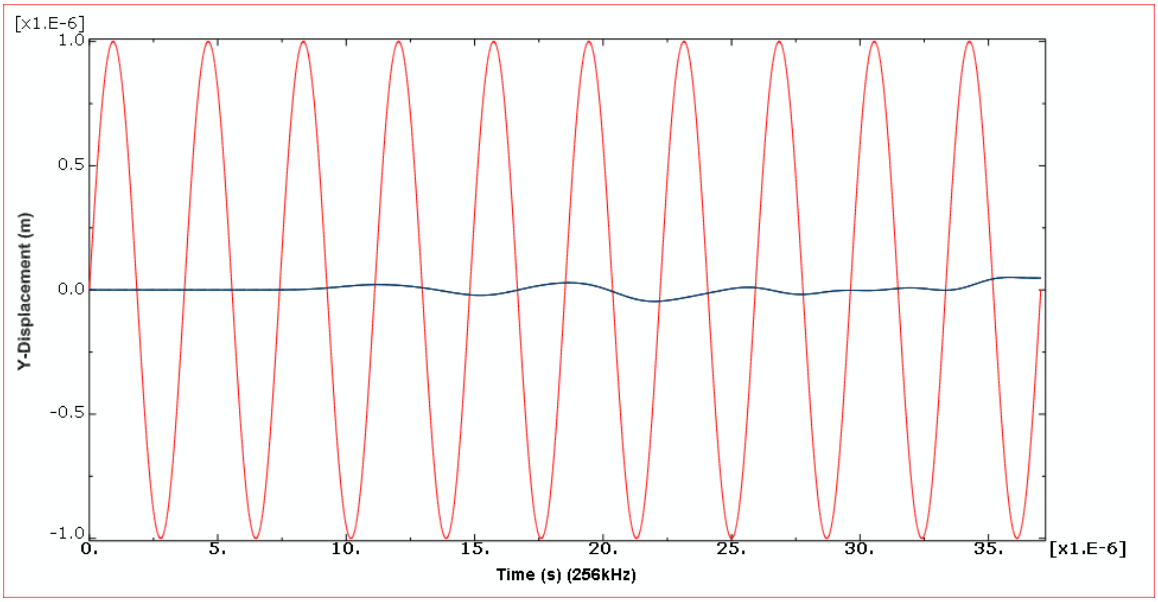

Figure 7.6 Y-Displacement measured at the input and output

X and Y displacement magnitudes at the input and output of the 2D PhnC are compared as shown in Fig 7.5 and Fig 7.6. Both the displacement components measured at the output

are about 10% of the applied input displacement. This shows that the PhnC effectively attenuates the input signal.

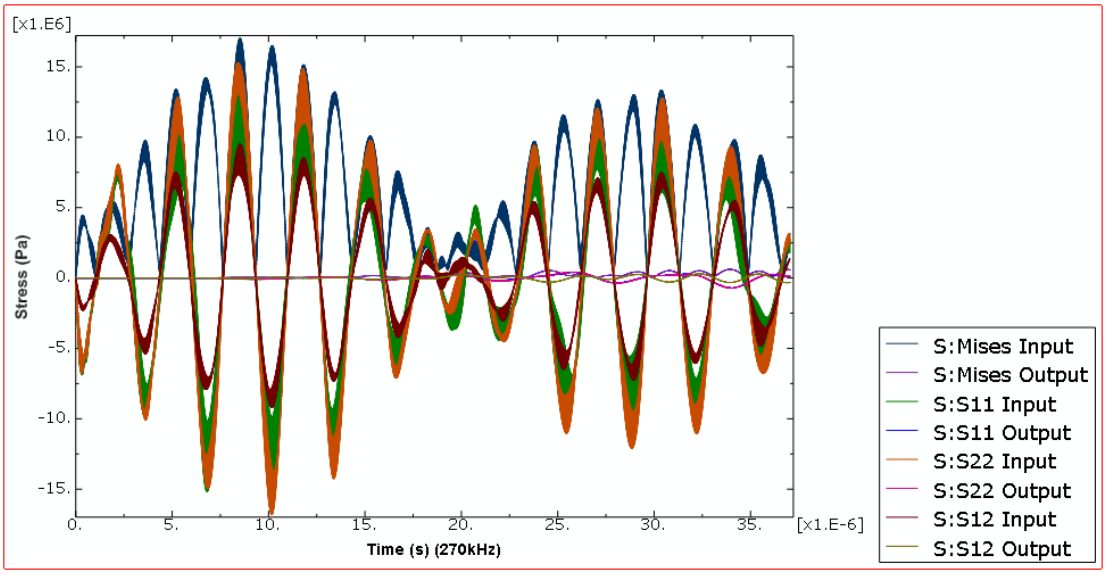

Figure 7.7 Stress components measured at the input and output (stress x$10^{6,}$ time x10^{-6})

Stress components measured at the input and output of the 2D PhnC are compared as shown in Fig 7.7. Both the stress components measured at the output are about 10% of the applied input. This shows that PhnC effectively attenuates the stress.

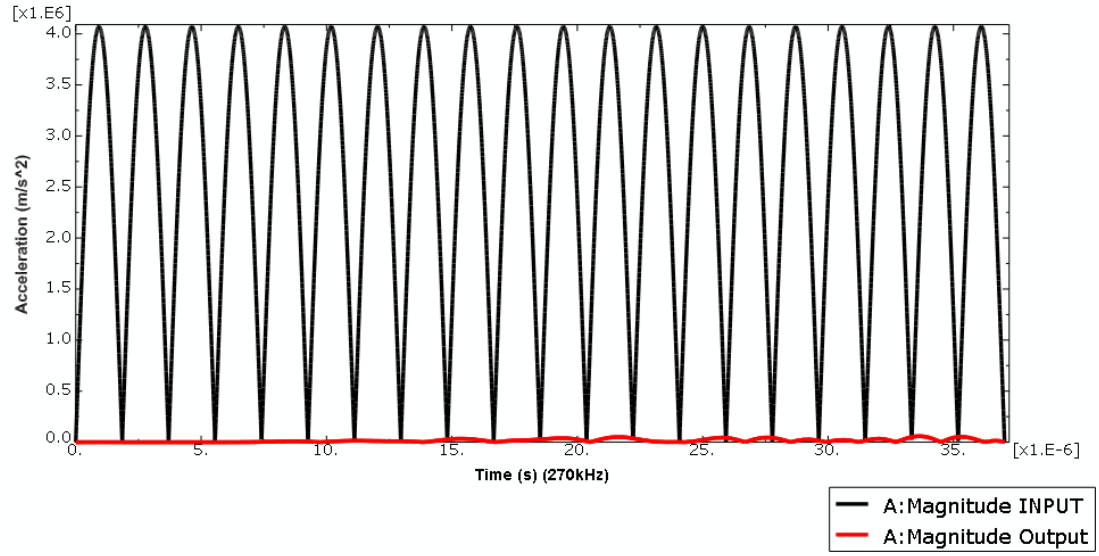

Figure 7.8 Acceleration magnitude measured at the input and output (acceleration x10^{6}, time x10^{-6})

Acceleration magnitude measured at the input and output of the 2D PhnC are compared as shown in Fig 7.8. Acceleration measured at the output are about 2.5% of the applied input. This shows that there is very less response at the measured output.

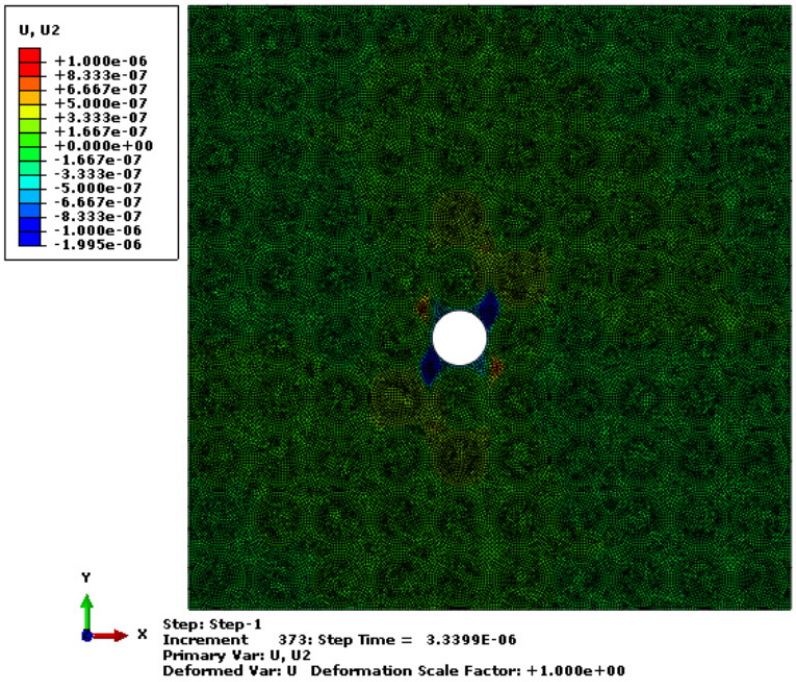

Figure 7.9 Displacement figure for sound isolation

Displacement magnitude for the 2D PhnC is shown in Fig 7.9. Displacement magnitude is seen to be confined only to the area of the input. This shows that PhnC effectively attenuates the input signal.

As seen from the results, the displacement at the measured output is an order of magnitude less compared to the input. The stress components show a similar trend. The Epoxy-CNT Phononic crystals have a potential to be used as vibration absorbers, and sound isolators for the ultrasonic frequency range. For vibration and sound isolation these PhnCs can provide large drop in displacement and stress response.

7.3 SOUND GUIDING

In this section, sound guiding in a 2D Epoxy-CNT PhnC is studied using ABAQUS's finite element explicit code. A 270 kHz frequency is chosen as the input, as this frequency falls

right in the center of the widest band gap predicted by band structure calculations. The PhnC of size 100X100 mm^2 with 10X10 array of idealized CNT cylinders was considered for wave guiding analysis. The same unit cell size of 10X10 mm^2 and CNT cylinder volume fraction of 67% and of radius 4.6 mm are used. All the external edges of the FEM model are constrained in order to prevent the PhnC from moving. A vibrating object is simulated by applying a 270 kHz periodic displacement at the center hole of the PhnC. This loading is applied for 10 cycles and the sound guiding characteristics are studied. CPE4R plane strain quadrilateral elements are used to calculate the wave guiding properties of the finite element model. The analysis is performed for 10 cycles in order to better capture the wave propagation through the PhnC. Figures 7.10 and 7.11 below shows the geometry of the 2D PhnC used for wave guiding analysis.

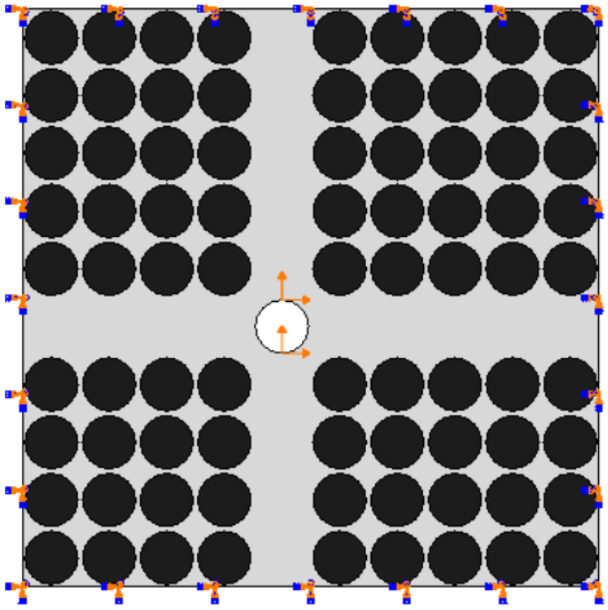

Figure 7.10 Geometry of the PhnC designed for wave guiding

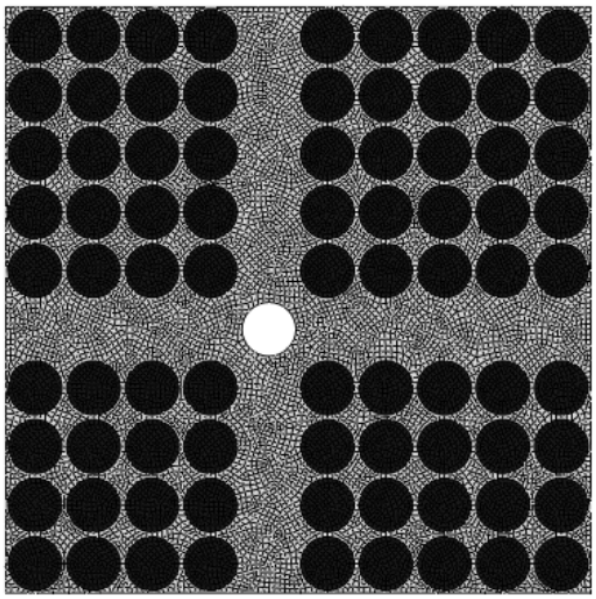

Figure 7.11 FEM Model of the PhnC designed for wave guiding

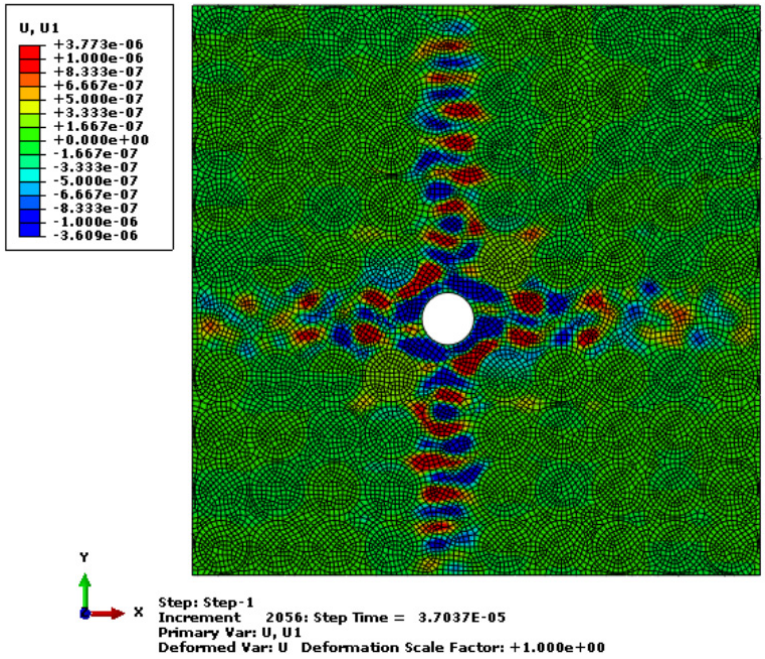

Figure 7.12 X-component of displacement for sound guiding

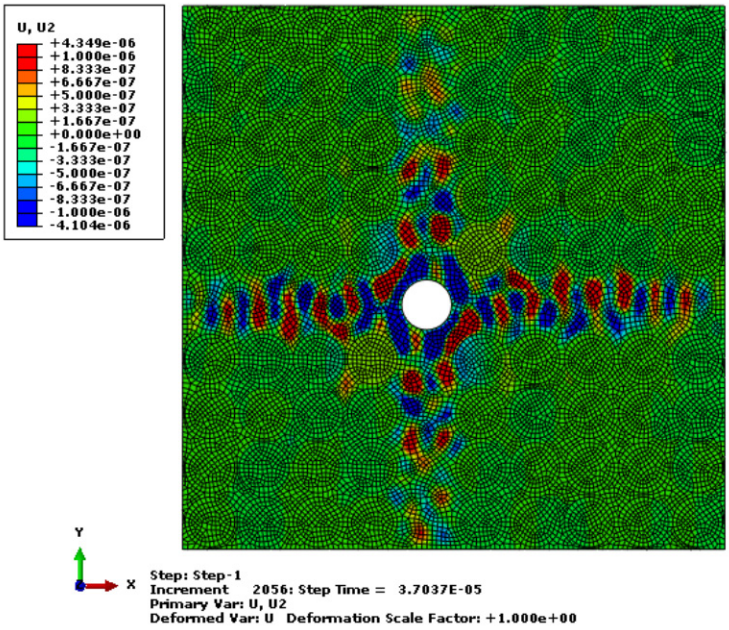

Figure 7.13 Y-component of displacement for sound guiding

Figures 7.12 and 7.13 shows that periodic input of amplitude 1-micron displacement is effectively guided along the path. This wave signal can be seen to travel along the guided path without losing its amplitude.

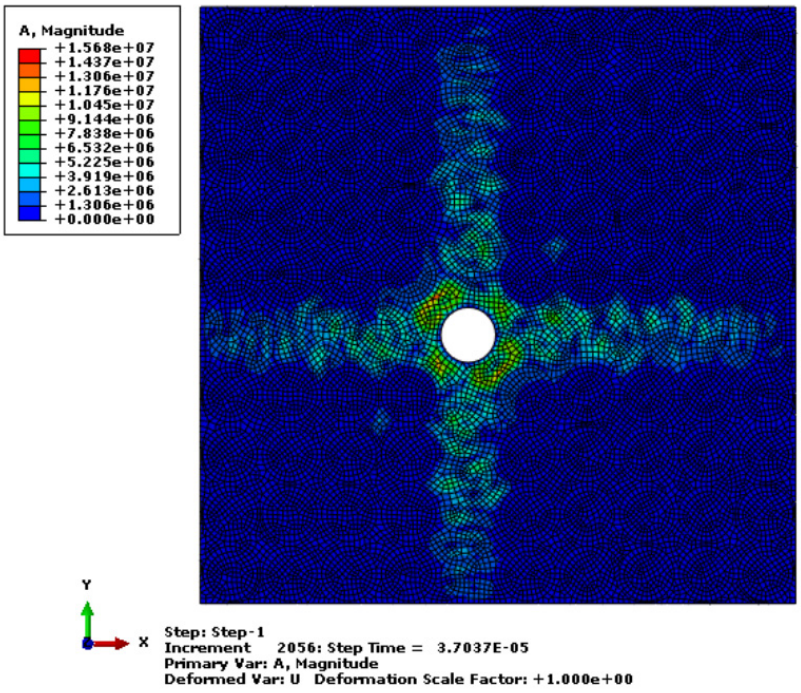

Figure 7.14 Acceleration magnitude for sound guiding

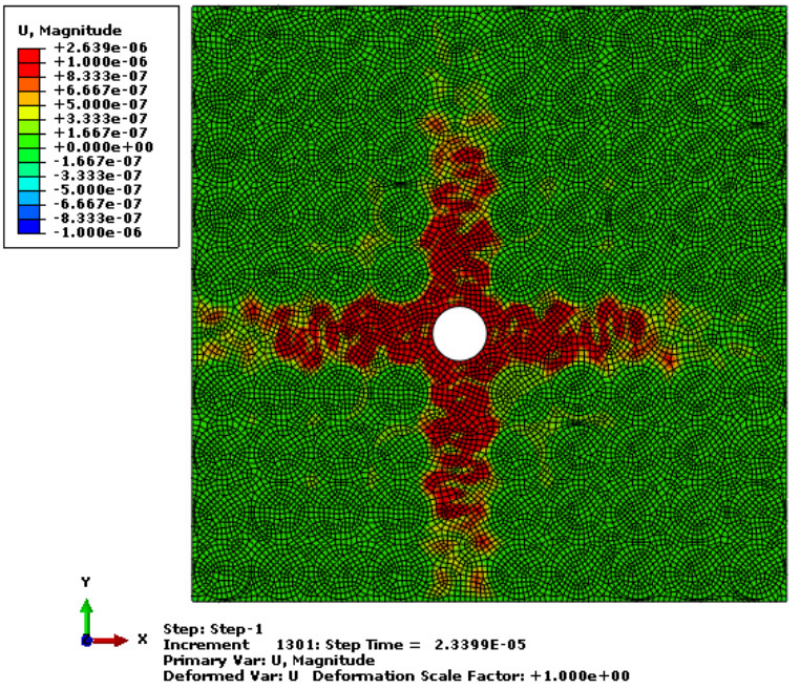

Figure 7.15 Displacement for sound guiding

Figures 7.14 and 7.15 shows the acceleration and displacement magnitude of wave guide. The input signal can be seen to travel along the guided path without much loss of amplitude.

As seen from the results, the applied sound or vibration is guided effectively by the PhnC less compared to the input. The stress components show a similar trend. The Epoxy-CNT Phononic crystals have a potential to be used as frequency filters and acoustic wave guides for the ultrasonic frequency range. For vibration and sound guiding these PhnCs carry the wave effectively through the designed path.

For comparison, a pure epoxy plate is also analyzed with the same 270 KHz 1-micron displacement input at the center hole as shown in Figure 7.16. The results shown in Figure 7.17 do not show any wave guiding effect with the pure epoxy plate. The input periodic displacement is propagated along the diagonal direction within the plate without any scattering.

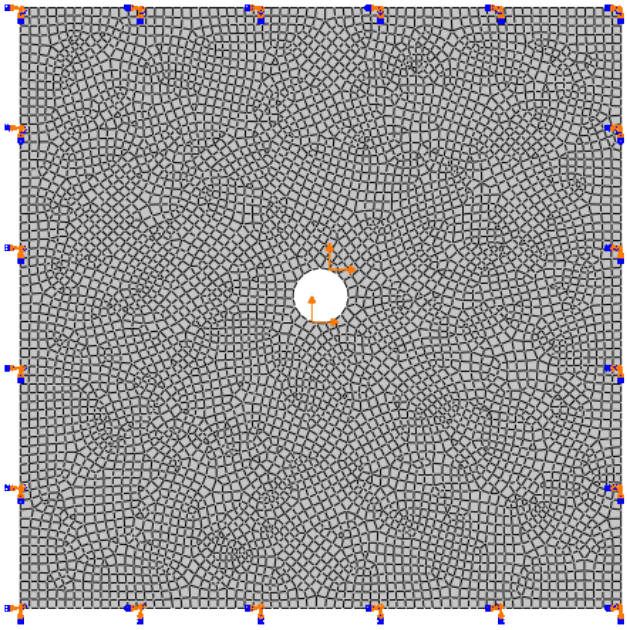

Figure 7.16 Geometry of the Pure Epoxy plate for comparison purposes.

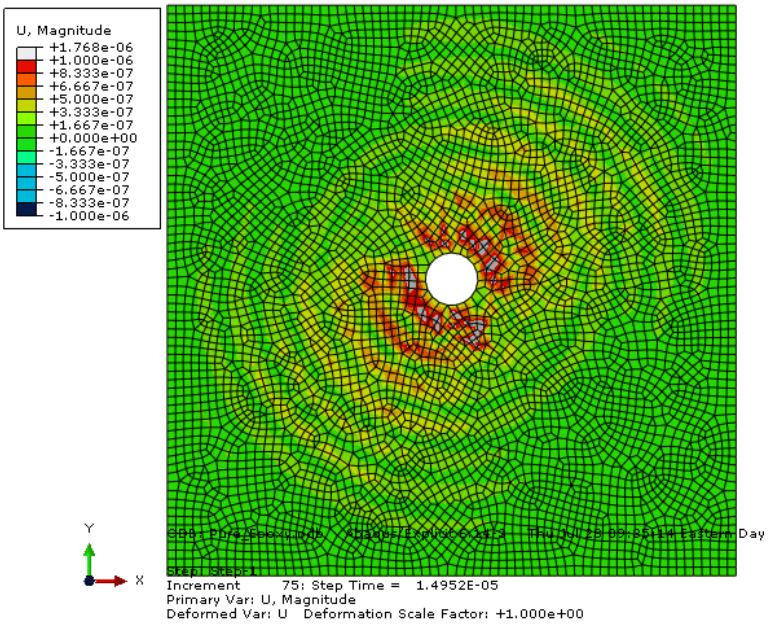

Figure 7.17 Displacement plot for the pure epoxy plate for comparison purposes

7.4 CONCLUSION

Based on the results, Epoxy-CNT Phononic crystals show a good potential to be used for vibration isolation, frequency filtering and acoustic wave guiding for the ultrasonic frequency range. The band structure calculations for 1D, 2D and 3D Epoxy-CNT Phononic crystals show multiple frequency band gaps spanning the ultrasonic range. The wave attenuation simulations show a large drop in response and the displacement and stress are an order of magnitude less than the applied input. The wave guiding simulations show that the applied wave frequency is carried effectively through the designed path without losing its amplitude and frequency contents. These metamaterials also have an advantage of being lighter and stiffer because of embedded carbon nanotube materials.

8 SUMMARY

Nanotube based periodic materials can achieve effective control over sound waves. This control over sound waves was demonstrated in this dissertation for nanotube based materials with periodicity in one, two and three directions. Elastodynamics theory was relied upon to derive governing equations for these inhomogeneous materials with interface and periodic boundary. These equations were solved to obtain the frequency band gaps existing in these periodic materials. Numerical methods including finite element method was relied upon to solve the dispersion relations. Frequency band gaps were searched for all wave directions and polarization. It was found that partial band gaps exist in these periodic materials and these band gaps attenuated waves travelling with longitudinal, transverse and coupled polarization. These band gaps were further correlated with frequency response calculations. Stress attenuation and guiding properties were also studied and interfacial stresses were also reported for future structural integrity calculations and tests.

One dimensionally periodic Epoxy carbon nanotube materials were analyzed for wave attenuation purposes. Geometrical dimensions of these composites were chosen mainly for ultrasonic frequency range. First the dispersion relation for transverse and longitudinal wave types for these composites was obtained. Solving the dispersion relations gave rise to frequency gaps existing due to Bragg's effect. It was found that these composites can block multiple frequencies for both transverse and longitudinal wave types. Interfacial and stress attenuation properties were also studied. These composites effectively attenuated the incoming input pulse.

One dimensional periodic idealized aluminum boron nitride nanotube layered materials were studied for wave guiding purposes. These materials were analyzed for wave guiding under Blast and Impact conditions for military applications. Wave guiding properties of straight and serpentine shapes were also studied and found to be effective carriers of mechanical energy.

Two dimensional periodic Epoxy carbon nanotube materials were analyzed for wave attenuation purposes. Geometrical dimensions of these composites were chosen mainly for ultrasonic frequency range. Dispersion relations using the finite element method were solved for transverse, longitudinal and coupled wave types for calculating frequency band gaps. It was found that these composites can block multiple frequencies for both transverse, longitudinal and coupled wave types. These composites effectively attenuated the incoming input. Sound isolation and frequency pulse filtering simulations were performed.

Three dimensional periodic Epoxy carbon nanotube materials were analyzed for wave attenuation purposes. Geometrical dimensions of these composites were chosen mainly for ultrasonic frequency range. Dispersion relations using the finite element method was solved for transverse, longitudinal and coupled wave types for calculating frequency band gaps. It was found that these composites have partial frequency band gaps in one or more directions but not complete band gaps in all directions for the frequencies studied.

Carbon nanotube materials have a potential to be used in controlling, directing and manipulating elastic waves to achieve wave guiding and attenuation. Based on the results presented, 1D, 2D and 3D nanotube based PhnCs can achieve frequency band gaps in the ultrasonic range and these results present nanotube based PhnCs as potential candidates for frequency filtering, demultiplexing and imaging applications in ultrasonic range. Strong wave guiding properties can also be achieved by these materials and this effect can be exploited for use in impact and blast energy dissipation. These materials have a potential to be incorporated into body armors to carry energy away from the area of impact. Incorporating these materials in soldier helmets could also guide blast energy around the helmets which could reduce the severity of the trauma injuries. Military equipment and armored vehicles could also make use of these materials to dissipate blast energy from the impact site for protection purposes.

9 FUTURE WORK

This work was mainly focused on establishing the conceptual and theoretical base for using nanotube materials for wave guiding and attenuation purposes. Experimental validation of these materials would be the first step toward validating the concepts presented in this dissertation. Although, materials with such ideal properties cannot be achieved, manufacturing and testing with high stiff materials such as carbon whiskers instead of nanotube yarns is suggested for validation. Sound transmission and attenuation properties are crucial for rating the performance of these materials, Therefore, acoustic and vibration testing is suggested for practical considerations. Since cost can be an issue for manufacturing these composites as nanotube materials are expensive. Developing cheaper methods for manufacturing nanotubes would be beneficial to further this research.

Testing and manufacturing of straight nanotube layered yarns embedded in epoxy under impact wave guiding is suggested. Since carrying tests under high frequency inputs can be challenging, testing under impact instead of high frequency periodic input is suggested for experiments. Shock tube tests is suggested for testing layered wave guide specimens. This test results would prove beneficial for military applications subjected to blast such as helmets and artillery. Comparative tests of these nanotube based specimens with materials like Kevlar is also suggested. Shear test is also suggested for testing the delamination characteristics of these materials. It is also suggested to perform bullet impact tests on body armors incorporated with layered wave guides to study energy dissipation characterists. Incorporating these materials in body armors could quickly carry away impact energy away from the impact area. Military equipment and armored vehicles could also make use of these materials to dissipate energy from blasts from the impact site.

Theoretical analysis of these materials for hypersonic frequencies is also suggested for thermal applications. Band structure for hypersonic frequencies can be obtained by following the same theoretical approach elaborated in this dissertation. Since the geometry tends to become very small for hypersonic frequency applications, using actual nanotubes are suggested for use in test specimens instead of carbon whiskers.

Further analysis of 2D Epoxy-CNT Phononic crystals with various inclusion patterns would be beneficial. This study would be helpful to study the influence of inclusion patterns on the width of the frequency band gap. Manufacturing simple frequency filters and sound isolators for proof of concept would help to enhance this research to build ultrasonic applications. Further analysis of 3D Epoxy-CNT Phononic crystals with different inclusion shapes is suggested. This study would be helpful to find a complete frequency band gap to build complete wave isolators i.e. “acoustic black holes”.

10 REFERENCES

1. Deymier, P.A., *Acoustic metamaterials and phononic crystals*. Springer series in solid-state sciences,. 2013, Berlin ; New York: Springer. xiv, 378 p.
2. Craster, R.V. and S.b. Guenneau, *Acoustic metamaterials : negative refraction, imaging, lensing and cloaking*. Springer series in materials science. 2013, Dordrecht ; New York: Springer. xiii, 323 pages.
3. Sigalas, M., et al., *Classical vibrational modes in phononic lattices: theory and experiment.* Zeitschrift Fur Kristallographie, 2005. **220**(9-10): p. 765-809.
4. Gao, Y., et al., *Impact of nanotube density and alignment on the elastic modulus near the top and base surfaces of aligned multi-walled carbon nanotube films.* Carbon, 2012. **50**(10): p. 3789-3798.
5. Veselago, V.G. and E.E. Narimanov, *The left hand of brightness: past, present and future of negative index materials.* Nat Mater, 2006. **5**(10): p. 759-762.
6. Pendry, J.B. and D.R. Smith, *Reversing light with negative refraction.* Physics Today, 2004. **57**(6): p. 37-43.
7. Maldovan, M., *Sound and heat revolutions in phononics.* Nature, 2013. **503**(7475): p. 209-217.
8. Fink, M., *ACOUSTIC METAMATERIALS Nearly perfect sound absorbers.* Nature Materials, 2014. **13**(9): p. 848-849.
9. Aravantinos-Zafiris, N., et al., *Phononic crystals and elastodynamics: Some relevant points.* Aip Advances, 2014. **4**(12).
10. Xiang, H.J., et al., *Periodic materials-based vibration attenuation in layered foundations: experimental validation.* Smart Materials and Structures, 2012. **21**(11).
11. Sukhovich, A., et al., *2D–3D Phononic Crystals*, in *Acoustic Metamaterials and Phononic Crystals*, A.P. Deymier, Editor. 2013, Springer Berlin Heidelberg: Berlin, Heidelberg. p. 95-157.
12. Garretón, L.G., et al., *Phononic and photonic band gap structures: modelling and applications -International Congress on Ultrasonics, Santiago de Chile, January 2009.* Physics Procedia, 2010. **3**(1): p. 357-364.
13. Page, J.H., et al., *3D Phononic Crystals*, in *Wave Scattering in Complex Media: From Theory to Applications*, B.A. van Tiggelen and S.E. Skipetrov, Editors. 2003, Springer Netherlands: Dordrecht. p. 282-307.
14. Yang, S., et al., *Focusing of Sound in a 3D Phononic Crystal.* Physical Review Letters, 2004. **93**(2): p. 024301.
15. Joannopoulos, J.D., *Photonic crystals : molding the flow of light*. 2nd ed. 2008, Princeton: Princeton University Press. xiv, 286 p.

16. Kushwaha, M.S., et al., *Theory of Acoustic Band-Structure of Periodic Elastic Composites.* Physical Review B, 1994. **49**(4): p. 2313-2322.

17. Chen, H.Y. and C.T. Chan, *Acoustic cloaking and transformation acoustics.* Journal of Physics D-Applied Physics, 2010. **43**(11).

18. Norris, A.N., *Acoustic cloaking theory.* Proceedings of the Royal Society a-Mathematical Physical and Engineering Sciences, 2008. **464**(2097): p. 2411-2434.

19. Croenne, C., et al., *Negative refraction of longitudinal waves in a two-dimensional solid-solid phononic crystal.* Physical Review B, 2011. **83**(5).

20. Lee, M.K., et al., *Negative refraction experiments with guided shear-horizontal waves in thin phononic crystal plates.* Applied Physics Letters, 2011. **98**(1).

21. Cai, L.W. and J. Sanchez-Dehesa, *Analysis of Cummer-Schurig acoustic cloaking.* New Journal of Physics, 2007. **9**.

22. Cummer, S.A., et al., *Scattering theory derivation of a 3D acoustic cloaking shell.* Physical Review Letters, 2008. **100**(2).

23. Cummer, S.A. and D. Schurig, *One path to acoustic cloaking.* New Journal of Physics, 2007. **9**.

24. Pai, P.F. and G. Huang, *Theory and design of acoustic metamaterials*. 2015, Bellingham, Washington (USA): SPIE Press. xv, 334 pages.

25. Al-Lethawe, M.A., et al., *All-angle negative refraction for surface acoustic waves in pillar-based two-dimensional phononic structures.* New Journal of Physics, 2012. **14**.

26. Baron, A., et al., *[INVITED] Self-assembled optical metamaterials.* Optics and Laser Technology, 2016. **82**: p. 94-100.

27. Inoue, K. and K. Ohtaka, *Photonic crystals : physics, fabrication, and applications*. Springer series in optical sciences,. 2004, Berlin ; New York: Springer. xii, 320 p.

28. Singh, B.K., M.K. Chaudhari, and P.C. Pandey, *Photonic and Omnidirectional Band Gap Engineering in One-Dimensional Photonic Crystals Consisting of Linearly Graded Index Material.* Journal of Lightwave Technology, 2016. **34**(10): p. 2431-2438.

29. Sukhoivanov, I.A. and I.V. Guryev, *Photonic crystals : physics and practical modeling*. Springer series in optical sciences,. 2009, Heidelberg ; New York: Springer. xix, 242 p.

30. Doutres, O. and N. Atalla, *Experimental estimation of the transmission loss contributions of a sound package placed in a double wall structure.* Applied Acoustics, 2011. **72**(6): p. 372-379.

31. Liu, Z., et al., *Locally resonant sonic materials.* (1095-9203 (Electronic)).

32. Antos, R., V. Vozda, and M. Veis, *Plane wave expansion method used to engineer photonic crystal sensors with high efficiency.* Optics Express, 2014. **22**(3): p. 2562-2577.

33. Low, K.L., M.Z.M. Jafri, and S.A. Khan, *Band Gap Calculation Using the Plane Wave Expansion Method for Metallic Substrate Photonic Crystals (PC) with Air Rods in E Polarizing Mode.* Chinese Journal of Physics, 2009. **47**(6): p. 853-861.

34. Po-Feng, H., W. Tsung-Tsong, and S. Jia-Hong, *Three-dimensional phononic band gap calculations using the FDTD method and a PC cluster system.* IEEE Transactions on Ultrasonics, Ferroelectrics, and Frequency Control, 2006. **53**(1): p. 148-158.

35. Gorishnyy, T., et al., *Hypersonic phononic crystals.* Physical Review Letters, 2005. **94**(11).

36. Otsuka, P.H., et al., *Broadband evolution of phononic-crystal-waveguide eigenstates in real- and k-spaces.* Scientific Reports, 2013. **3**.

37. Armenise, M.N., et al., *Phononic and photonic band gap structures: modelling and applications.* Physics Procedia, 2010. **3**(1): p. 357-364.

38. Gomopoulos, N., et al., *One-Dimensional Hypersonic Phononic Crystals.* Nano Letters, 2010. **10**(3): p. 980-984.

39. Wu, M.L., et al., *Elastic wave band gaps of one-dimensional phononic crystals with functionally graded materials.* Smart Materials & Structures, 2009. **18**(11).

40. Whitworth, R.W., *Fundamentals of Solid-State Physics - Christman,Jr.* Nature, 1989. **338**(6211): p. 175-176.

41. Giorgio, A., A.G. Perri, and M.N. Armenise, *Fast modelling of deeply and fully etched gratings based on the Bloch-Floquet theorem.* International Journal of Numerical Modelling-Electronic Networks Devices and Fields, 2001. **14**(6): p. 507-522.

42. Mandelik, D., et al., *Band-gap structure of waveguide arrays and excitation of Floquet-Bloch solitons.* Physical Review Letters, 2003. **90**(5).

43. Kittel, C., *Berkeley physics course*. 1965, New York,: McGraw-Hill.

44. Bedford, A. and D.S. Drumheller, *Introduction to Elastic Wave Propagation*. 1996: Wiley.

45. Tham, C.Y., V.B.C. Tan, and H.P. Lee, *Ballistic impact of a KEVLAR® helmet: Experiment and simulations.* International Journal of Impact Engineering, 2008. **35**(5): p. 304-318.

46. Naik, N.K. and V.K. Ganesh, *Prediction of on-axes elastic properties of plain weave fabric composites.* Composites Science and Technology, 1992. **45**(2): p. 135-152.

47. Naik, N.K. and V.K. Ganesh, *An analytical method for plain weave fabric composites.* Composites, 1995. **26**(4): p. 281-289.

48. Ganesh, V.K. and N.K. Naik, *Failure behaviour of plain weave fabric laminates under in-plane shear loading: effect of fabric geometry.* Composite Structures, 1995. **30**(2): p. 179-192.

49. Logan, D.L., *First Course in the Finite Element Method*. 2007: Thomson.

50. Petyt, M., *Introduction to Finite Element Vibration Analysis*. 1998: Cambridge University Press.